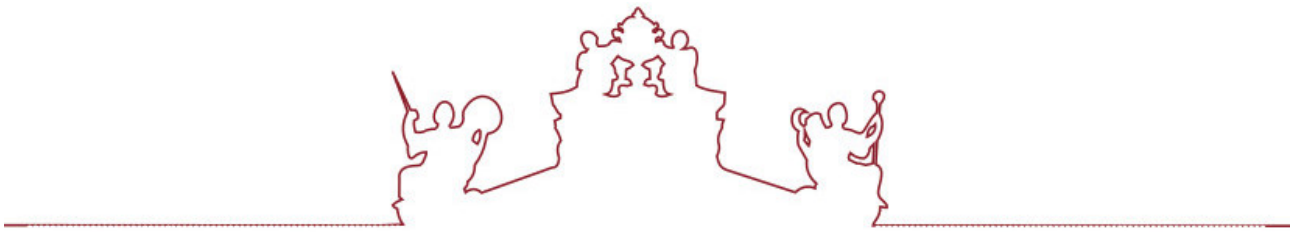

Universidade de Évora - Instituto de Investigação e Formação Avançada
Università degli Studi di Roma "La Sapienza" Aristotle University of Thessaloniki

Mestrado em Ciência dos Materiais Arqueológicos (ARCHMAT)

Dissertação

PVA/Borax-based Hydrogel for Stone Conservation: Evaluation of Cleaning Performance through a Multi-Technical Approach

Andrea Louise Matulac

Orientador(es) | Gabriele Favero

Évora 2023

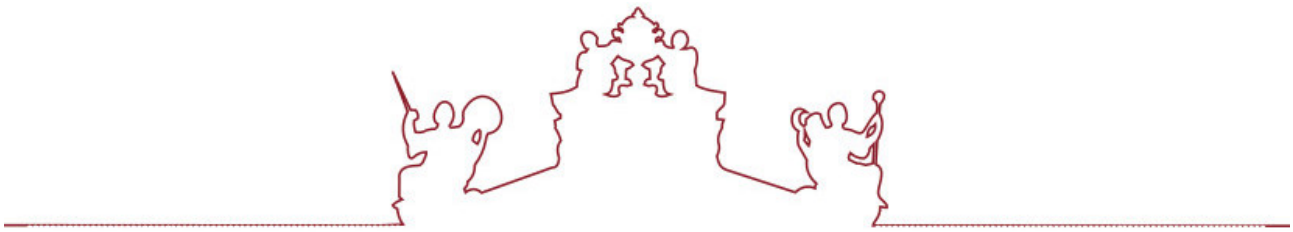

Universidade de Évora - Instituto de Investigação e Formação Avançada
Università degli Studi di Roma "La Sapienza" Aristotle University of Thessaloniki

Mestrado em Ciência dos Materiais Arqueológicos (ARCHMAT)

Dissertação

PVA/Borax-based Hydrogel for Stone Conservation: Evaluation of Cleaning Performance through a Multi-Technical Approach

Andrea Louise Matulac

Orientador(es) | Gabriele Favero

Évora 2023

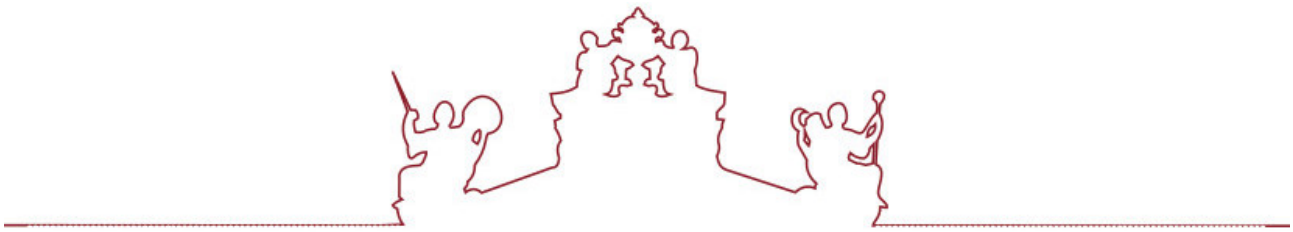

A dissertação foi objeto de apreciação e discussão pública pelo seguinte júri nomeado pelo Diretor do Instituto de Investigação e Formação Avançada:

Presidente	|	Donatella Magri (Università degli Studi di Roma "La Sapienza")
Vogais	|	Alessando Ciccola (Università degli Studi di Roma "La Sapienza") Eugenio del Re (Università di Roma La Sapienza) Gabriele Favero (Università degli Studi di Roma "La Sapienza") Ioannis Kozaris () MARIA STEFANIDOU () Nicola Schiavon (Universidade de Évora)

Évora 2023

PVA/Borax-based High Viscosity Polymeric Dispersions for Stone Conservation: Evaluation of Cleaning Method through a Multi-Technical Approach

Facoltà di Scienze, Matematiche, Fisiche e Naturali
Dipartimento di Biologia Ambientale
Corso di laurea in Scienze dei Materiali Archeologici (ARCHMAT)

Andrea Louise Matulac
Matricola 2091708

Relatore
Gabriele Favero

Correlatore
Alessandro Ciccola
Laura Giuliani

A.A. 2022-2023

ACKNOWLEDGEMENTS

I am sincerely grateful to all those who have contributed to the completion of this endeavor. Their relentless support has been invaluable throughout this journey.

First and foremost, I extend my gratitude to my supervisors Laura Giuliani, Alessandro Ciccola, and Gabriele Favero, for their continuous guidance and insights. Their dedication and expertise have been instrumental in shaping the direction of my research and in delivering the best possible output. I also want to extend my appreciation to my colleagues in the laboratory whose camaraderie and collaboration created a stimulating environment for learning and growth.

I also want to thank the European Commission and the ARCHMAT consortium composed of Nicola Schiavon, Panagiotis Spathis, and Donatella Magri, for providing me with the opportunity to pursue an Erasmus Mundus Joint Master Degree. The resources, knowledge, and experience offered by the program have aided my holistic development.

I also want to thank my friends, especially Kathryn, Lionel, Leanne, and Arnob, with whom I could not have survived the last two years without. The homemade dinners, late night talks, and aimless wandering were my source of comfort and joy. I am fortunate to be surrounded by good people on bad days.

My heartfelt gratitude goes out to my family back in the Philippines for their love, encouragement, and belief in me. Their sacrifices and understanding are the pillars of my being and I am truly blessed to have them by my side.

Lastly, I acknowledge the divine presence of God, whose grace has guided me through every decision I made. This accomplishment would not have been possible without Him.

Title: PVA/Borax-based High Viscosity Polymeric Dispersions for Stone Conservation: Evaluation of Cleaning Method through a Multi-Technical Approach

ABSTRACT

Carbonate stones used in connection with cultural heritage materials are subjected to different degradation phenomena in function of their chemical and physical properties. Two important issues that need to be addressed are: (1) the formation of corrosion products from metallic impurities or metallic artifacts in contact with the stone and (2) the photo-oxidative weathering of resins on stone which render them insoluble. In such cases, the choice of cleaning method is critical because the removal has to be confined to the contaminants and should not further damage the stone. High viscosity polymeric dispersions (HVPDs), which have good mechanical properties, high solvent and active component retention, low toxicity, and low environmental impact, seem to be a promising solution. For this thesis project, the two main HVPDs evaluated were polyvinyl alcohol cross-linked with borax (PVA/B) and its variant with agarose (PVA/B-AG) on the substrates Carrara Marble, Lecce Stone, and Travertine. For the cleaning of bronze corrosion products, ethylenediaminetetraacetic acid (EDTA) and potassium sodium tartrate (PST) were added as chelants. Based on characterization studies, all of the HVPDs pass the criteria of peelability, have minimal water desorption, retain more than half of their volatile fraction, and do not leave residues under four hours. Regarding the first issue, SEM and FORS analysis reveal that treatment using PVA/B-AG with EDTA or PST are both effective in the removal of corrosion products and the restoration of the surface close to its original state. Two applications are necessary, with the second one modulated to avoid lightening. The use of EDTA is recommended over PST due to its higher removal efficiency. FT-IR ATR results confirm the complexation of the chelants with copper, their sequestration, and their interaction with the HVPD components. Regarding the second issue, FORS analysis demonstrate the significant reduction in the redness and yellowing of the surface after the treatment with PVA/B and PVA/B-AG. Flaking off and delamination were observed in both cases, but FT-IR ATR results show the capability of the latter to adhere the acrylate polymer. Water vapor permeability test results also reinforce that the resin is being removed based on the improvement of the stone's breathability. Altogether, the results demonstrate the eco-friendliness and versatility of PVA/B-based HVPDs as a cleaning tool. This also opens avenues for its adoption not just in the removal of hydrophilic but also hydrophobic materials detrimental to cultural heritage objects.

Keywords: Polymeric Dispersion, Chelants, Cleaning, Stone, Corrosion, Resin

TABLE OF CONTENTS

INTRODUCTION

Natural stones have always played a fundamental role in the creation of sculptures, monuments, and architecture. They have been used to realize artistic visions and to construct grand structures, religious edifices, public squares, and iconic landmarks.[1] Italy, in particular, has a rich history of using various natural stones especially carbonates. The selection reflects aesthetic preferences, regional traditions, and cultural identities.[1–3] On a practical note, the selection can also be attributed to geological availability, transportation feasibility, and the intended use in that period.[1,4]

By definition, a stone is a mono- or poly-mineral aggregate formed naturally through lithification. After its formation, it immediately undergoes transformation through geochemical processes until eventually reaching equilibrium with its environment. However, if the environmental parameters change, the equilibrium is disrupted and the stone has to counteract it.[4] For example, when stones go from burial (high temperature and pressure) to subaerial conditions (low temperature, atmospheric pressure, fluid contact), physical and chemical weathering happens. The identity and properties of the stones change as a consequence.[2,4]

Once extracted from their environment, stone durability depends on factors encountered during its construction. Quarrying releases the latent tension present in natural stone resulting in cracking. Dressing and processing also produces cracks, both at the surface and at the bulk, which propagate and favor the action of degradation agents. Moreover, if the material is not well-suited for its application and not handled properly, maintenance might not be sufficient long-term.[1,5] Assuming the construction is done correctly, the usage and exposure of the stone mainly influence the mechanism and rate of its degradation. [1–3] Common culprits include salt crystallization,[6] aqueous dissolution,[7] microbiological growth,[8] temperature fluctuations,[9] mechanical loads,[10] presence of metallic artifacts that undergo corrosion,[11–13] aging of polymer coatings,[14,15] and human contact.[1–3]

Due to their intrinsic nature, both chemical and physical, stones will always be susceptible to various degradation phenomena.[2] Cleaning –the removal of contaminants and undesired substances –is therefore imperative. However, poorly executed and inappropriate interventions only exacerbate damage. The goal is to therefore restore the stone back as close to its initial state as possible without further affecting its integrity in a non-toxic and non-polluting way.

As part of a doctoral project focused on the development of innovative soft matters for the cleaning of stone assets, this research will delve into two pressing issues which continue to affect carbonate-based stones. The first issue involves the leaching of corrosion products from metallic impurities inherently present in the stone or metallic artifacts in direct contact with the stone (e.g. clamps, pins, nails, and plaques) and the concomitant discoloration altering the stone's appearance.[13,16] While the corrosion products are often concentrated at the interface of the metal and the stone, without intervention the damage extends throughout the stone.[13,16] The second issue involves the aging of Paraloid® B72, an acrylic resin, commonly used by restorers as a protective coating. The resin undergoes natural aging and photo-oxidative weathering instigating polymer chain scission and cross-linking reactions, which results in the production of harmful insoluble by-products, a change in properties, and an observable yellowing in appearance.[14,15,17]

The choice of cleaning treatment is complicated because the removal has to be confined to the contaminants or undesired substances without any unwarranted effect on the stone itself. In recent years, gels and gel-like high viscosity polymeric dispersions (HVPDs) have garnered interest due to their good mechanical properties, high solvent and active component retention, low toxicity, and low environmental impact.[18,19] In particular, polyvinyl alcohol cross-linked with borax (PVA/B) is a promising material because of its facile preparation and use.[18] This dynamic network can be loaded with chelants, such as disodium ethylenediamine tetraacetic acid (EDTA) and potassium sodium tartrate (PST), to enhance contaminant sequestration.[20–23] Ligands with high affinity and stability towards metals ions undergo coordination, leading to the dissolution of the corrosion products into the aqueous media and reconfinement back into the soft matter.[20,21] The material can also be applied to the surface and left in contact, then removed by peeling with little to no residues left.[24,25] When necessary, modification of plasticity or rigidity can also be obtained through the addition of agarose (AG) in the network without sacrificing the other properties of the material.[26,27]

This chapter will discuss thoroughly the following: (1) the characteristics of the three lithotypes, specifically, Carrara Marble, Lecce Stone, and Travertine, (2) the macroscopic and microscopic changes brought about by the bronze corrosion products and the aging of Paraloid® B72, (3) the measures taken so far to solve these problems, and (4) how PVA/B-based HVPDs can be utilized in cleaning.

1.1 LITHOTYPES, PROPERTIES, AND USES

Carbonate stones are sedimentary in type, formed from the accumulation of organic and inorganic particles followed by cementation. The main compounds found in these stones are calcium carbonate ($CaCO_3$) and calcium magnesium carbonate ($CaMg(CO_3)_2$).[28,29] Calcium carbonate exists as either its calcite or aragonite polymorph. From a geochemical point of view, calcite is more stable and abundant at surface conditions due to its rhombohedral crystal structure. Meanwhile, aragonite is only metastable and denser due to its orthorhombic crystal structure. The conversion of aragonite to calcite has a low free energy of transition and is thermodynamically favored, except at an extremely high temperature and pressure.[28] Calcium magnesium carbonate exists as dolomite. This mineral is formed when a significant amount of magnesium substitutes for calcium in calcite.[28] It is not unusual for all these aforementioned minerals to occur together. However, a carbonate stone consisting mainly of calcium carbonate is classified as limestone while that mainly consisting of calcium magnesium carbonate is classified as dolostone.[28]

Calcium carbonate is often produced from seawater and freshwater.[30] Calcium ions (Ca^{2+}) originate from the dissolution of calcium-bearing biotic and abiotic substances. Meanwhile, the bicarbonate (HCO_3^-) and carbonate (CO_3^{2-}) ions come from the two-step dissolution of atmospheric carbon dioxide (CO_2) in water. The free calcium ions react with free bicarbonate and carbonate ions to form calcite or aragonite. Calcite is favored in the presence of chloride, nitrate, and sodium bicarbonate. Aragonite is favored in the presence of divalent ions such as lead, manganese, barium, strontium, magnesium and sulfate.[28,30]

$$CaX_2\,(s) + H_2O\,(l) \rightleftharpoons Ca^{2+}\,(aq) + X^-(aq) + H_2O\,(l) \qquad \text{Rxn 1}$$

$$CO_2\,(g) + H_2O\,(l) \rightleftharpoons H_2CO_3\,(aq) \qquad \text{Rxn 2}$$

$$H_2CO_3\,(aq) \rightleftharpoons H^+\,(aq) + HCO_3^-\,(aq) \qquad \text{Rxn 3a}$$

$$HCO_3^-\,(aq) \rightleftharpoons H^+\,(aq) + CO_3^{2-}\,(aq) \qquad \text{Rxn 3b}$$

$$Ca^{2+}\,(aq) + 2HCO_3^-\,(aq) \rightleftharpoons CaCO_3\,(s) + H_2CO_3\,(aq) \qquad \text{Rxn 4a}$$

$$Ca^{2+}\,(aq) + CO_3^{2-}\,(aq) \rightleftharpoons CaCO_3\,(s) \qquad \text{Rxn 4b}$$

The precipitation of calcium magnesium carbonate is similar in process. Magnesium is another common ion in water which originates from magnesium-containing compounds.[28,30]

$$MgX_2\,(s) + H_2O\,(l) \rightleftharpoons Ca^{2+}\,(aq) + X^-(aq) + H_2O\,(l) \qquad \text{Rxn 5}$$

$$Ca^{2+}\,(aq) + Mg^{2+}\,(aq) + 4HCO_3^-\,(aq) \rightleftharpoons CaMg(CO_3)_2\,(s) + 2H_2CO_3\,(aq) \qquad \text{Rxn 6a}$$

$$Ca^{2+}\,(aq) + Mg^{2+}\,(aq) + 2CO_3^{2-}\,(aq) \rightleftharpoons CaMg(CO_3)_2\,(s) \qquad \text{Rxn 6b}$$

Based on Le Chatelier's Principle, the dissolution of calcite, aragonite, and dolomite is controlled by the amount of atmospheric carbon dioxide dissolved in water and the resulting pH of the water. At lower temperatures and higher pressures, the dissolution of gaseous carbon dioxide in water to form carbonic acid in solution is favored. Conversely, higher temperatures and lower pressures result in the precipitation of carbonates. In nature, many aquatic life forms are responsible for the formation of most carbonate rocks, since organisms either produce shells and other skeletal parts of carbonates or induce the precipitation of carbonates as a byproduct of their biological activities.[30,31]

Table I. Three most common minerals found in carbonate stones and their crystalline structure.[29]

Mineral	Unit Cell	Image
Calcite	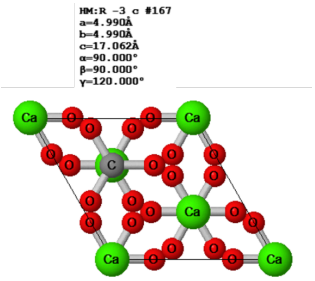	
Aragonite	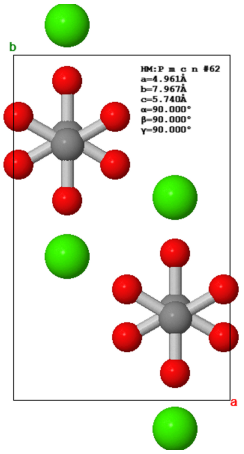	
Dolomite	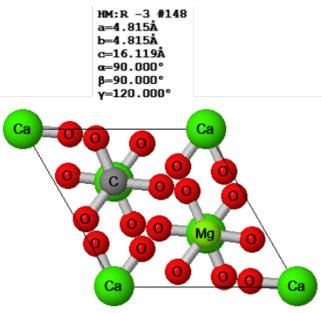	

1.1.1 LITHOTYPE A: CARRARA MARBLE

Figure 1. Images of Madonna della Pietà by Michelangelo Buonarroti made of Carrara Marble.

Carrara marble is highly prized by Classical, Renaissance, and modern sculptures; its purity, grain size, color, and workability make it an excellent ornamental and statuary stone.[32] It is Hettangian in age and found in the Apuane Alps within the Northern Apennines. In outcrops, it is either massive or brecciated with angular elongate white marble fragments in a matrix of gray marble. Its commercial quarrying was started by the Romans during the second century B.C. It was referred to then as Luni Marble, after the ancient port city situated about 17 km from the quarries. Three main areas were exploited by the Romans, namely, Torano, Miseglia, and Colonnata. Torano includes the Mandria, Polvaccio, Sponda, and Crestola quarries. Miseglia includes the Fantiscritti, La Tagliata, and Canalgrande quarries. Colonnata includes Fossacava, Calagio, and Bacchiotto quarries. The use of Carrara marble mellowed and became sporadic throughout the Medieval period then flourished again in the Renaissance period.[x] In the present time, the aforementioned quarries have the highest production in the world and account for almost all of the marble imported into the United States.[32]

This stone is characteristically homogenous, with a white to gray ground color, shining grains, and smoky gray veins running through it irregularly.[4] Carrara marble consists of calcite with variable but low amounts of accessory minerals. The lowest relative amount of calcite is 96% with accessory minerals dolomite, muscovite, plagioclase, and epidote ranging from 1 to 4%. Trace amounts of quartz, chlorite, graphite, pyrite, hematite, and magnetite are occasionally detected. Calcite is 50-200 μm in diameter, has subhedral to euhedral equigranular crystals, and of bigranular or equigranular textures.[4]

1.1.2 LITHOTYPE B: LECCE STONE

Lecce stone is widely used in the Baroque architecture of southern Italy. It is warm and golden in color, fine-grained and generally homogeneous in texture. Being soft and malleable, it was the perfect material for the expression of sculptors and stonemasons.[4] The streets of the old city of Lecce and the entire Salento region also have noble palaces and

churches from the Middle Ages and Renaissance period built and decorated with this stone. Up until today, it is still being used to create sculptures and artisan objects. [33,34]

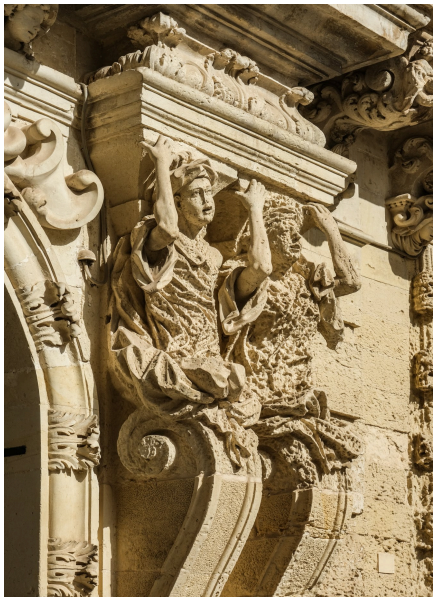

Figure 2. Image of Cariatidi di Palazzo di Marrese made of Lecce Stone.

Lecce stone is Miocenic in age and found in the Salento region. This region is characterized by a Cretaceous base, composed of pure and dolomitic limestones, with calcareous sediments from the Quaternary period at the outcrop. Due to its availability and accessibility, it has been used for centuries. Stone supply has been guaranteed by the open-pit quarries and underground quarries although there are some variations. In the main extraction point in the city of Lecce, the variety was more durable and well-suited as building material compared to the soft, hygroscopic, heterogeneous ones from other towns.[33,34]

In terms of petrography, Lecce stone is considered a wackestone, a mud-supported carbonate rock that contains 10% grains within the very-fine-sand grade. It is mainly composed of calcareous microfossils and bioclasts, with glauconite and phosphate nodules as the fillers in cavities. Microcrystalline calcite, which functions as the cementing agent, is dispersed in the matrix only in relatively small amounts. This makes Lecce stone densely packed but poorly cemented.[4] In terms of mineralogy, its main component is calcite with low magnesium content. It also contains clay minerals such as illite, kaolinite, smectite, and chlorite ranging from 3 to 14%. Silicate minerals like quartz, feldspars, micas, and pyroxenes are found in even smaller fractions.[4] Owing to its composition, the porosity and water absorption is generally high. This subsequently affects its mechanical performance as seen in compressive and flexural strength lowering.[4]

1.1.3 LITHOTYPE C: TRAVERTINE

Travertine is often used as a building material and decorative polished stone. It is characterized by pitted holes and troughs in the surface but it can easily be polished to a shiny finish. It lacks planes of weakness resulting in high compression strength. It also has high porosity which makes it light in weight and good workability.[35] The Romans mined deposits of travertine for building temples, aqueducts, monuments, bath complexes, and amphitheaters.[35] It remains popular in modern architecture and is one of several natural stones used for paving patios and garden paths. It is also used for flooring, ceilings, facades, and

wall cladding. In Italy, the well-known travertine quarries are found in Tivoli and Guidonia Montecelio. However, there are also a hundred other locations including Rapalino near Pisa.[35]

Figure 3. Image of Colosseo, also known as Anfiteatro di Flaviano, using Travertine in its structure.

Travertine is a dense, finely crystalline, concrete limestone with a white to cream color. It has a fibrous or concentric structure with distinct splinters due to the rapid chemical precipitation of calcium carbonate around geothermal seepages, springs, and streams. Bacteria, algae, bryophytes, and reeds are frequently encrusted with travertine and their photosynthetic activity further enhances calcium carbonate precipitation.[29,35]

The formation process begins when groundwater rich in carbon dioxide comes in contact with limestone. The dissolved carbon dioxide acts as a weak acid and dissolves the limestone to form calcium bicarbonate. When the concentration of calcium bicarbonate increases, the equilibrium is disrupted, and calcium bicarbonate reacts with calcium ions to form calcium carbonate. An alternative process involves the reaction between groundwater rich in carbon dioxide and alkaline surface water. Hydroxyl ions react with bicarbonate ions to form carbonate ions, which then form insoluble precipitates with available calcium ions. The repetition of these processes lead to the formation of thick deposits of travertine. Other minerals, such as iron oxide, can be incorporated in travertine which imparts a range of shades from ivory to beige.[29,35]

1.2 DEGRADATION ISSUES OF STONES

Although stones can be considered one of the most stable materials used in buildings, monuments, and sculptures, it is well-known that they are threatened by various degradation phenomena. The processes involved are complex but can be attributed to the interconnected action of physical, chemical, mechanical, and biological factors simultaneously over prolonged periods of time.[2,3] Stone degradation is primarily due to natural causes, but it is important to emphasize that anthropogenic contribution can change, and even accelerate, the degradation process.[2,3,36]

The extent of damage is influenced by the intrinsic properties of the stone, such as its chemico-mineralogical composition and anisotropic fabric, along with environmental parameters, such as climatic and atmospheric conditions.[2,3] To expound, low-porosity

magmatic rocks containing quartz and siliceous minerals are usually more resistant to degradation compared to medium-to-high-porosity sedimentary rocks based on carbonate minerals.[2,3] Meanwhile, the conduciveness or harshness of the environment in which the stone is situated dictates the type of degradation it will be subjected to.[2,3]

Physical weathering refers to the disaggregation of stone caused by freeze-thaw cycles, thermal wet-dry cycles, and salts.[37] Variations in temperature result in the expansion and contraction of the stone and, in addition, water enters through cracks and pores then expands upon freezing.[37] Salt migration and crystallization in the pores of the stone can also produce mechanical stress, instigate osmotic swelling of clays, and alter the breathability of the stone fabric.[6,37] These processes also result in the progressive fragmentation of the stone along preferred anisotropic surfaces, including intra- and intercrystalline microcracks, cleavage planes, twin lamella, and joints.[6,37]

Meanwhile, chemical weathering is the result of reactions induced on the mineral constituents of the stone by water, carbon dioxide, or oxygen. The chemical changes take place at the molecular level and pore walls, fracture surfaces, and grain boundaries provide the sites for these reactions to occur.[38] A common example is carbonation, where carbon dioxide combines with water to form carbonic acid which is strong enough to dissolve the stone. When the carbonic acid seeps through underground, it can open up huge cracks and hollow out a significant portion of the stone.[31,38] Another example is the formation of rust when iron-containing minerals undergo oxidation, which breaks apart the rock as it goes contraction and expansion.[38,39]

Regardless of the type of weathering, the role of water cannot be understated. Together with the wind, water can exert mechanical force resulting in the erosion of stone and its features. Water can also display its ability as a chemical solvent or hydrolysis agent, dissolving substances present in the stone and depositing them somewhere else.[38,40] This can be observed in many historic buildings in urban areas, where the stone's decorative and architectural elements (e.g. columns, capitals, pinnacles, and spires) exposed to rainfall experience deformation and undergo irreversible reactions.[36,40]

There are also more contemporary degradation issues rooted in the interaction of stone with other materials in contact with it, such as mortars used for masonry or rendering, ceramic tiles used for roofing, metallic artifacts for structural and ornamental purposes, and polymers previously applied in conservation efforts.[36]

The research will focus on two main issues. The first issue arises when metal and stone are frequently combined or put into contact for decorative and structural purposes. Some cases include bronze monuments which stand on stone pedestals, copper-based bars and pins used to reinforce or stabilize fractured stones, and iron alloys used for the anatylosis of archaeological ruins.[12,13,41] The second issue is concerned with the aging and photo-oxidative degradation of polymers caused by UV radiation and the synergistic effects of temperature, moisture, and pollutants.[14,17,42] In the following section, these issues will be discussed in further detail to identify key points crucial in the development of an effective cleaning method to address them.

1.2.1 FORMATION OF BRONZE CORROSION PRODUCTS ON STONE SURFACES

Upon exposure to outdoor environments, metals tend to corrode due to their physio-chemical properties, sometimes even at accelerated rates.[11,43,44] The corrosion products can be washed away by rainwater or condensed water vapor, absorbed by the porous stones into its capillary network, and then deposited in subsurface volume giving rise to staining.[45] Copper products impart a green or bluish colors, iron products gives the well-known rusty color, and lead oxides result in red or black stains.[11] The co-presence of different metals can cause the formation of mixed compounds with unusual colors.[11,43] The concentration of the corrosion products generally decreases from the core going to the surface.[11,13] The extent of staining depends on several factors including stone porosity, metal composition, amount, frequency and pH of rain events, but generally the spread increases with time. While the damage often does not result in significant pressure, cracking, or pulverization of stone, the chromatic discontinuity deprives the stone of its aesthetic value.[11,13,16]

The problem begins with metal corrosion, the natural process of deterioration of metals and their alloys as they interact with the surrounding environment, usually in the presence of water or air. As the solid metal oxidizes by losing electrons, other substances are reduced by gaining electrons. During the reaction, the metal transforms into cations that proceed to form either dissolved species or solid corrosion products.[43]

For archaeological materials, the corrosion layer could either be destructive (vile patina)[x] or protective (noble patina).[46,47] Whether it was one or the other is a function of endogenous and exogenous factors. Examples of endogenous factors include alloy composition, production technology, and metallurgical form and features. Meanwhile, exogenous factors include acidity or alkalinity, oxygen levels, humidity, temperature, and microorganisms to which the material is exposed.[11] Sometimes, the formation of a corrosion patina is intentional (artistic patina), meaning actions were deliberately taken in order to produce a compound on the

surface for a stylistic or pragmatic purpose. The layer could have varying composition, color, and thickness. In most cases, the artist produced a coating to cover defects and junctions or to create a desired chromatic effect.[47]

A corrosion patina acts as an interface between the metal substrate and the external environment. The stability and reactivity of the patina with the environment can strongly modify the aging of the archaeological material.[11] For example, a statue made to remain indoors usually has a weaker patina because, in its original location, it is submitted to a less aggressive environment, while outdoor statues have a more resistant patina.[11,47]

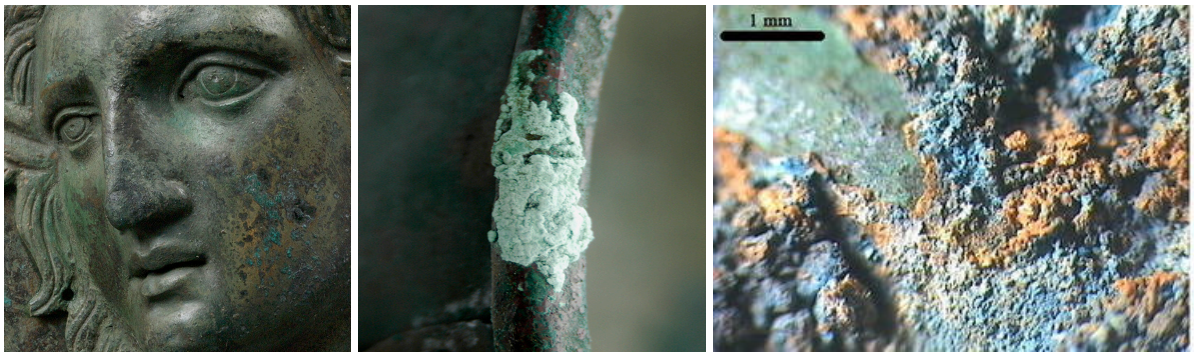

Figure 4. Corrosion of bronze materials seen at different magnifications (1x, 10x, and 40x) to highlight patina formation.

One of the most prevalent metal alloys used since ancient times is bronze. It is a copper-based alloy with tin, zinc, and lead. It can also contain trace amounts of other metals, such as aluminum, manganese, phosphorus, and silicon. For this kind of material, usually protective patinas spontaneously form.[11]

The fundamental chemistry behind bronze corrosion processes has been thoroughly studied.[11,43] In moist ambient temperature air, copper undergoes a reduction-oxidation reaction with oxygen to form a layer of cuprite (Cu_2O). This can be seen as a powdery red or dark compact layer. The rate of the reaction varies according to temperature and relative humidity. Although the initial corrosion rate might be rapid, as the cuprous oxide forms a passivation layer over the metal and shields it, the final corrosion rate is much slower. The rate is determined by the diffusion of copper through the formed oxide layer. The copper (I) oxide can be further oxidized to form copper (II) compounds which are characteristically blue-green in color. [11,43]

$$\tfrac{1}{2}\ O_2 + 2e^- \rightarrow O^{2-} \text{(reduction; cathodic process)} \qquad \text{Rxn 7a}$$

$$2Cu \rightarrow 2Cu^+ + 2e^- \text{ (oxidation; anodic process)} \qquad \text{Rxn 7b}$$

$$2Cu + \tfrac{1}{2}\ O_2 \rightarrow Cu_2O \text{ (overall reaction)} \qquad \text{Rxn 7c}$$

In many cases, the presence of other ions can extensively affect the inertness of the patina. Chloride ions can cause localized formation of copper chlorides, rendering the material susceptible to ionic diffusion and electronic migration. Chloride ions can penetrate the otherwise protective film of Cu_2O and react with the underlying metal to form nantokite (CuCl).[48,49] This so-called "bronze disease" is a form of pitting corrosion where the inner region is actively dissolving under the Cu_2O film and the corrosion products are continuously deposited in a mound above the Cu_2O film. Hence, the Cu_2O film functions as a bipolar electrode with oxidation and reduction reactions occurring on opposite sides. Consequently, there is a concentration gradient of copper ions between the pit bottom and mound top. In the presence of high concentrations of chloride ions, CuCl can further react to form a series of soluble complexes such as $CuCl_2^-$ and $CuCl_3^{2-}$. These complexes then react with available hydroxide ions to produce copper hydroxychloride minerals. [11,43]

$$Cu^+ + Cl^- \rightarrow CuCl \qquad \text{Rxn 8}$$

$$2CuCl + H_2O \rightarrow Cu_2O + 2HCl \qquad \text{Rxn 9}$$

$$4CuCl + 4H_2O + O_2 \rightarrow 2Cu_2(OH)_3Cl + 2HCl \qquad \text{Rxn 10}$$

It is also essential to look into sulfate ions and their interaction with the corrosion patina. Acid rain, which has become more prevalent in recent years, is the primary source of sulfate ions that react with bronze. Large amounts of sulfur dioxide (SO_2) are released into the atmosphere by natural sources and by the burning of fossil fuels. This gas dissolves in rainwater to give sulfurous acid (H_2SO_3), which is oxidized by oxygen to form sulfuric acid (H_2SO_4).[40,48,49]

$$SO_2\,(g) + H_2O\,(l) \rightarrow H_2SO_3\,(aq) \qquad \text{Rxn 10}$$

$$2H_2SO_3\,(aq) + O_2\,(g) \rightarrow 2H_2SO_4\,(aq) \qquad \text{Rxn 11}$$

Low-pH rainwater elicits the dissolution of the patina on an exposed bronze, leading to streaking and disfigurement.[40] Corrosion crusts of bronze readily produce acidified copper sulfate ($CuSO_4$) solutions, thereby influencing Cu_2O growth. Since it is an equilibrium reaction, increase in sulfuric acid concentration stifles the growth of cuprite and favors the formation of copper sulfates instead. Similar to the chloride complexes, copper sulfate reacts with available hydroxide ions to form copper (II) compounds. Most reaction models for the mineralization of copper hydroxysulfates suggest that the aqueous-phase reactions occur throughout the corrosion crust. In some other cases, however, the outer sulfate crust can supply ions to the aqueous front and then serve as sites for solidification as the aqueous phase evaporates. [40,48,49]

$$Cu_2O + H_2SO_4 \rightleftharpoons Cu + CuSO_4 + 2H^+ + ½\ O_2 \quad \text{Rxn 11}$$

$$4Cu^{2+} + SO_4^{2-}\ 6OH^- \rightleftharpoons Cu_4(OH)_6(SO_4) \quad \text{Rxn 12}$$

While the identity of the corrosion products can vary from one case to another, several studies demonstrate that copper hydroxychloride and copper hydroxysulfate compounds comprise the majority of products that leach from the corroded bronze metal and reprecipitate or recrystallize within the porous stone matrix.[16,48,50]

Table II. Common corrosion products found in bronze patinas, their crystallography, and their characteristics.[11,16]

Mineral	Chemical Formula	Crystal System	Color	Luster
Atacamite	$Cu_2(OH)_3Cl$	Varies	Bright green, dark emerald green to blackish green	Adamantine, Vitreous
Botallackite	$Cu_2(OH)_3Cl$	Monoclinic	Mountain green, bluish green to green	Vitreous
Antlerite	$Cu_3(SO_4)(OH)_4$	Orthorhombic	Emerald green to blackish green	Vitreous
Brochantite	$Cu_4(SO_4)(OH)_6$	Monoclinic	Green, emerald green, blackish green, light green	Vitreous, Pearly
Cuprite	Cu_2O	Isometric	Dark red to cochineal red, sometimes almost black	Adamantine, Sub-Metallic, Earthy
Posnjakite	$Cu_4(SO_4)(OH)_6 \cdot H_2O$	Monoclinic	Sky blue to dark blue, may be slightly greenish blue	Vitreous

The mechanism of surface staining involves the dissolution of the patina by rainwater, which transports soluble ions through vincinal porous stone, and the reprecipitation or recrystallization of the corrosion products from bulk to surface.[12,13,16,51] The first part, which is sometimes called the runoff process, proceeds simultaneously but independently of the corrosion process in the metal. Runoff rate is mainly a function of rain duration time, but it is 10 to 25 times higher for green-patinated layers than brown-patinated layers since they have a higher wetting capacity and water absorption.[52] For the second part, the product-rich solution penetrates into the pores of the stone in specific thermodynamic conditions then proceeds to reprecipitation or recrystallization.[52] Different corrosion products deposit on the surface depending on their solubility constant (K_{sp}) and other physico-chemical parameters such as

ionic strength, pH, and temperature.[13,53] The damage depends on the shape, supersaturation, pore size, and the repulsion between the corrosion products and the pore walls. Porosity therefore represents a crucial parameter in the degradation since it regulates runoff mobility. The pressure exerted by the corrosion products is directly proportional to the product concentration and inversely proportional to the pore radius.[52,54] There is also a correlation between the degradation and the textural features of the stone. Sparitic calcareous matrices offer greater resistance to reprecipitation or recrystallization. [52]

Figure 5. Digital images of copper staining on stone including The Thinker by Rodin, Student Statue in the Sapienza University of Rome, and a stone piece in the Museum of Modern Art in Aalborg, Denmark.[13,45,51]

1.2.2 AGING OF PARALOID® B72

There are several causes for stone degradation, but rain has the most extensive effect because it acts as a solvent of the binding medium and as a carrier of environmental pollutants.[55] Synthetic polymeric materials which exhibit water repellency, breathability, and stability have therefore been used as protective coatings for stone.[56]

It is essential that these materials do not degrade and introduce complications over time. Comprehensive studies have been done to elucidate the molecular changes that happen after prolonged exposure to light, heat, moisture, air, and harsh atmospheric conditions.[57,58] Unfortunately, studies show that many polymeric materials used in the protection of cultural heritage suffer from irreversible alterations over time.[14,15,17]

The most basic and prevalent degradation mechanism for polymers is photolysis, wherein long chains break into shorter ones through the attack of high-energy photons on the

molecular backbone. The reduction in weight results in changes in the mechanical properties of the polymer as well as alterations in color (e.g. fading and yellowing) and texture (e.g. crazing, corrugation, and protraction).[59–61] Photolysis can also release highly reactive radicals, which react with other available bonds or with available oxygen and water. The instigated oxidation results in embrittlement and chalking, sometimes even mechanical failure. With increased oxygen uptake, oxidation also leads to formation of volatiles, peroxides, and new functional groups such as carbonyls.[60] Polymer degradation can also be worsened by fluctuating temperatures. Upon heating and cooling, polymers experience distinct phase transitions when passing through specific temperatures, which induce changes to their specific volume, mechanical properties, and physical behavior. Elevated temperatures can also accelerate the kinetics of reactions that are already underway.[14,15,62]

Perhaps, the most pressing issue that arises is the partial or total insolubilization of the degraded polymers making complete removal difficult and overall counterproductive to the goal of stone conservation.[14,15] The decreased porosity and permeability of stone causes the nucleation and growth of salts at the interface between the polymer layer and the stone surface, leading to the flaking and disaggregation of the stone surface layers and the disruption of the polymer coating.[60]

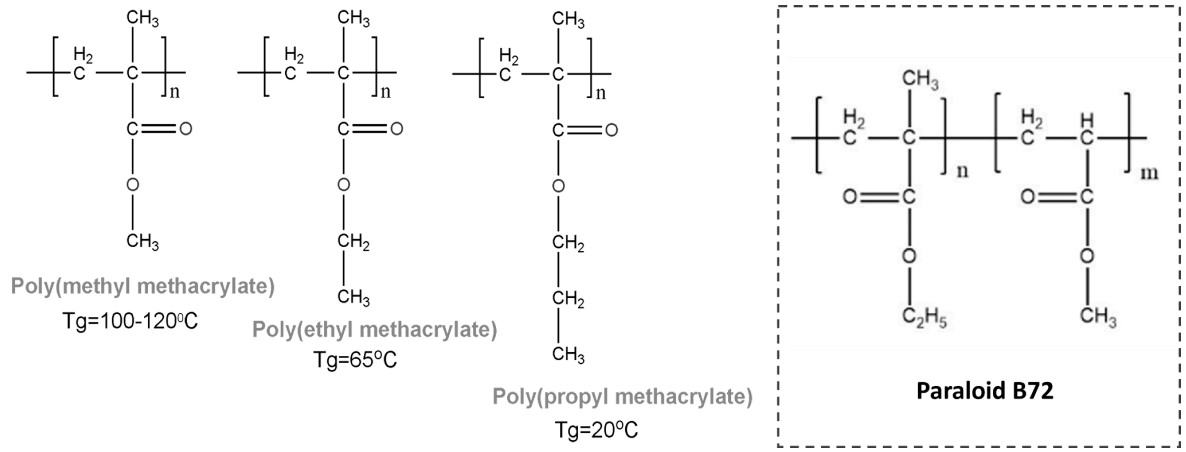

Figure 6. Chemical structure of acrylate polymers commonly used as protective coatings and the copolymer making up the commercial product Paraloid® B72.

Altogether, these pose a problem with acrylic and methacrylic ester polymers which have been used for stone facades of churches and buildings, monuments, and pedestals due to their well-suited mechanical properties, optical clarity, and overall stability.[36]

For aged poly(methyl methacrylate) (PMMA), there was extensive chain scission and cross-linking accompanied by the evolution of volatile materials such as methanol, carbon dioxide, carbon monoxide, methyl formate, methane, and hydrogen gas. Yellowing was also observed due to the formation of conjugated by-products.[17] Investigations reveal that, under ultraviolet irradiation, methyl groups in the α-position and alkoxy groups in esters

significantly accelerate degradation. For other methacrylic-based materials, the rate of degradation is even higher attributing to the presence of unstable bulky ester groups. In the the case of aging through artificial solar light irradiation ($\lambda > 295$ nm), the initial degradation seems to be related to the presence of chromophores in the material. The latter oxidation reactions are favored by the presence of labile hydrogen atoms located on the tertiary carbon of the ester side groups. [14,15]

For copolymers of acrylic and methacrylic esters, the degradation process is a bit more complex. Under the same aging conditions, acrylate units are more reactive towards oxidation relative to methacrylate units. For both monomeric chain scission prevails when the ester group is small but fast and extensive cross-linking happens when the ester group has bulkier butyl group.[14,15]

Paraloid® B72 is a 70:30 copolymer of ethyl methacrylate and methyl acrylate. It comes in clear little pellets which can be dissolved in a variety of organic solvents such as acetone, ethanol, dimethyl formamide, and methylene chloride. Based on studies, Paraloid B72 only exhibits gradual development of chain scission and cross-linking. Relative to other products, it showed good stability against oxidation reactions. [14,15,42]

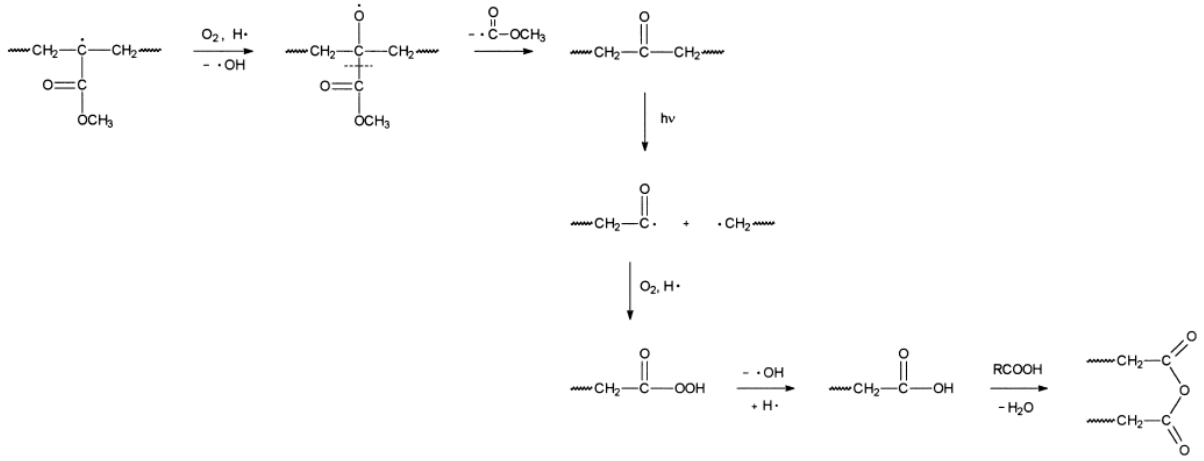

Figure 7. Degradation mechanism of Paraloid® B72 during thermal photo-oxidation weathering.[14,15,62]

Mixtures of acrylic polymers and silicone have also been used as coatings since the early seventies of the last century. They were initially applied to sandstones but were eventually to limestones and marbles. One particular mixture is called Bologna Cocktail (BC), composed of commercial Paraloid® B72 and Dri-Film® 104. It was widely agreed to have suitable penetration depth, good stability against photo-oxidative degradation, and resistance to acid action. [14,15] In a study, it was subjected to artificial weathering on marble substrates through a combined exposure to UV/Vis light exposure and saline solution. Molecular modifications have been identified for the two components in relation to their application method. The photo-oxidative degradation is enhanced when the mixture is applied as a thin film but

limited when applied as a thick coating. The difference in behavior is hypothesized to be due to the low penetration of oxygen into the bulk, confining the photo-oxidative reactions to the external polymeric surface.[14,15]

The photo-oxidative degradation of the acrylic component of BC is similar to Paraloid B72. Chain scissions and cross-linking predominate, with the formation of intramolecular and terminal double bonds and oxidized species such as γ-lactones. However, the overall removability of BC is lower than Paraloid® B72. This appears to be due to the cross-linked silicone network which entraps the acrylic polymer chains with higher molecular weight but allows for the solubilization of the acrylic polymer chains with lower molecular weight. On the other hand, Dri-Film 104 was no longer detectable. The hydrolytic breakage of the silicon-oxygen bonds and subsequent solubilization of the silicon-based substances.[14,15]

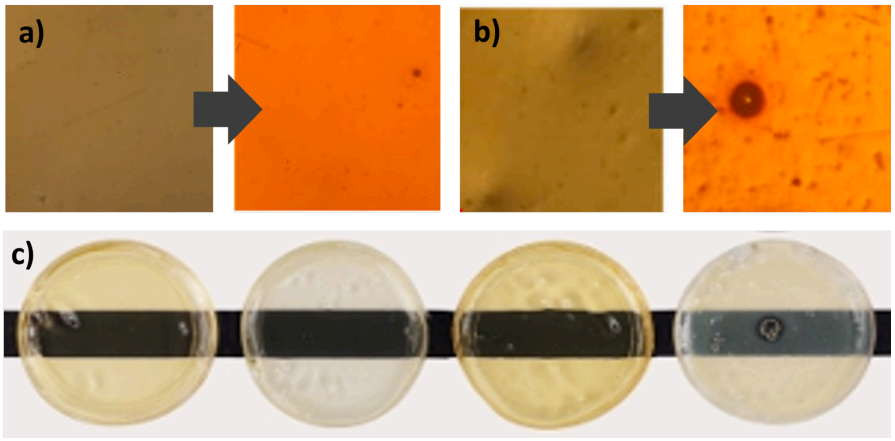

Figure 8. Changes in color and surface morphology after accelerated photo-oxidative aging of (a) epoxy, (b) vinyl epoxy, and (c) acrylic resins.[17,42]

1.3 CLEANING CONSIDERATIONS AND PROPOSED SOLUTION

Cleaning is the process of removing undesired substances (e.g. dirt, remnants of catastrophic events, harmful interventions, degraded components) from the surface of cultural heritage materials. It is complex and challenging due to the many considerations that come into its everyday practice. The cleaning process should also be cost-effective, environmentally friendly, and safe for the conservators. From a scientific perspective, the conundrum lies in the removal (i.e., solubilization, swelling, adsorption) of the target substances without affecting the other components present. The operation must be controlled, selective, and sensitive. Several cleaning approaches have been used over time but there is constant search for safe, innovative, and more effective ways.[18,19]

1.3.1 GENERAL CLEANING METHODOLOGIES FOR STONES

The methods currently employed in the cleaning of stone can be classified into water-based, chemical, and physico-mechanical methods. Water softens and carries away dirt and dissolves

soluble contaminants such as gypsum and salt. Chemicals can react with surface impurities, paints, or consolidants to convert them into water-soluble forms. Organic solvents can also be used to dissolve lipophilic substances contained in darkened layers. Physico-mechanical methods include the use of grinders, sanding discs, sandblasters, and engraving tools to manually remove undesired substances.[18,19,57]

Expounding on each classification, water-based methods are generally safe for removing dirt in stone when the application conditions are regulated. The soaking of surfaces with spraying or misting water can remove sulfated crusts and soot, but can also damage patinas, polychromies, and the stone itself which are sensitive to prolonged moisture. To facilitate the cleaning process, non-ionic detergents or surfactants are preferred, in combination with gentle scrubbing with a natural bristle. In cases of acid-sensitive surfaces, such as carbonate-based stones, steam cleaning can be done to provide extended wetting with a large specific area. However, it is essential to note that there is always a risk of water penetration from the surface to the interior. This can result in staining, efflorescence, sugaring, exfoliation, and biogenic growth. [57,63]

Different kinds of chemicals have been used in the removal of discolorations in stone (e.g. stains from metal, flora, fauna, paints, coatings, and graffiti). Acidic compounds are prohibited for cleaning calcareous stones due to the extreme reactivity of calcite in acids. Acids are also not recommended for silica-rich surfaces and acid-resistant minerals due to their oxidizing power. Meanwhile, alkaline compounds are recommended for calcareous stones, along with non-ionic surfactants which facilitate the dissolution of the undesired substances. For the removal of organic matter, alkaline compounds containing strong hydroxides and phosphates are combined together with organic solvents. While effective, chemical cleaning can be hazardous to the lithic substrate, the operators, and the environment, thereby eliciting a stricter protocol during interventions.[57,63]

Similar to water-based methods, there remains an issue of penetration when it comes to chemical methods. To circumnavigate this, absorbent poultices such as clay minerals and cellulose have been employed. Poultices containing EDTA and AC as active ingredients have been used to remove black crusts. Ion-exchange resins containing carbonate and hydroxide ions have also been utilized to reform calcium carbonate and calcium hydroxide from gypsum layers. In practice, conservators often use Japanese paper between the stone and poultice to avoid leaving residues. [57,63]

Physico-mechanical methods rely on contact and the force applied using handheld tools or heavy equipment to erode dirt and undesired substances. The pressure exerted and the nature

of the particles used affects the impact. Coarser particles result in surface etching, surface rounding, and subsurface cracking. Finely ground silica, nut shells, glass beads, and pelletized dry ice are often employed. If the stone is made of softer material, then disaggregation might happen. Overall, the uncontrollability of physico-mechanical methods are strayed from unless there are no other viable alternatives.[57,63]

1.3.1 GELS AND HIGH VISCOSITY POLYMERIC DISPERSIONS

The limitations associated with the traditional cleaning methods paved the way for the development of new materials for cleaning. In the 1980s, gels were introduced as a new carrier material for solvent systems to deliver them to the substrate in a controlled and selective manner.[18,64,65] Gels seemed promising because they released the liquid phase, whether aqueous or organic, slowly and limited to the interface of the gel and the substrate. The confinement of the solvents into the three-dimensional network of the gel also reduced evaporation rate and this enhanced liquid phase retention allows longer application times relative to poultices. This is especially crucial for organic solvents which are often volatile and toxic.[18]

When discussing gels, it is important to establish a definition for it. However, due to its characteristic variability and numerous applications in different fields, narrowing it to one remains difficult. Presently, the International Union of Pure and Applied Chemistry (IUPAC), defines a gel as a "non-fluid colloidal network or polymer network that is expanded throughout its whole volume by a fluid", imparting it with properties in between those of a solid and a liquid. In the conservation field, the emphasis is on the use of two components, the gelator and the fluid, and their ability to maintain form under the stress of their own weight and to undergo strain when subjected to any mechanical stress. Almdal also provided a rheologic criterion to determine whether the soft matter can be described as a gel or not. According to him, real gels display a plateau in the storage modulus G′(ω), which is higher than the loss modulus G"(ω) over a wide range of frequencies. Hence, those which exhibit a plateau in G′(ω) but has G′(ω) less than G"(ω), are not real gels. Other polymer-solvent mixtures characterized by a high elastic modulus, fall under other gel-like materials, with G′(ω) and G″(ω) parallel throughout the entire frequency range.[18,20]

There are also different classifications of gels. Gels can be classified according to the source of the gelator (natural or synthetic), its composition (homopolymer, copolymer, interpenetrating network), and its cross-linking mechanism (chemical or physical). Gels can also be classified according to its fluid (organic solvent or water). In the conservation field, gels are generally classified as either thickeners, rigid gels, and peelable gels. While most

materials used in the field cannot be considered gels from a rheological point of view, they are conventionally called as such.[64,66]

The classification of the gel has practical consequences on its application. Chemical gels require 200 to 650 kJ mol^{-1} of energy, while physical gels only need approximately 1 to 120 kJ mol^{-1}. Chemical gels are therefore irreversible while physical gels are thermoreversible or, in other words, can undergo sol-gel transition through variation of temperature. In terms of cleaning mechanisms, there is also a difference due to the cohesion forces (between the gel components) and the adhesion forces (between the gel and sample surface). Since chemical gels are often solids with strong cohesion forces, they ensure a residue-free treatment. Physical gels are flexible and have optimal contact with the surface to be treated. However, they are relatively prone to leaving residues which may require an additional step of removal.[64,66]

The gel's suitability for removing a material is also affected by its type. Organogels consist of a hydrophobic polymer network holding organic solvents, making them useful for removing non-polar materials (e.g. consolidants, coatings, and varnishes).[x] Meanwhile, hydrogels consist of a network of hydrophilic polymers holding mainly water, sometimes with water-miscible solvents and water-soluble compounds, making them useful for removing polar materials (e.g. deposits, dirt, salts). [64,66]

For cleaning, the most well-known thickeners are cellulose derivatives (e.g. Tylose® , Klucel®, and Carbopol®). These polymers are first dispersed in a fluid to form a paste then applied to the surface.[18] One commonly used thickener contains polyacrylic acid polymers dissolved in basic aqueous solutions. The alkalinity converts the carboxylic acid to carboxylates, resulting in the unfolding of the polymer chains and formation of a three-dimensional structure. With the aid of surfactants, organic solvents and enzymes can be added to the gel. The drawback of these materials is that their weak cohesion forces result in residues on the surface after the treatment.[18,65] Meanwhile, rigid gels are made of natural polysaccharides (e.g. agar, agarose, and gellan gum) dispersed in water. They are thermo-reversible, have good shape stability, and have high retention of water. Rigid gels can be applied in two ways. In the first method, the gel is delivered through a heated syringe in the semi-solid phase to facilitate application in specific and well-confined areas. In the second method, the polymer dispersed in the fluid is sprayed for the application in larger areas. The limitation is the damage it causes to sensitive substrates due to the mechanical action involved in their use. [18,65] Lastly, peelable gels (e.g. partially hydrolyzed polyvinyl acetate/borax and polyvinyl alcohol/borax) can be applied to surfaces with rough and

irregular structures. They maintain high elasticity which allows them to be easily removed from the surface by means of tweezers.[24,64,66]

1.3.2 IN FOCUS: AGAROSE GELS AND POLYVINYL ALCOHOL/BORAX HVPDS

Agarose gels are widely used in the cleaning of works of art.[67] Agarose is a non-ionic polysaccharide of high molecular weight. It is extracted from red marine seaweeds and is composed of ß-1,3-linked-D-galactose and α-1,4-linked 3,6-anhydro-L-galactose.[x] Agarose undergoes thermoreversible gelation. When heated in water above 85 °C, random coils form. When cooled, the random coils transform into single and double helices which then form a network. Each single chain has a left-handed three-fold helix symmetry. Meanwhile, the two chains in the double helix are bound by a translation along the helix axis. The double helix forms an interior cavity which extends along the length of the axis, similar to but of smaller diameter than that of V-amylose from plastids. The interior cavity of agarose is lined with oxygen atoms available for hydrogen bonding with water molecules, thermodynamically stabilizing the structure. Meanwhile, the exterior contains protruding hydroxyl groups which also engage in hydrogen bonding with water molecules and other helices.[68]

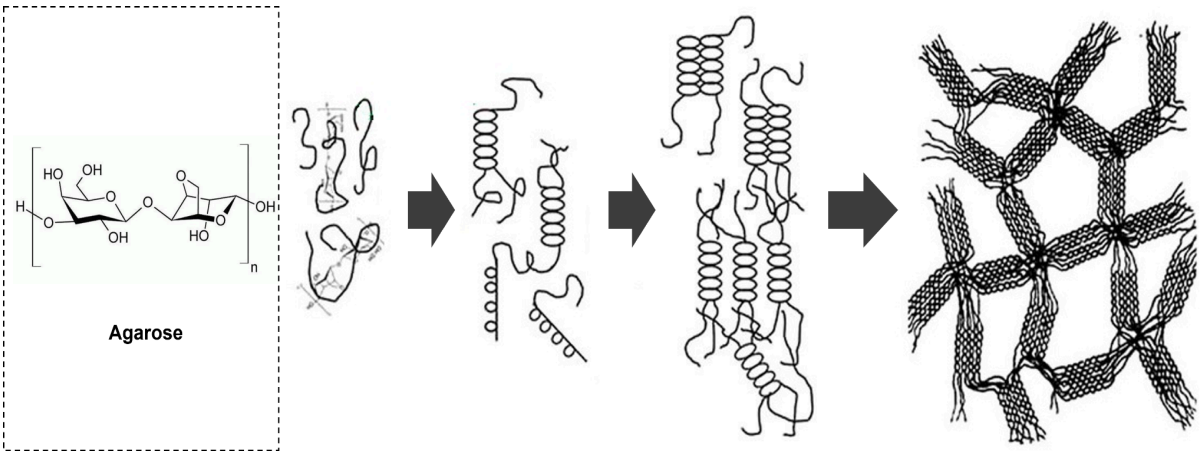

Figure 9. Structure of the natural saccharide agarose, its double helical structure, and its network formation.

Despite the advantage of being able to form inclusions with a variety of cleaning agents, agarose gels are limited by their rigidity. They cannot fit into irregular surfaces which reduces contact area and hinders them from complete cleaning.[66] HVPDs based on polyvinyl alcohol and borax (PVA/B) was then sought as an alternative. PVA is a water-soluble polymer formed from the hydrolysis of polyvinyl acetate (PVAc). The presence of atactic hydroxyl groups in the backbone allows for extensive intra- and intermolecular hydrogen bonding. As a consequence, heating is required for the dissolution of PVA in water especially when the molecular weight and the degree of hydrolysis is higher. Usually, sodium tetraborate is used as a cross-linker for PVA/B hydrogels.[24,69]

$$[CH_2CH(CH_3COO)]_x \rightarrow [CH_2CH(CH_3COO)]_y + [CH_2CH(OH)]_z \quad \text{Rxn 14}$$

$$Na_2B_4O_7.10H_2O \rightarrow 2\ B(OH)_3 + 2\ B(OH)_4^- + 2Na^+ + 3H_2O \quad \text{Rxn 15}$$

The cross-linking of PVA with borax occurs through a di-diol complexation reaction. In the first step, the tetrahydroxy borate anion reacts with a PVA chain diol to form a complex. In the second step, the other hydroxyl groups attached to the boron react with the adjacent diols. The system can also be loaded with binary or ternary solvent systems and chelants. The loadable concentration varies according to the degree of hydrolysis of the polymer, the extent of cross-linking, and the presence of other components.[23,24,69]

The PVA/B hydrogel formed is characterized by its peculiar viscoelastic behavior. From a rheological point of view, these are not real gels and only exhibit gel-like behavior. Their storage modulus G′(ω) exhibits a plateau, however, G′(ω) is less than G″(ω) in the plateau region.[x] Nonetheless, their plasticity eases their conformity to surface morphology while still being peelable with the use of tweezers. [23,24,69]

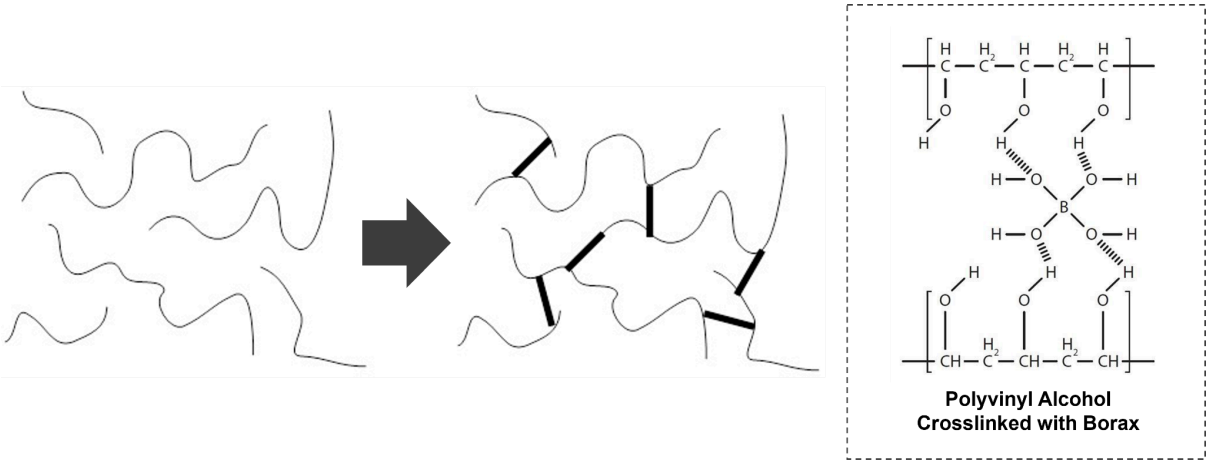

Figure 10. Chemical cross-linking of PVA chains with borax in water to form a three-dimensional structure.

1.4 RESEARCH AIMS

Several studies have proven that PVA/B-based HVPDs are effective in cleaning cultural heritage materials.[21,24,69] Their viscoelasticity allows facile application, conformity to the surface morphology of the substrate, and peeling off. They can also be loaded with other cleaning systems, such as organic solvents, surfactants, and chelants. They also have good liquid phase retention which extends contact time without drying. In addition, they are environmentally friendly and reduce the risk of toxicity for the operator. For porous substrates, however, the PVA/B-based HVPDs can leave behind residues. [21,24,69] On the other hand, agar gels have good shape stability but their rigidity has always limited their adoption to flat surfaces rather than irregular. When applied during their sol-gel phase, they can also cause damage to fragile materials.[67,70]

To offset these limitations, in this study, PVA/B-based HVPDs are tested in the cleaning of carbonate-based stones. Agarose is blended into the three-dimensional polymer network to adjust rheological properties while retaining their individual effectiveness in cleaning.[26,27,66] The research will focus on the removal of two contaminants on carbonate-based stones: metallic corrosion products and an acrylic resin insoluble when aged, namely, Paraloid® B72.

Two chelants were chosen for the removal of bronze corrosion products. The selection of the chelants is based on the criteria that they are capable of forming complexes with copper ions, they have physico- chemical inertness towards the stone, they are water-soluble, and they are compatible with both PVA/B and agarose. The first chelant is disodium ethylenediaminetetraacetic acid (EDTA) which has six oxygen- and nitrogen-containing metal-complexing sites. This enables one molecule to interact with all the reactive centers of a metal ion. This also permits a multiple number of metal-enclosing chelate rings to form which results in maximum stability.[71] Meanwhile, the second chelant is potassium sodium tartrate (PST) which is a double salt of tartaric acid. It only has carboxylic acid groups, making it more environmentally friendly than other amino-carboxylic acid chelants. Its complexation occurs through the hydroxyl groups and, similar to EDTA, forms a chelate ring to achieve metal-ligand stability.[71]

For the removal of Paraloid® B72, acetone is often added to gels or HVPD formulations.[72,73] However, for eco-compatibility, it will not be included in the formulations to be tested. This allows the determination of the effectiveness of the HVPD alone, which only has water in its liquid phase, to remove a hydrophobic substance.

To investigate the cleaning performance of PVA/B-based HVPDs in removing bronze corrosion products and Paraloid® B72 from Carrara Marble, Lecce Stone, and Travertine, a multi-technical approach will be used. The rheological properties, water holding capacity, and loss of volatile fraction will be first examined to determine the suitability of HVPDs for cleaning. Fiber optic reflectance spectroscopy (FORS) will be used to measure colorimetric changes in the stone before and after the treatment. Scanning electron microscopy - energy dispersive spectroscopy (SEM-EDS) will be used to view the morphology of the surface and the elemental composition of selected points. Finally, Fourier-transform infrared attenuated total reflectance spectroscopy (FT-IR ATR) will be used to characterize the HVPDs and elucidate their interaction with the contaminants.

2.1 MATERIALS

Polyvinyl alcohol (99+% hydrolyzed, M.W. = 89,000 - 98,000 g/mol, Sigma-Aldrich), disodium tetraborate decahydrate (pharmaceutical grade, M.W. = 381.37 g/mol, PanReac AppliChem ITW), agarose (electrophoresis grade, Euroclone S.p.A.), disodium ethylenediaminetetraacetic acid dihydrate (reagent grade, M.W. = 372.24 g/mol, PanReac AppliChem ITW), and potassium sodium tartrate tetrahydrate (reagent grade, M.W. = 282.23 g/mol, PanReac AppliChem ITW) were used as is for the preparation of the HVPDs. Copper sulfate anhydrous (pure, M.W. = 159.60 g/mol, PanReac AppliChem ITW) and bronze disks (Bronze Alloy 555, National Research Council) were used for the simulation of bronze corrosion product formation and leaching into carbonate stone. Paraloid® B72 (commercial, M.W. = 105,000 g/mol, T_g = 40 ºC) dissolved in acetone (technical grade, 99.8% purity, M.W. = 58.08 g/mol, Lab-Scan) was used for the coating of the stone block surfaces prior to aging. All three stones cut into 5 cm x 5 cm x 2 cm blocks were sourced from StilMarmi.

2.2 SUBSTRATE PREPARATION

2.2.1 ARTIFICIAL CORROSION PATINAS

To mimic real-life cases of sulfate-induced patination of bronze and the leaching of corrosion products into carbonate stone, a 17 mM $CuSO_4$ aqueous solution was brought to a boil, with the bronze disks inside, then the heat source was removed. The bronze disks were submerged at a 50 mM of $CuSO_4$ mM aqueous solution at room temperature for 15 days afterwards.

In a glass chamber, the stone blocks were then allowed to immerse for two weeks with the bronze disks to allow the penetration and distribution of corrosion products. The stone blocks were then allowed to air-dry for a week until constant weight was observed.[48]

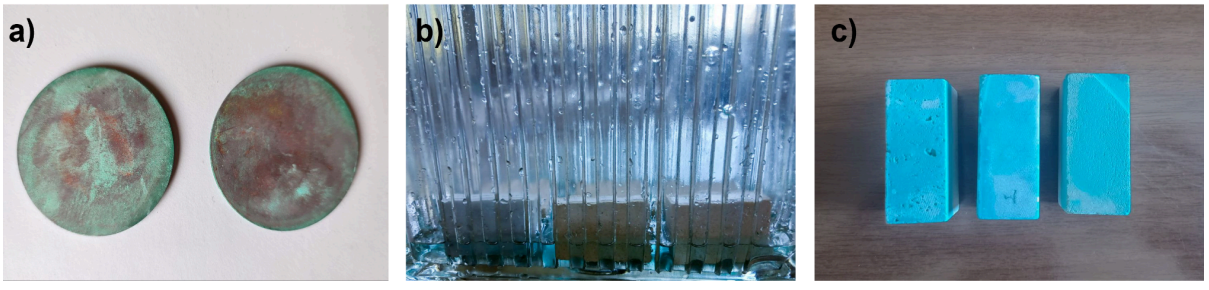

Figure 11. Photos of a) bronze disks after sulfate-induced corrosion, b) experimental setup for the immersion of stone blocks, and c) stone blocks after leaching of bronze corrosion products.

2.2.2 ARTIFICIAL ACCELERATED AGEING

A 3% w/v solution of Paraloid® B72 in acetone was applied by brushing on the stone block surfaces until a coating thickness of approximately 2 mm was achieved. The coating thickness was monitored through the gravimetric method stated in Section 5.3 of ISO 2808:2019. The formula used for the thickness calculations is shown in Equation 1, where T is thickness in µm, m is mass expressed in g, ρ is density expressed in g/cm^3, and A is area expressed in cm^2.[x]

$$T = \frac{10\,x\,m}{\rho\,x\,A} \qquad \text{Eqn. 1}$$

The QUV Accelerated Weathering Tester (Solar Eye Model, Q-Lab) was used as the aging chamber. The equipment was calibrated using a UC10/UV smart sensor using the AUTOCAL system. The coated stone blocks were then exposed to a temperature of 65 ºC in addition to light illumination (4 front and 4 rear UVA-340 lamps, 295 - 365 nm nm, irradiance 0.65 W/m^2) for 250 hours.[14,15,66]

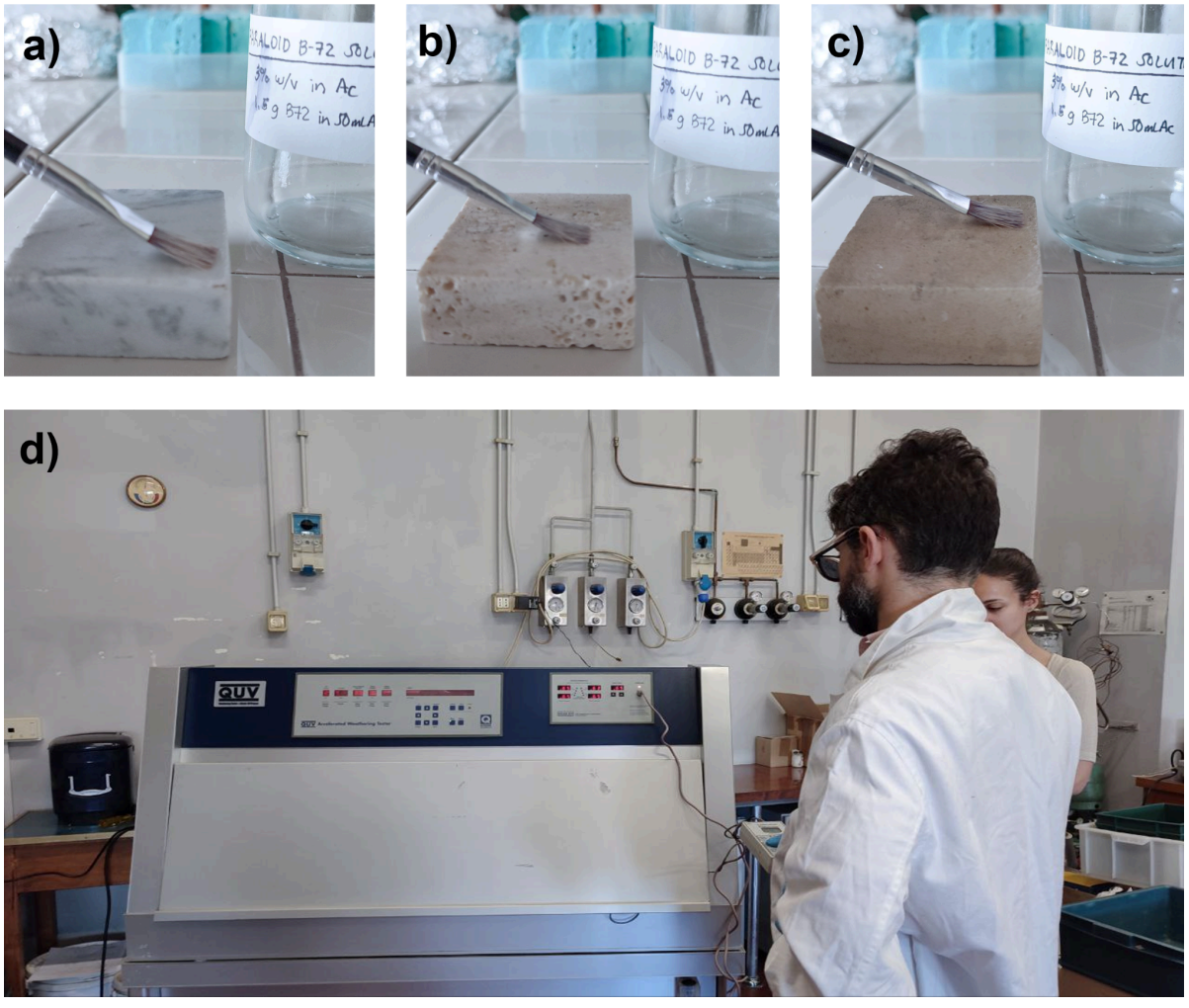

Figure 12. Photos of Paraloid® B72 coating application in a) Carrara Marble, b) Lecce Stone, c) Travertine, and d) their aging in the QUV Accelerated Weathering Tester.

2.3 HVPD SYNTHESIS AND CHARACTERIZATION

There are several criteria with which we can evaluate the suitability of the soft matter for the target applications. First, it is essential that the soft matter can be synthesized easily to make sure that it can be adopted by conservators without any difficulty. The chemicals used in the formulation should also have minimal risk for both the conservator and the environment. Second, due to the intrinsic instability of polymeric dispersions, water can be lost when subjected to external forces or temperature fluctuations. The loss of water through passive diffusion or through evaporation can lead to shrinking, change in texture, and residue formation. It is therefore practical to determine the water holding capacity and loss of volatile fraction of the soft matter. Third, tests on rheological properties allow us to determine whether the material is a gel or an HVPD and provide us with an idea of their viscoelastic behavior and peelability. Lastly, spectroscopic characterization helps deepen the understanding of the interactions between components on a molecular level.

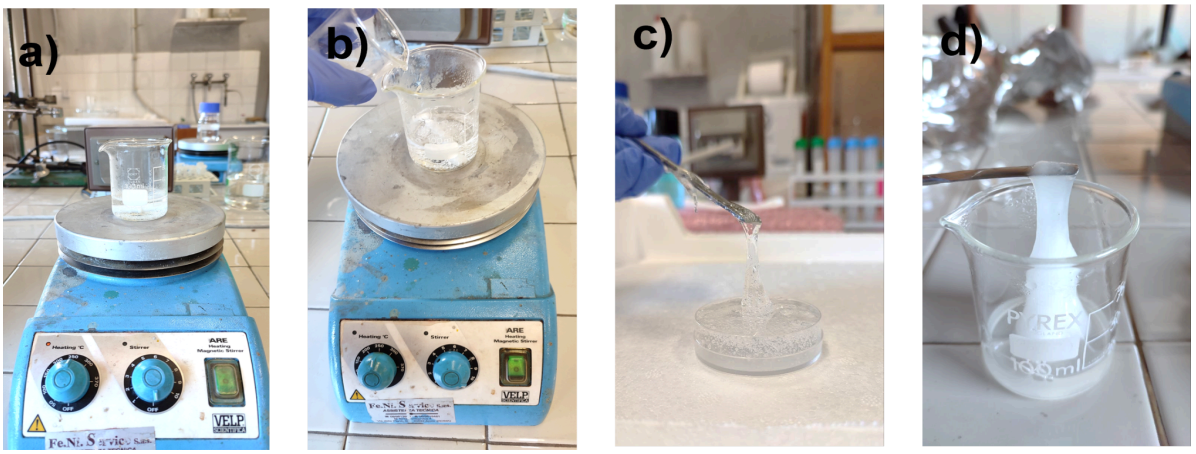

Figure 13. Preparation of HVPDs including a) dissolution of components and b) addition of borax solution for cross-linking. The product should be c) clear and viscous if made successfully, but d) white and heterogeneous if made unsuccessfully.

2.3.1 PREPARATION

Eleven HVPD formulations (PD1-PD11) were used in total, all of which follow the same preparation procedure (see Table III). PVA was first added to distilled water and dissolved at temperatures ranging from 80 to 100 ºC. A change from a white turbid color to a clear solution was observed. The chelant and agarose were then added separately and consecutively until complete dissolution. The 6% w/v borax stock solution was added last with vigorous stirring until gelation was complete. It should be noted that the borax solution had to be heated and stirred prior to each use because sodium tetraborate tends to recrystallize quickly. The prepared dispersions were then stored in polypropylene syringes (10-mL capacity) with as little air as possible to avoid evaporation and drying. The prepared

dispersions were then left in the refrigerator at approximately 5 °C until needed for characterization or application.[46,69]

No other solvents were used aside from water to keep them as environment-friendly as possible. Agarose was added at a concentration 0.5 wt.% to impart rigidity without sacrificing the dispersion's flexibility. Higher concentrations of agarose that were tested led to whitening and syneresis. Based on Boral *et al*,[74] increasing network density influences the swelling-deswelling kinetics of the bundled helices of agarose. An internal osmotic stress is created in the microenvironment resulting in the expulsion of water. Likewise, the concentration of chelants was also limited by its effect on gelation. Based on Carretti *et al*,[21] higher concentrations of chelants disrupt the hydrogen bonding in the network and change the level of alkalinity which leads to syneresis. Between the two chelants, lower concentrations of EDTA relative to PST leads to syneresis due to its bulkier molecular shape and basic functional groups.

Table III. Summary of HVPD formulations used for cleaning bronze corrosion products and Paraloid® B72 in stone blocks of Carrara Marble, Lecce Stone, and Travertine.

Code	Formulation	Composition
PD1	PVA:B = 4:1	1.00 g PVA + 7.00 g Borax solution + 17.00 g H_2O
PD2	PVA:B = 4:1 + 0.5 wt. % EDTA	1.00 g PVA + 7.00 g Borax solution + 0.13 g EDTA + 16.87 g H_2O
PD3	PVA:B = 4:1 + 1.0 wt. % EDTA	1.00 g PVA + 7.00 g Borax solution + 0.25 g EDTA + 16.75 g H_2O
PD4	PVA:B = 4:1 + 1.0 wt. % PST	1.00 g PVA + 7.00 g Borax solution + 0.25 g PST + 16.75 g H_2O
PD5	PVA:B = 4:1 + 1.5 wt. % PST	1.00 g PVA + 7.00 g Borax solution + 0.38 g PST + 16.62 g H_2O
PD6	PVA:B = 4:1 + 2.0 wt. % PST	1.00 g PVA + 7.00 g Borax solution + 0.50 g PST + 16.50 g H_2O
PD7	PVA:B = 4:1.5 + 0.5 wt. % EDTA	1.00 g PVA + 10.00 g Borax solution + 0.13 g EDTA + 13.87 g H_2O
PD8	PVA:B = 4:1.5 + 1.5 wt. % PST	1.00 g PVA + 10.00 g Borax solution + 0.38 g PST + 13.62 g H_2O
PD9	PVA:B = 4:1 + 0.5 wt. % Agarose	1.00 g PVA + 7.00 g Borax solution + 0.13 g Agarose + 16.87 g H_2O
PD10	PVA:B = 4:1 + 0.5 wt. % Agarose + 1.5 wt. % EDTA	1.00 g PVA + 7.00 g Borax solution + 0.13 g Agarose + 0.38 g EDTA + 16.49 g H_2O
PD11	PVA:B = 4:1 + 0.5 wt. % Agarose + 2.0 wt. % PST	1.00 g PVA + 7.00 g Borax solution + 0.13 g Agarose + 0.50 g PST + 16.37 g H_2O

2.3.2 LOSS OF VOLATILE FRACTION

The loss of volatile fraction was studied by means of gravimetric measurements. Small circular samples (6 mm diameter, 3 mm thickness) were put on a glass slide and left exposed at room temperature. The weight of the samples were monitored for set intervals between 30 minutes to 6 hours. After the experiment, the samples were left to dry and weighed daily until no change in weight was observed. All measurements were made in triplicate.[24]

The evaporation kinetics were expressed as volatile fraction loss versus time and the formula used for weight decrease is shown in Equation 2, where W_{VF} is volatile fraction loss in function of time, W_t is the weight in a specific time, W_w is the initial weight, and W_d is the final dry weight.[x]

$$W_{VF} = \frac{(W_t - W_d)}{(W_w - W_d)} x\ 100\% \qquad \text{Eqn. 2}$$

2.3.2 WATER HOLDING CAPACITY

Small cylindrical samples (6 mm diameter, 3 mm thickness) were put in microfuge tubes then centrifuged at 2000 rpm for 5 minutes at 20 °C. The weight of the samples were measured after a minute of standing still and water pour-out. The process was repeated for set intervals between 30 minutes to 6 hours. All measurements were made in triplicate. The weight ratio after and before centrifugation was used to characterize water holding capacity as shown in Equation 3, where W_i is the weight before and W_f is the weight after centrifugal dehydration.[75,76]

$$WHC = \frac{W_f}{W_i} x\ 100\% \qquad \text{Eqn. 3}$$

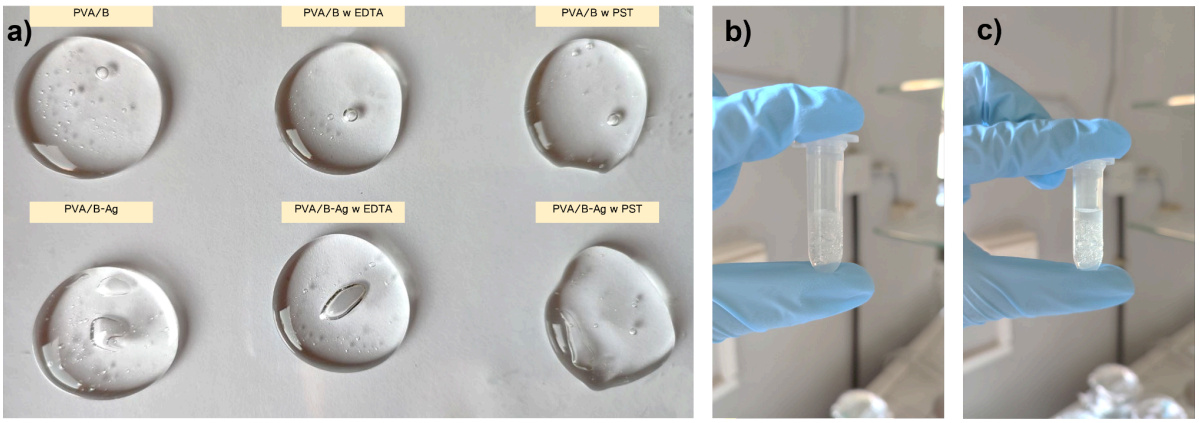

Figure 14. Photos showing a) the evaporation process of the HVPDs for the loss of volatile fraction test, as well as b) pre-centrifugation and c) post-centrifugation for the water holding capacity test.

2.3.3 RHEOLOGICAL PROPERTIES

All experiments were done using the TA Discovery HR-1 instrument and all data was processed through its accompanying TRIOS software. It was operated by Luca Paoletti and

Claudia Migliorini, with the supervision of Dr. Pietro Maricardi. The rheometer geometry used was flat-flat, knuckled, in aluminum, with a diameter of 20 mm. The gap operating speed was set to 500 μm. For sample preparation, the dispersions were left to stabilize at 25 ºC for 2 hours before transferring from the syringes in which they were supplied to the extrusion pan, avoiding excessive bubble formation. Analyses were then carried out at 25 ºC, using approximately 800 μL of sample each.

Frequency Sweep experiments were done to evaluate the rheological properties of the samples. Measurements were made over a range of oscillation frequencies at a constant oscillation amplitude and temperature. The analytical conditions were as follows: 300 seconds of static conditioning of the sample at 25 ºC, logarithmic frequency sweep at 25 ºC at 1% strain in the frequency range from 50 to 0.01 Hz, with 7 acquisition points per increment, conditioning time of 12 seconds per point and sampling time equal to 3 seconds. Below the critical level (γ_c), if the storage (G') and loss (G") moduli were independent of frequency, the material is considered solid or highly structured. However, if the two parameters were dependent on the frequency, the material is fluid-like. The experiment therefore help distinguish between real gels and high-viscosity polymeric dispersions.

The intrinsic elastic shear modulus (G'_0) and apparent relaxation time (τ_c) can also be derived from the curves. G'_0 is the average of the last three highest frequency points of G′ and this parameter describes the stiffness of the system. For PVAc-derived systems, the threshold is 400 Pa in order to have enough elasticity to be peeled off. Meanwhile, τ_c is the reciprocal of the crossover frequency point (ω_c) of the two moduli. Shifting ω_c to lower frequencies increases τ_c, reflecting better shape stability or resistance to deformation.[18,21,77,78]

Flow Sweep experiments were also performed to evaluate the dynamic viscosity of the samples. The analytical conditions were as follows: 300 seconds of static conditioning of the sample at 25 ºC, logarithmic stress sweep at 25 ºC in the range from 1 to 1 x 10^4 Pa, with 7 acquisition points per increment. The data was acquired at steady state with 180 seconds of acquisition for each point, 20 seconds of sampling, consecutiveness on 3 samplings, and 5% tolerance. Monitoring the viscosity of a material according to the rate at which it is sheared provides important information about its pseudoplasticity or dilatancy behavior.

2.3.4 CHEMICAL STRUCTURE AND INTERACTIONS

Infrared (IR) spectroscopy is generally a non-destructive technique that provides extensive information about the chemical and structural properties of different classes of materials including gels and high viscosity polymeric dispersions. Among the scientific principles involved in the use of IR spectroscopy, the vibrational activity is the most relevant one. The

IR activity of a certain fundamental vibrational mode depends on the general IR selection rule which states that the permanent dipole moment (μ) of a given functional group must have a non-zero derivative, with respect to the normal coordinate, for the equilibrium configuration of a given functional group. Thus, a vibration causes a change in the corresponding dipole moment, resulting in the absorption of IR radiation. The larger the change, the more intense the absorption will be.[79,80]

All spectra were obtained using the FT/IR-410 spectrometer and the Attenuated Total Reflectance (ATR) sampling technique. This involved pressing the samples against a high-refractive-index diamond crystal and measuring the infrared spectrum using totally internally reflected infrared light. Instrument specifications include a high-intensity ceramic light source with the range of 350 to 7800 cm^{-1}, a DLaTGS detector, and an 8000-Hz filter. Permanent optical alignment was guaranteed by the corner-cube retro-reflective mirrors with an auto-alignment feature.

The sample chamber was kept close during the measurements and the conditions were regulated using the Pure Air Circulator Unit (PACU) by Thorlabs, Inc. Three points for each sample were measured. All spectra were taken from 400 to 4000 cm^{-1}, with 32 scans, 4 mm/s scanning speed, 2 cm^{-1} resolution, and Blackman-Harris apodization. Carbon dioxide corrections, water vapor corrections, and ATR conversions were done with the instrument's built-in software. Subsequent spectra processing (e.g. background removal, averaging, baseline subtraction, normalization, and analysis) was performed using the OriginLab software.

2.4 EVALUATION OF CLEANING PERFORMANCE

There are many ways in which the cleaning performance of the HVPDs can be monitored. Preliminary tests were first conducted through the application and removal of HVPDs to narrow down the formulations which result in a significant removal of the contaminants and the conditions in which they can be used. To check whether the breathability of the stone is affected by the addition and removal of the acrylic resin, water vapor permeability is monitored. For the two issues at hand, morphological structure is helpful in visualizing the extent of damage brought about by the contaminants and whether recovery of the original surface is possible with cleaning. Monitoring colorimetric change allows the quantification of the perceptibility of the change and the removal efficiency of the cleaning method.

2.4.1 APPLICATION AND REMOVAL OF HVPDS

The stone blocks were divided into sections for testing. The dispersions were carefully spread on the surface with a spatula in the confines of the section and gently removed with tweezers or peeled off after a given amount of time. The dispersions were covered with parafilm to reduce evaporation during treatment and consequently minimize residues.

In order to determine which HVPDs were the most suitable for the intended application, different conditions were investigated. For removing bronze corrosion products from carbonate samples, dispersions with different chelant concentrations were first applied to contaminated stone blocks. The concentrations were increased at increments of 0.50 wt.% until monophasicity was no longer observed. Based on visual examination, one set was removed at 4 hours when there was already a clear difference in color while another set was removed at 6 hours when residues were clearly formed. To address the issue of residues, the extent of cross-linking was modified by increasing the amount of Borax solution added. Since their application yielded no significant colorimetric change, the alternative explored was the introduction of agarose into the formulation.

Table IV. Summary of experiments conducted to determine the most effective HVPD formulation for the cleaning of bronze corrosion products and Paraloid® B72.

Contaminant	Parameter	Variations	Stone Substrate
Bronze Corrosion Products	Treatment Period	4 hours vs. 6 hours	Travertine
	Chelant Concentration	PD2 vs. PD3 PD4 vs. PD5 vs. PD6	Travertine
	Extent of Cross-linking	PD2 vs. PD7 PD5 vs. PD8	Travertine
	Agarose Component	Presence	Carrara Marble, Lecce Stone, Travertine
Paraloid® B72	Treatment Period	2 hours vs. 24 hours	Carrara Marble, Lecce Stone, Travertine
	Agarose Component	Presence	Carrara Marble, Lecce Stone, Travertine

2.4.2 WATER VAPOR PERMEABILITY

It is crucial to monitor changes in the breathability of stone upon the application of a coating as well as its removal, which can be quantified through water vapor permeability (WVP).[x] In order to measure this, the stone blocks were fixed on a glass platform in makeshift cylindrical polyvinyl chloride containers partially filled (500 mL) with distilled water. The containers were

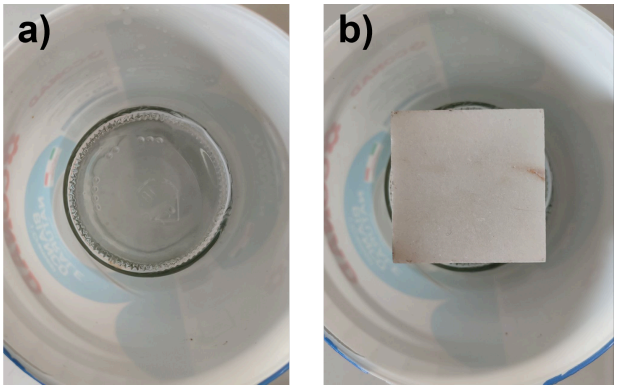

Figure 15. Photos showing the internal arrangement of the sealed container with a) the glass platform surrounded by distilled water and b) the stone placed on top with five sides exposed.

sealed and kept at room temperature. The stone weights were quickly measured at intervals of 30 mins until 6 hours on the first day, then once every 24 hours for 7 days afterwards. The measurements were taken quickly before returning the stone blocks to the sealed container in order to reduce any interference from atmospheric exposure.[x] The formula used is shown in Equation 4, where W_t is the weight at a given time, W_o is the starting weight, and A is the area of exposed surface. Percent changes of the maximum water vapor transmission in the stone were calculated against a negative control.[81,82]

$$WVP = \frac{W_t - W_o}{A} \qquad \text{Eqn. 4}$$

2.4.3 MORPHOLOGICAL STRUCTURE

Scanning electron microscopy (SEM) coupled with energy dispersive x-ray spectroscopy (EDS) is one of the most commonly used methods for understanding the microstructure and surface morphology of materials. It is possible to obtain a high resolution, high depth of field image as well as an elemental composition for a bulk material, or a particular area of that material In SEM-EDS, an electron beam with sufficient energy is bombarded onto the material. Several different interactions occur as the beam reaches and enters the material, leading to the emission of photons and electrons from or near the sample surface. Different modes exist for characterization of materials such as secondary electrons imaging and backscattered electrons imaging.[83]

All micrographs and elemental spectra were taken using the Scanning Electron Microscope FEI Quanta 400 equipped with an EDAX Genesis microanalysis system. The instrument uses a tungsten emitter, a voltage range of 1-30 kV, an Everhart-Thornley secondary detector (ETD), a dual backscattering detector (DualBSD), and multiple vacuum settings. Parameters for each micrograph and spectrum are detailed accordingly. Due to logistical reasons, SEM-EDS studies were only done for the removal of corrosion products and not the removal of Paraloid® B72.

2.4.4 COLORIMETRIC CHANGE

Fiber optics reflectance spectroscopy (FORS) is a non-invasive technique that allows *in situ* measurements of color and its variations. It is based on the analysis of the reflectance spectra, in which the intensity of the backscattered radiation is reported as a function of the wavelength of the incident radiation. The intensity, reported as percentage of reflected light from the sample, is compared to a white reference.[84,85]

To mathematically describe the color, the CIELAB color system was used. The system contains one parameter for lightness (L^*) and two parameters for color (a^* and b^*). The L^* values range from pure black (0) to white (100). The chromatic a* axis extends from green ($-a^*$) to red ($+a^*$), while the chromatic b* axis extends from blue ($-b^*$) to yellow ($+b^*$).[84,85]

Any visible color can be triangulated and placed within CIELAB color space. Color differences and discriminability can also be calculated from the relative distance between two points within the color space. This difference is often expressed as ΔE_{ab}^* and the formula is shown in Equation 5. It is important to note that while delta E quantifies the magnitude of color difference, it does not indicate the direction of the difference. [66,84,85]

$$\Delta Eab^* = \sqrt{(L_2 - L_1)^2 + (a_2 - a_1)^2 + (b_2 - b_1)^2} \qquad \text{Eqn. 5}$$

Instrument set-up was composed of BWTEK BPS 101 tungsten halogen light source, Thorlabs bifurcated optic cable, and a BWTEK Exemplar LS charge-coupled device detector. All measurements were taken with the BWSpec software, with an integration time of 1000000 μs and a multiplier of 5. To ensure that the same spot is measured for each sample, a labeled transparent mask is overlaid on the substrate. All measurements were done in triplicates. Delta values were calculated against the plain stone as control. The formula for removal efficiency is shown below in Equation 6, based on the study by Al-Emam *et al*.[66]

$$\%Removal\ Efficiency = \frac{(\Delta E_{ab-plain} - \Delta E_{ab-cleaned})}{\Delta E_{ab-plain}} x\ 100\% \qquad \text{Eqn. 5}$$

3.1 CHARACTERIZATION OF HVPDS

3.1.1 RHEOLOGICAL PROPERTIES

In order for the gel or gel-like HVPD to have adequate performance in terms of ease of application and complete removal through peeling action, the material should exhibit viscoelastic behavior even upon the incorporation of additives. Its mechanical properties should be preserved and, in particular, the G'_0 value should remain greater than 400 Pa.[18,21]

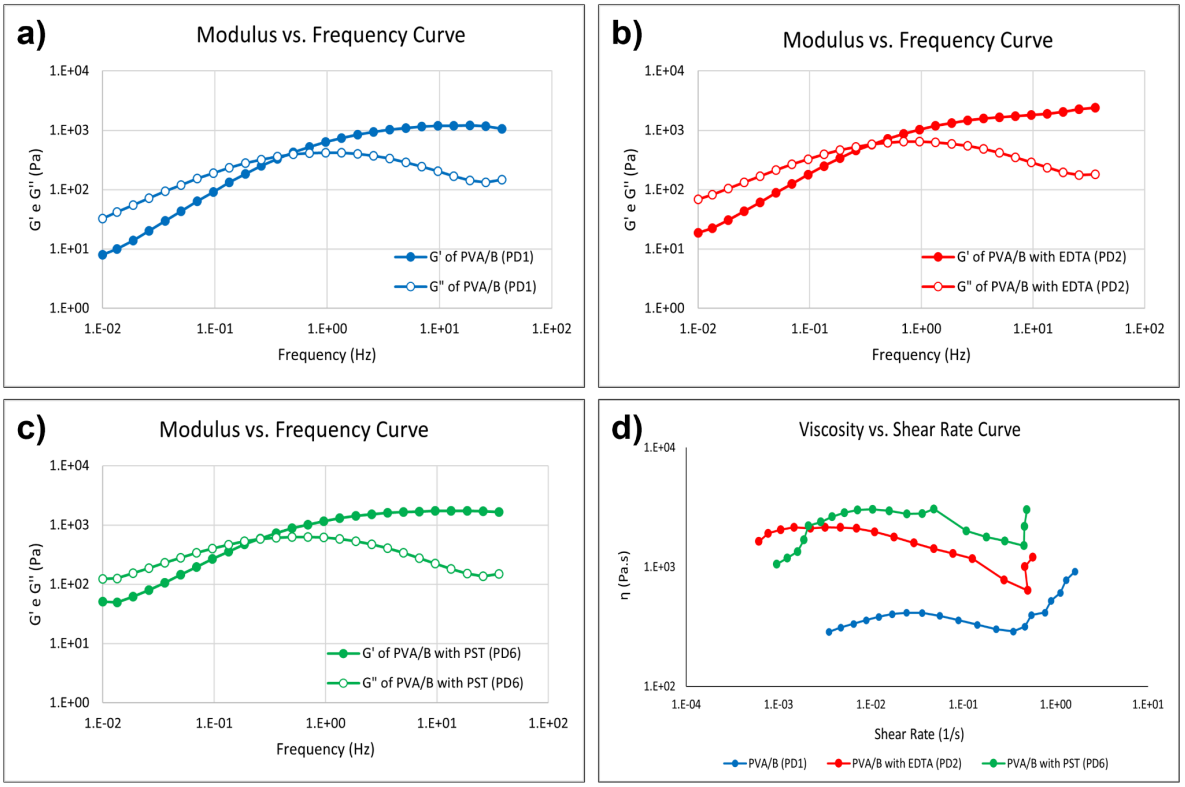

Figure 16. Frequency sweeps conducted at 25 °C for a) PVA/B, b) PVA/B with 0.5 wt.% EDTA, and c) PVA/B with 2.0 wt.% PST. Flow sweeps conducted at 25 °C for d) the three HVPDs.

Based on the frequency sweeps, the PVA/B systems are viscoelastic (see Figure 18). Initially, at lower frequencies, G" dominates which indicates viscous behavior. Later on, at higher frequencies, G' dominates which indicates elastic behavior. The material therefore undergoes a transition from being fluid-like to highly structured, behaving like a gel.[18,86] All three HVPDs also have a G'_0 much higher than 400 Pa, passing the criterion of peelability. [18,21]

The addition of EDTA and PST increases the G'_0 of PVA/B pointing to a stiffer material. The chelant addition also increases τ_c demonstrating better shape stability (see Table V). These show that the two salts have a structuring effect on the system, increasing component entanglement. These results can be attributed to the strengthening of the network due to the hydrogen bonding between the amine, hydroxyl, and carboxylate groups of the chelants and the hydroxyl groups of the PVA chains. It can also be related to the strong electric field

introduced by the multi-charged organic salts which induce water realignment and, consequently, improvement of the mutual solubility of PVA/B and water.[20,87,88]

Based on the flow sweeps, all three PVA/B systems follow non-Newtonian behavior (see Figure 18). At lower shear rates, the three HVPDs exhibit pseudoplasticity. They do not have a yield stress but behave nonlinearly. They flow instantaneously upon application of stress and undergo shear thinning. However, at higher shear rates, the gels exhibit dilatancy. The viscosity increases with the shear rate, which suggests that the PVA/B systems develop greater spacing between chains during agitation. This demonstrates the dynamic and reversible nature of the cross-linking mechanisms which hold the HVPDs together.[77]

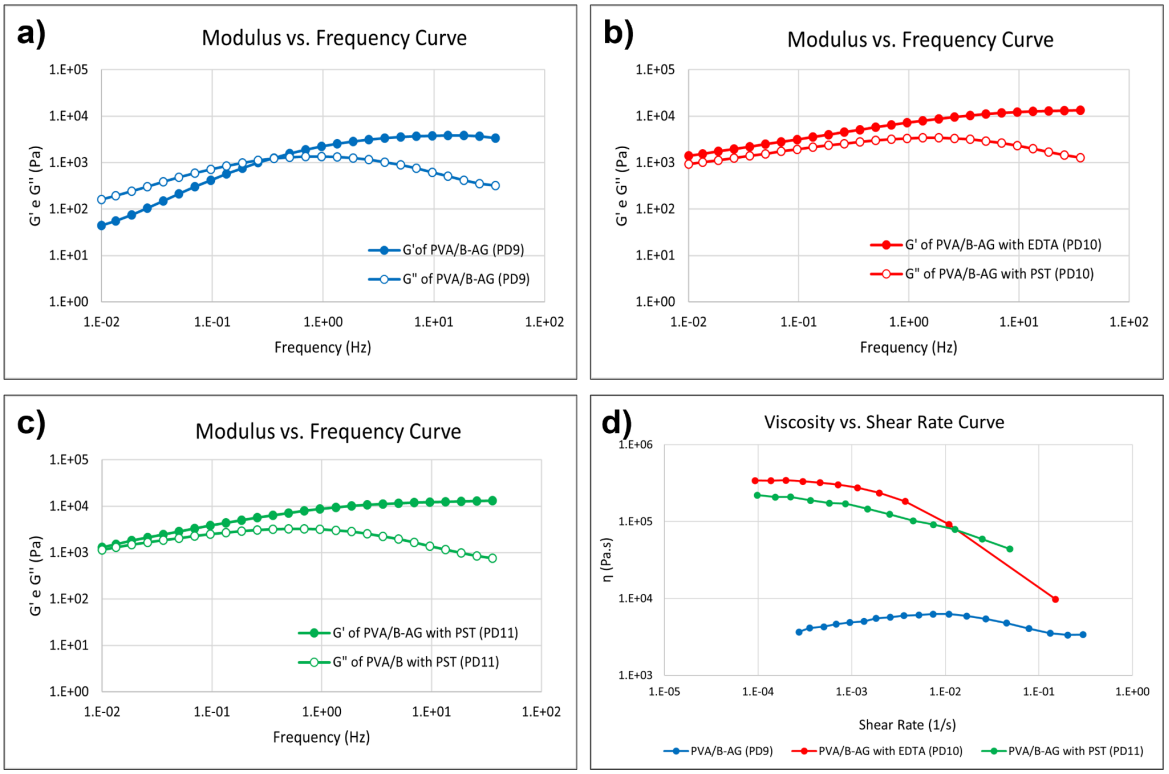

Figure 17. Frequency sweeps conducted at 25 ºC for a) PVA/B-AG, b) PVA/B-AG with 1.5 wt.% EDTA, and c) PVA/B-AG with 2.0 wt.% PST. Flow sweeps conducted at 25 ºC for d) the three HVPDs.

Based on the frequency sweeps, the PVA/B-AG systems behave differently (see Figure 19). The addition of agarose significantly increases G'_0 and τ_c, pointing to a much stiffer material and better shape stability (see Table V). Owing to its bundled double-helix structure, agarose provides a robust three-dimensional structure that interpenetrates with the PVA/B network. [18,86] All three HVPDs still have a G'_0 much higher than 400 Pa and pass the criterion of peelability necessary for adoption. [18,21]

PVA/B still behaves like a gel, but with the addition of EDTA and PST, the viscoelastic behavior is no longer observed. The value of G' is consistently higher than G", and there is an absence of ω_c or distant parallelism, demonstrating a much higher mechanical rigidity. This

could be attributed to the increased physical interactions within the material. The addition of agarose and chelants increase points of hydrogen bonding and component entanglement.[20,87,88]

Based on the flow sweeps, throughout the shear rates tested, the PVA/B-AG systems only exhibit pseudoplasticity (see Figure X). They do not have a yield stress but behave nonlinearly. They flow instantaneously upon application of stress and undergo shear thinning. This suggests that the PVA/B-AG systems tend to rearrange and realign in response to shear. The movement goes hand in hand with increasing disentanglement, resulting in decreasing viscosity values.[77]

Table V. Intrinsic elastic shear modulus, crossover frequency, and apparent relaxation time for the six HVPDs obtained from their respective frequency sweeps.

	G'_0 (Pa)	ω_c (Hz)	τ_c (s)
PD1	1.14×10^3	5.00×10^{-1}	2.00
PD2	2.22×10^3	5.00×10^{-1}	2.00
PD6	1.69×10^3	2.58×10^{-1}	3.88
PD9	3.39×10^3	3.60×10^{-1}	2.78
PD10	1.33×10^4	-	-
PD11	1.3×10^4	-	-

The rheological properties observed for the PVA/B and PVA/B-AG systems are supported by literature findings. The systems seem to follow a sticky reptation mechanism where entangled polymer chains form reversible cross-links with highly attractive sticker molecules, i.e., EDTA and PST. There are many stickers per chain so, at a high degree of association, there are very few unassociated stickers. It is therefore difficult for a sticker to find a new partner to associate with after dissociating with an old one. This leads to the sticker maintaining its current association, prolonging the effective lifetime of the reversible cross-linking. This is evident in the significant difference in the rigidity between PVA/B and PVA/B-AG systems, with the latter having higher network density and lower component mobility. Moreover, due to the structures of EDTA and PST, the correlation length of the chains and their affinity to the aqueous phase increase. It is important to emphasize, however, that the chelants remain free and labile in this model which means these species can still migrate throughout the material and be used to sequester contaminants at the interface. [20,87]

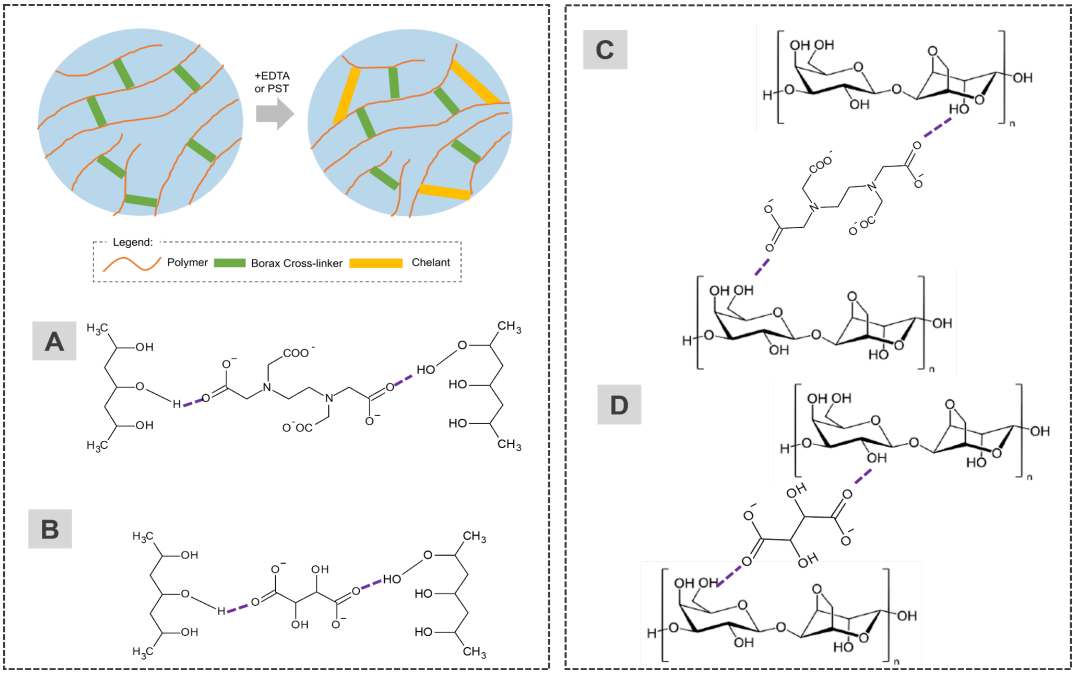

Figure 18. Chelants acting as reversible intra- and intermolecular cross-linkers between the hydroxyl groups of PVA chains (a-b) and agarose coils (c-d) based on the sticky reptation model.

3.1.2 WATER HOLDING CAPACITY

The data reveals minimal change overall in the water holding capacity of the six HVPDs (see Figure 22). Over the span of four hours, the water holding capacity of the HVPDs decrease but remained above 99%. This shows that there is minimal desorption of water from the HVPDs onto the porous matrix; the area of cleaning action is restricted within the interface of the HVPDs and the stone substrate. This outcome can be attributed to the abundant presence of hydroxyl groups in the PVA chain and agarose helical bundles, along with the ionic and hydrophilic nature of the chelants loaded into the HVPDs. The combination of these components increases the osmotic pressure around the polymer chains which lead to better water retention properties.[89,90]

Among the six HVPDs, PD6 has the highest water holding capacity. This suggests that the PVA/B system with PST has more bound water relative to the non-loaded HVPD. It is possible that there might be a high degree of association between PST and the PVA chains, resulting in the entrapment of water molecules in the network. Conversely, PD2 has a lower water holding capacity. This suggests that the PVA/B system with EDTA has more free water relative to the non-loaded HVPD. It is possible that the association between EDTA and the PVA chains result in much larger gaps in the network due to the chelant's bulkier shape, allowing higher mobility of water molecules.[87] It is also possible that EDTA changes the microenvironment of the HVPD due to its ionic strength, favoring the solvation and stabilization of the salt with water instead of the polymer chains.[89]

For the HVPDs containing agarose, PD9 had higher water holding capacity than PD10 and PD11. The addition of agarose to the PVA/B system improved its water holding capacity due to its hydrophilicity and the affinity of its internal cavity to host water molecules. However, the addition of chelants lower the water holding capacity, with the effect more extensive when EDTA is added relative to PST. This can be attributed to the increased correlation length between the polymer chains associated with chelant cross-linkers. The increased spacing improves allows for the mobility of water molecules.[87]

These results fall in line with other studies concerning PVA/B and PVA/B-AG systems. Water holding capacity is known to reflect the morphology of gels and gel-like systems, defined by both the coarseness and the stiffness of the network.[91] HVPDs of PVA/B generally have large interconnected pores, but HVPDs of PVA/B-AG have slightly thicker walls and smaller pores.[66] The latter can hold more water because it has higher surface area available for binding water.[91] The addition of salt ions, whether inorganic and organic, below a critical concentration, are also known to generally increase network density, reduce pore size, and increase water holding capacity.[92–94]

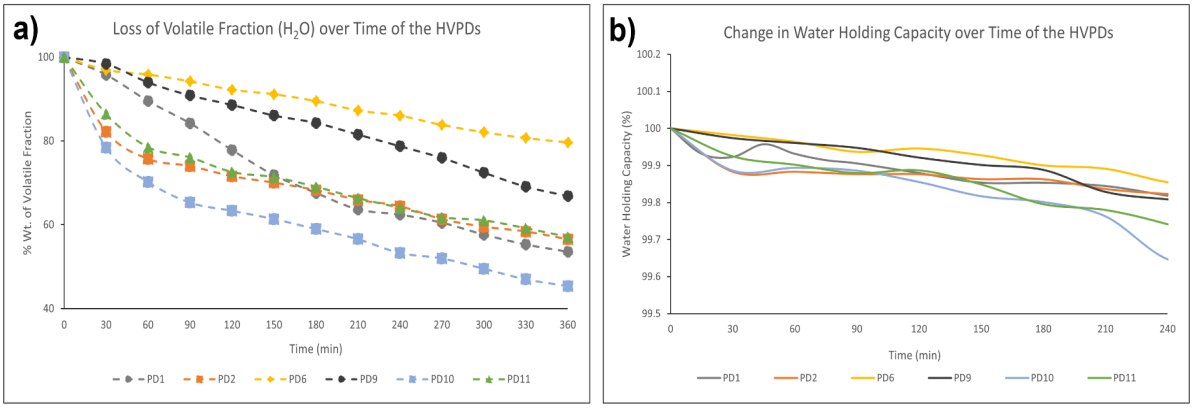

Figure 19. Experiment results for a) loss of volatile fraction and b) time-dependent change in water holding capacity for six main HVPD formulations.

3.1.3 LOSS OF VOLATILE FRACTION

Based on the results, the six HVPDs continuously lose water content over time due to evaporation (see Figure 22). The extent to which they lose water, however, varies. Between a system with and without agarose, PVA/B loses a higher percentage of volatile fraction over time compared to PVA/B-Agarose. At the end of six hours, PD1 only has 54% of its volatile fraction while PD9 still has 67%. This can be attributed to the structure of agarose whose internal cavity binds a greater fraction of water molecules. Moreover, due to the higher network density of the HVPD, water is also easily trapped in the confined spaces between adjacent and cross-linked macromolecules.[68]

With the addition of chelants, there is a change in the percent weight of the volatile fraction remaining. PD2 has 57% while PD10 has 45% at the end of six hours. This reinforces the hypothesis that EDTA acts as a reversible cross-linker and its high correlation length promotes water mobility. Meanwhile, PD6 has 80% while PD11 has 57% at the end of six hours. This also supports what has been discussed thus far that PST has a high degree of association with the hydroxyl groups of the polymer chains which leads to water entrapment.[27,87]

There have been extensive studies on the effects of salts in the liquid phase retention of gels or HVPDs. For PVA/B systems, the interaction of water and polymer weakens in favor of the multi-layered hydration of the salts added and promotes water mobility throughout the network.[92,93] For agarose-containing systems, water mobility is hindered both by interactions with the hydroxyl groups of agarose and by the high network density of the polysaccharide matrix. When salts are introduced, coil-helix transition and helix-helix interactions reduce due to ionic interference, facilitating the release of water trapped within the gel or HVPD network.[94]

Overall, it can be concluded that the dehydration of the HVPDs is primarily driven by evaporation kinetics rather than desorption. In the adoption of the cleaning method, therefore, it is practical to account for the temperature and humidity when planning the procedure. It might also help to cover the setup to avoid the premature drying of the HVPD.

3.1.4 CHEMICAL STRUCTURE AND INTERACTIONS

For all the six HVPDs, the components consistently present are PVA, Borax, and water. There is a weak band at 1648 cm^{-1} attributed to O-H bending. It does not shift in wavenumber or change in intensity regardless of the sample. There is also a strong broad band at around 3360 cm^{-1} for O-H stretching. Its intensity changes from sample to sample but is not very useful for elucidating component interactions. Instead, it reflects the contribution of the water present during analysis. [66,80] In the PVA/B spectrum (PD1), the other bands can be assigned as follows: 2944 cm^{-1} for asymmetrical -CH_2 stretching, 2924 cm^{-1} for symmetrical -CH_2 stretching, 1549 and 1506 cm^{-1} for the C-C stretching, 1338 cm^{-1} for -CH_3 rocking, 1317 cm^{-1} for C-O-H bending, 1236 cm^{-1} for -CH_2 wagging, 1089 cm^{-1} for the C-O stretching of secondary alcohols, and 933 cm^{-1} for -CH_2 stretching. [66,80] It is essential to highlight the band at 1432 cm^{-1} contributed by B-O-C asymmetric stretching which shows the cross-linking of PVA with borate ions.[66,80]

With the addition of chelants, there are a few changes in the spectrum. In the PVA/B with EDTA spectrum (PD2), the band for N-H stretching for the amine group should be found

around 3300 cm^{-1} but cannot be seen clearly due to overlap with the band for O-H bending. However, the spectral shape and intensity of the peaks around 2915 cm^{-1} changed due to the contribution of the N-C-H stretching in the chelant. The twin bands centered at 1360 cm^{-1} corresponds to C-O-O^- stretching, particular to the carboxylate group of EDTA whose carbon-oxygen bond exhibits both single and double bond properties. There is also a shift in the band for C-O stretching from 1089 cm^{-1} to 1069 cm^{-1}, possibly due to a change in bond length now that there is interaction between the polymer chain and the chelant. The band around 1100 cm^{-1} also seems broader due to the additional overlapping bands, including those around 1147 cm^{-1} for C-O-C stretching and 1106 cm^{-1} for C-N stretching.[95,96] Meanwhile, in the PVA/B with PST spectrum (PD6), there are less visible changes. There is an additional band around 890 cm^{-1} characteristic to the C-O-O^- stretching of PST which also have characteristics in between a single bond and double bond.[97,98]

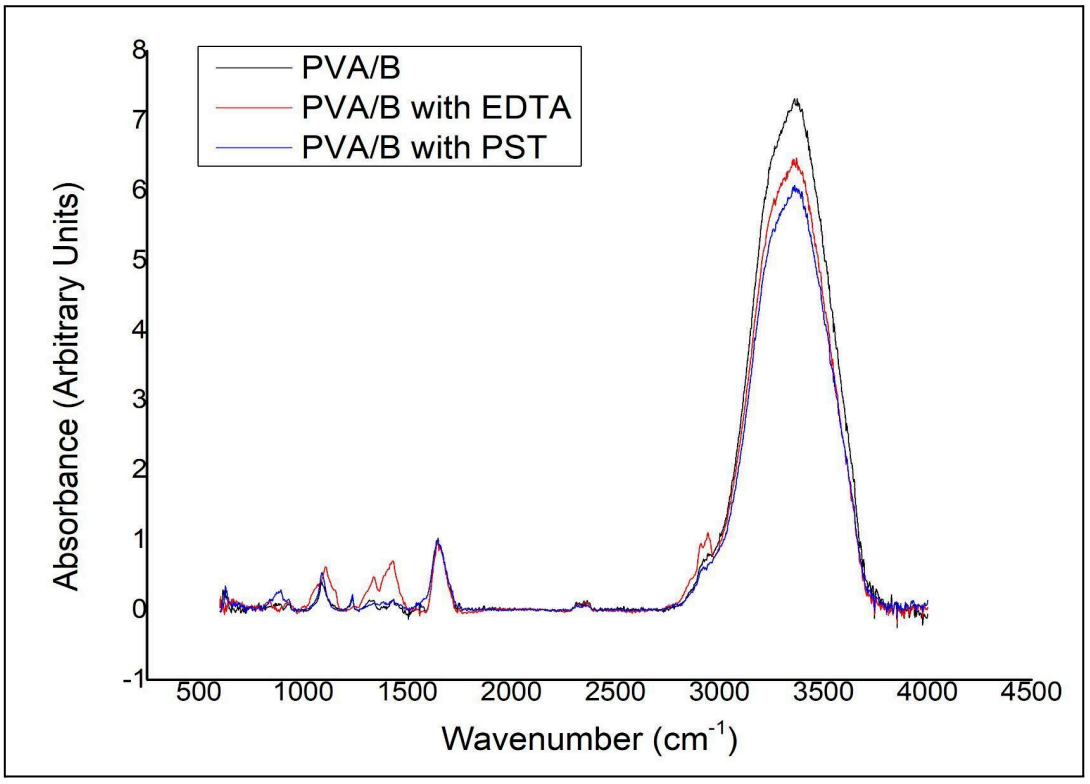

Figure 20. Superimposed ATR-FTIR spectra of the PVA/B system without chelants (black), with EDTA (red), and with PST (blue).

For the PVA/B-AG system (PD9), the spectrum is highly similar to that without agarose. What is important to highlight are the bands at 1069 cm^{-1} for the C-O-C stretching of the glycosidic linkage and at 931 cm^{-1} characteristic to 3,6-anhydrogalactose stretching. The bands at 892 cm^{-1} for B-O stretching from residual $B(OH)_4^-$ ions and at 626 cm^{-1} for B-O-B linkages within borate networks are also apparent in the spectrum albeit weak.[66,80]

With the addition of chelants, there are not a lot of visible changes in the spectrum. The bands of the HVPD dominate, making interpretation difficult. In the PVA/B-AG with EDTA spectrum (PD10), there is a band at 1386 cm^{-1} for C-O stretching of the carboxylate group

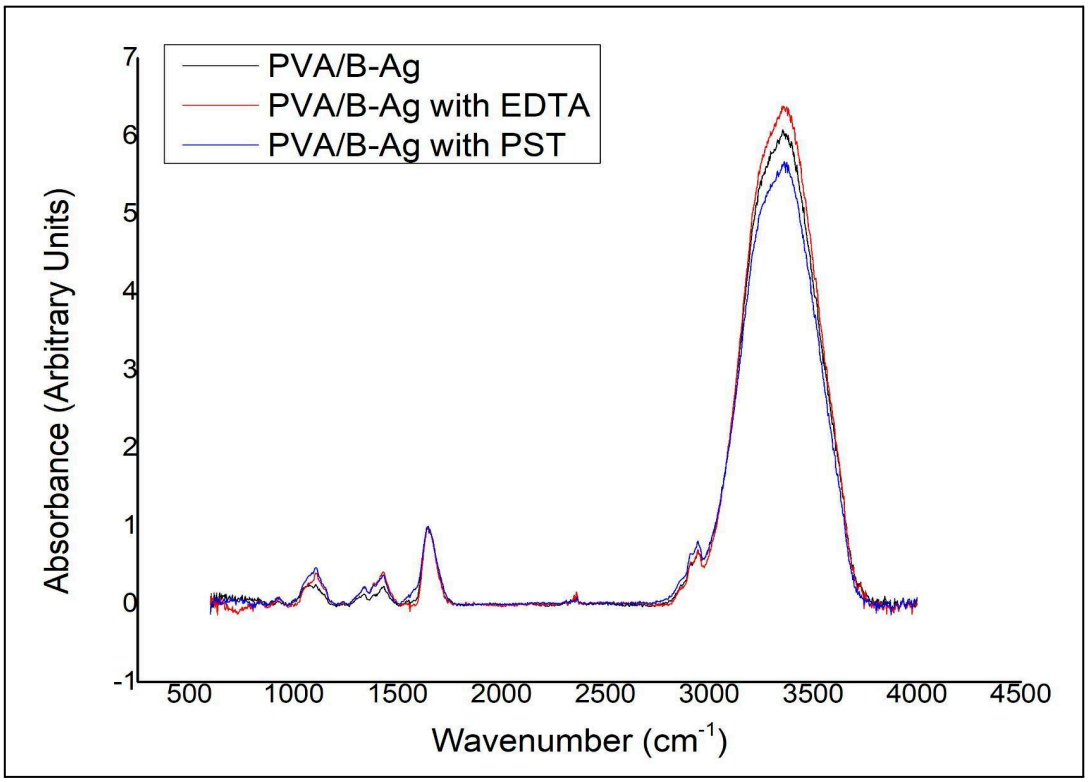

Figure 21. Superimposed ATR-FTIR spectra of the PVA/B-AG system without chelants (black), with EDTA (red), and with PST (blue).

and at 1110 cm^{-1} for C-N stretching of the tertiary amines.[95,96] There is also a slight shift in the position of the bands for asymmetric B-O-C stretching, symmetric -CH_2 stretching, and O-H bending which might be attributed to the role of EDTA as a reversible cross-linker. [95,96] Meanwhile, in the PVA/B-AG with PST spectrum (PD11), there is only a slight shift in the position of the band for symmetric -CH_2 stretching and tailing of the O-H bending which might also be attributed to the interaction of PST with the polymer chain.[97,98]

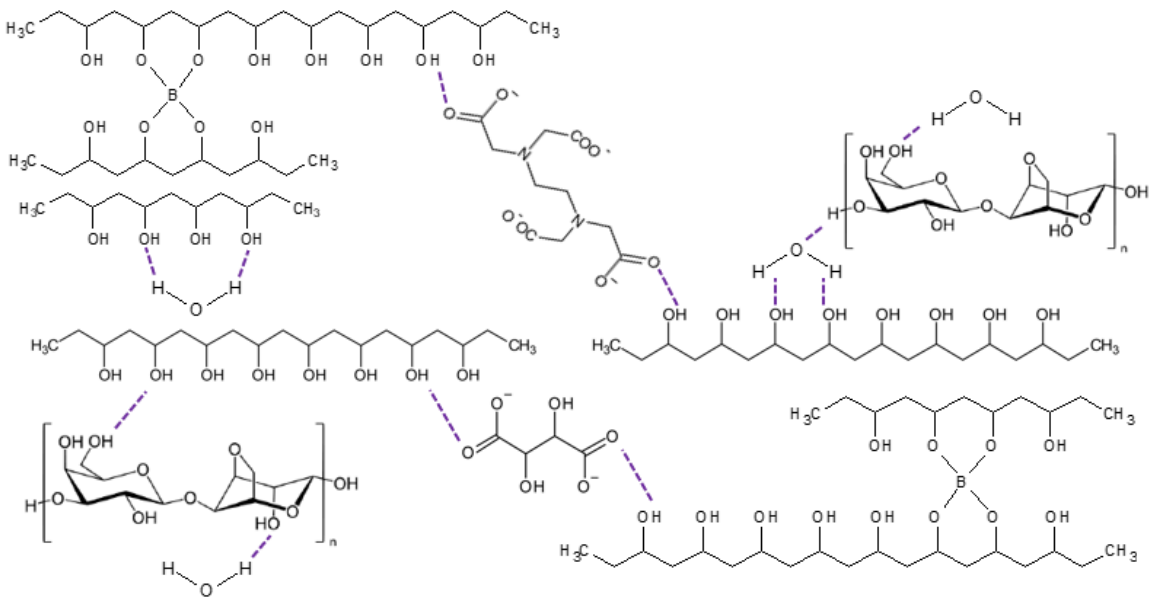

Figure 22. Possible intermolecular interactions between components: chemical cross-linking of PVA chains with borax, hydrogen bonding with agarose, and the dynamic reversible cross-linking with agarose and the chelants.

3.2 CLEANING OF BRONZE CORROSION PRODUCTS

3.2.1 ARTIFICIAL CORROSION PATINA & STONE CONTAMINATION

3.2.1.1 MORPHOLOGICAL STRUCTURE

Based on the SEM micrographs, it can be seen that the surface morphology of the carbonate stones are severely affected by the bronze corrosion products (see Figure 26). While cracks and pores were originally present in the stone grains, their surfaces were generally smooth and uniform. After contamination, their surfaces are consistently rugged and uneven due to the presence of precipitates and crystals.

From the SE image, Carrara Marble has a mixture of raw, point, double-terminated, and cluster crystals scattered throughout the surface. There are some visible striations, a sign of corrosion fatigue, which indicates cyclic stresses imposed by the corrosion product on the stone surface.[99] From the BSE image, there is a high contrast between the lighter calcium atoms which make up the substrate and the heavier atoms which make up the contaminants. EDS spectra were obtained at three points (see Figure 27). The first and second points yield very similar spectra with the following peaks: carbon $K_{\alpha 1}$ peak at 0.20 keV, oxygen $K_{\alpha 1}$ peak at 0.60 keV, copper $L_{\alpha 1}$ peak at 0.90 keV, sulfur $K_{\alpha 1}$ peak at 2.30 keV, calcium $K_{\alpha 1}$ peak at 3.60 keV, copper $K_{\alpha 1}$ peak at 8.00 keV. The copper, oxygen, and sulfur peaks have the highest intensities, suggesting those points are rich with corrosion products. For the third point, the calcium $K_{\alpha 1}$ peak has the highest intensity accompanied by an increase in the intensity of the carbon $K_{\alpha 1}$ peak, suggesting that point is mainly composed of calcium carbonate. Impurities

inherently in the stone, such as magnesium and silicon, also have visible $K_{\alpha 1}$ peaks at 1.20 keV and 1.70 keV, respectively.

The SE image of Lecce Stone also shows an abundance of crystals with raw, point, and double-terminated shapes forming aggregates. It is possible there were multiple nucleation sites due to the larger pore size, but the growth was stifled due to the rapid cooling of the product-rich solution.[100] The BSE image also shows high contrast where the area captured is mostly composed of heavier atoms rather than lighter ones. EDS spectra were obtained at two points (see Figure 28). For both, the peaks present are similar to that of Carrara Marble. Copper $L_{\alpha 1}$ and $K_{\alpha 1}$ peaks as well as sulfur $K_{\alpha 1}$ peak are present, but the oxygen $K_{\alpha 1}$ peak has the highest intensity which can be due to the contributions of the different polyatomic anions present in the compounds. In addition to magnesium and silicon, there is also an aluminum $K_{\alpha 1}$ peak at 1.40 keV.

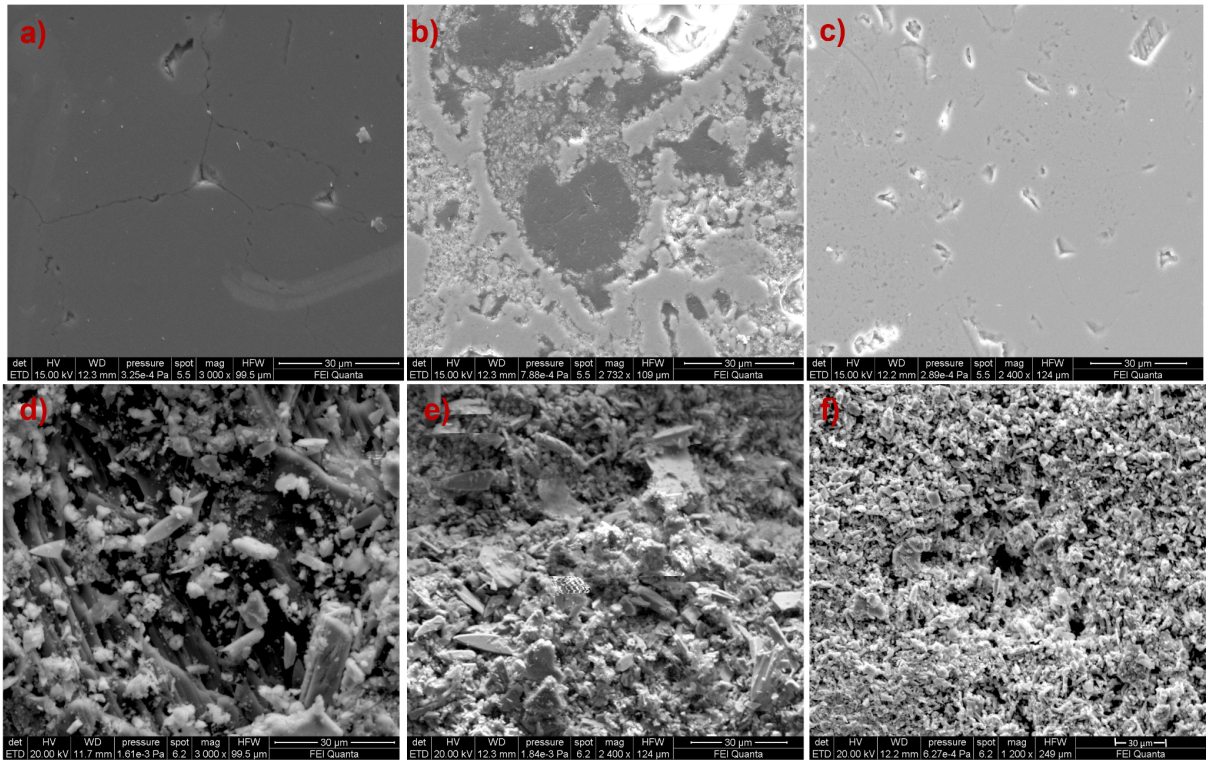

Figure 23. SE micrographs of the three lithotypes before (a-c) and after (d-f) contamination with bronze corrosion products. From left to right are SE images of Carrara Marble, Lecce Stone, and Travertine stone blocks.

The SE image of Travertine shows raw and tetrahedron crystals of different dimensions aggregated together. It is possible that, due to larger pore size and irregular pore shape, there were multiple nucleation sites some of which are favorable for crystal growth.[100] The BSE image shows low contrast so the composition of the contaminants throughout the surface might be more homogeneous. EDS spectra were obtained at two points (see Figure 29). Both yield similar results with the copper $L_{\alpha 1}$ peak having the highest intensity. Sulfur, oxygen,

calcium and carbon $K_{\alpha 1}$ peaks are also present. This implies that the corrosion products are well-distributed throughout the surface and have etched part of the calcium carbonate surface.

The extent of damage appears to worsen from Carrara Marble to Lecce Stone to Travertine which might be related to their porosities. Carrara Marble is the least porous substrate, so the copper-rich solution does not go through a capillary pore network and mostly interacts with the substrate through surface runoff. It can be noticed that the crystals formed on the surface of Carrara Marble are larger in size, reflecting fewer nucleation sites and promotion of crystal growth. Lecce Stone has higher porosity but its pore sizes are generally smaller (ranging from 600 nm to 5 μm). This provides a conducive environment for nucleation of crystals but not necessarily growth. The same can be stated for Travertine, which has an even higher porosity and larger pore size (ranging from 30 to 60 μm). This allows for nucleation and continuous crystal growth given a steady supply of the copper-rich solution.[49,53,54]

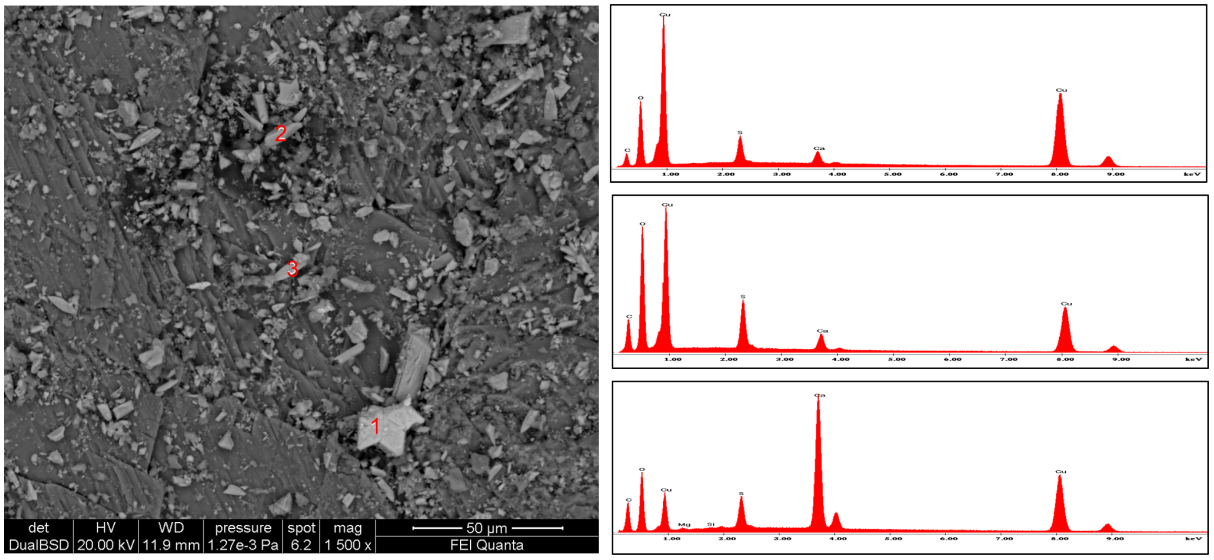

Figure 24. BSE micrograph of contaminated Carrara Marble and the corresponding EDS spectra of the selected points in red.

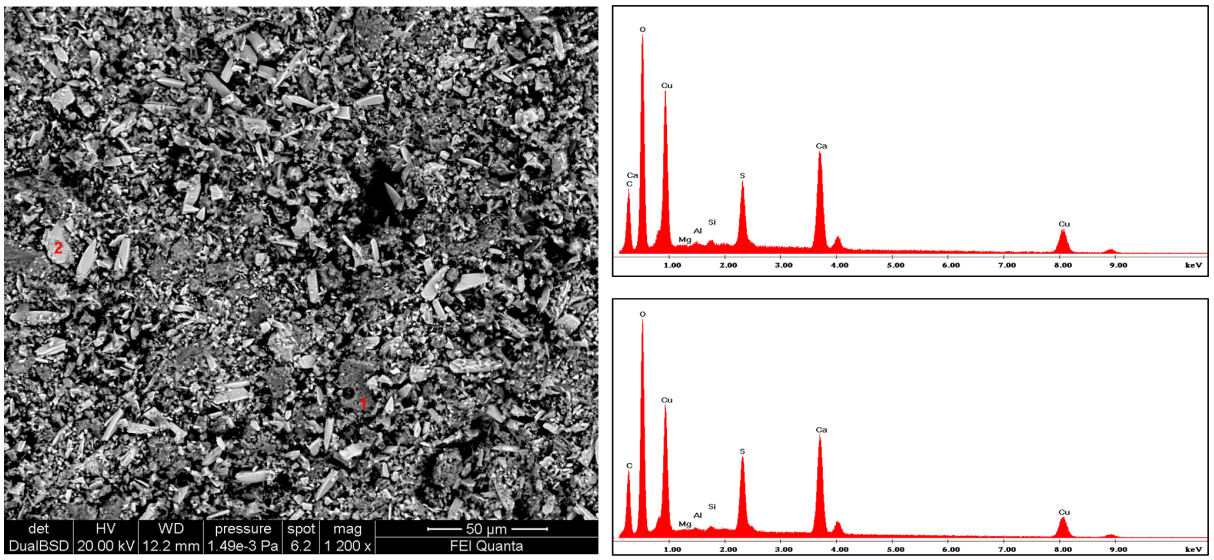

Figure 25. BSE micrograph of contaminated Lecce Stone and the corresponding EDS spectra of the selected points in red.

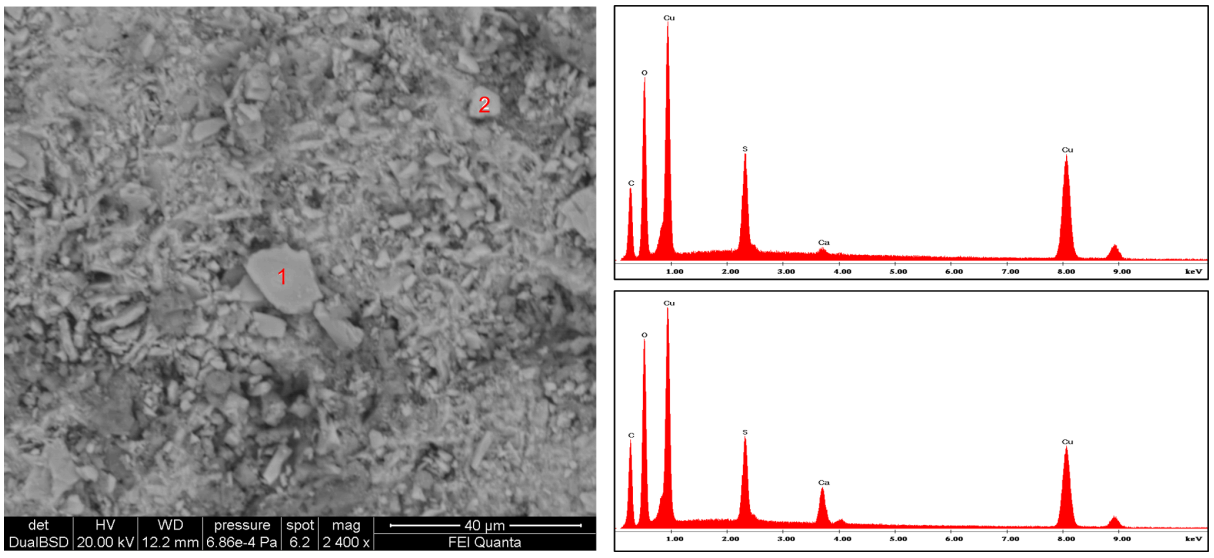

Figure 26. BSE micrograph of contaminated Travertine and the corresponding EDS spectra of the selected points in red.

3.2.1.2 COLORIMETRIC CHANGE

After the contamination of the three lithotypes, the area was divided into two for the application of the selected HVPDs. In the summarized table, the different colorimetric parameters reveal which direction the change happened relative to the plain stone (see Table VI). For the L* parameter, there is no general trend. With respect to the control, the contaminated stones either lighten or darken with delta values less than ten. For the a* parameter, the delta values are negative for all lithotypes which shows a general shift towards a greener color. For the b* parameter, the delta values are negative for all lithotypes, which shows a general shift towards a bluer color.

Table VI. Average colorimetric parameters of Area 1 and Area 2 in which the two selected HVPDs would be applied. Area 1 would be cleaned with PVA/B-AG with EDTA (PD10) while Area 2 would be cleaned with PVA/B-AG with PST (PD11).

	AREA 1				AREA 2			
Carbonate Stones	ΔL*	Δa*	Δb*	ΔE_{ab}*	ΔL*	Δa*	Δb*	ΔE_{ab}*
Carrara Marble	-0.76	-57.05	-16.68	59.86	2.42	-50.05	-10.40	51.28
Lecce Stone	-4.46	-23.26	-13.32	29.14	-6.62	-18.75	-0.32	29.00
Travertine	7.17	-26.33	-16.53	36.08	9.14	-24.22	-11.03	31.34

Looking more closely, the Δa* value for Carrara Marble is almost twice that of Lecce Stone and Travertine. The Δb* values for all three are close but also highest in Carrara Marble. This might be due to the difference in the nature and relative amounts of the corrosion products staining the surface. The ratio of copper hydroxide compounds to copper hydroxysulfate compounds might be higher in Carrara Marble, imparting a more greenish tint.[11,48]

The magnitude of ΔE_{ab}* is highest for Carrara Marble, then Travertine, then Lecce Stone. Relating these results to the SEM micrographs, the results might seem contradictory, but they are actually in accord. The formation of corrosion products in Carrara Marble are most likely concentrated on the surface. The corrosion products might have low penetration depth and form an external layer instead. Hence, the color reflected is more saturated compared to the other two substrates. For Lecce Stone and Travertine which have higher porosity, the products might have higher penetration depth. Between the two, Lecce Stone has smaller pore size and a pore capillary network, which makes diffusion of the products more extensive. Hence, the color reflected is less saturated. Note that these are all still hypotheses so further characterization of the substrates and their cross-sections might help elucidate the underlying factors affecting these results.[100]

3.2.2 CLEANING OF CARRARA MARBLE

3.2.2.1 MORPHOLOGICAL STRUCTURE

The contamination of Carrara Marble with bronze corrosion products transformed its smooth and even surface to highly irregular. Its cleaning with PD10 and PD11 resulted in a considerable change in the surface morphology (see Figure 31). The grains of the carbonate stone are visible again and the number of crystals was heavily reduced. The striations brought by fatigue corrosion remain. There were a few fibrils which got blurred and these are suspected to be residues left by the HVPDs. Focusing the electron beam on these spots results in overcharging due to the insulating nature of the network.

For the area cleaned with PD10, the BSE image shows a high contrast between the gray stone grains and the white corrosion products (see Figure 32). The first point of interest is a flat solid embedded in a crack. Its EDS spectrum shows the presence of impurities with a silicon $K_{\alpha 1}$ peak at 1.70 keV, aluminum $K_{\alpha 1}$ peak at 1.40 keV, magnesium $K_{\alpha 1}$ peak at 1.20 keV, and potassium $K_{\alpha 1}$ peak at 2.30 keV. The second point of interest is one of the crystals dispersed on the surface. Its EDS spectrum reveals that copper sulfates and hydroxides are still present, demonstrated by the copper $L_{\alpha 1}$ and $K_{\alpha 1}$ peaks at 0.90 keV and 8.00 keV, sulfur $K_{\alpha 1}$ peak at 2.30 keV, and oxygen $K_{\alpha 1}$ peak at 0.50 keV.

For the area cleaned with PD11, the BSE image also shows a high contrast between the stone grains and the corrosion products (see Figure 33). The first point of interest is one of the white crystals distributed throughout the area. Similar to the other results, the presence of copper, sulfur, and oxygen peaks show that some of the corrosion products are left. Meanwhile, the second point of interest is one of the gray stone grains making up the bulk. The results suggest that it is calcium carbonate, with the calcium $K_{\alpha 1}$ peak at 3.60 keV, carbon peak at 1.20 keV, and oxygens peak at 0.50 keV. There is also a magnesium $K_{\alpha 1}$ peak at 1.20 keV, indicating the substitution of some magnesium atoms in the place of calcium atoms.

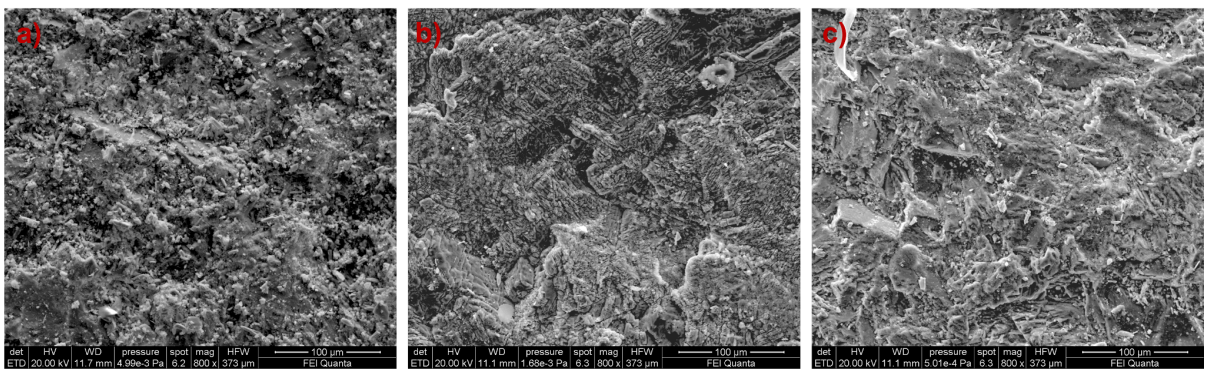

Figure 27. SE micrographs of Carrara Marble after (a) contamination with bronze corrosion products, (b) cleaning with PVA/B-AG with EDTA (PD10), and (c) cleaning with PVA/B-AG with PST (PD11).

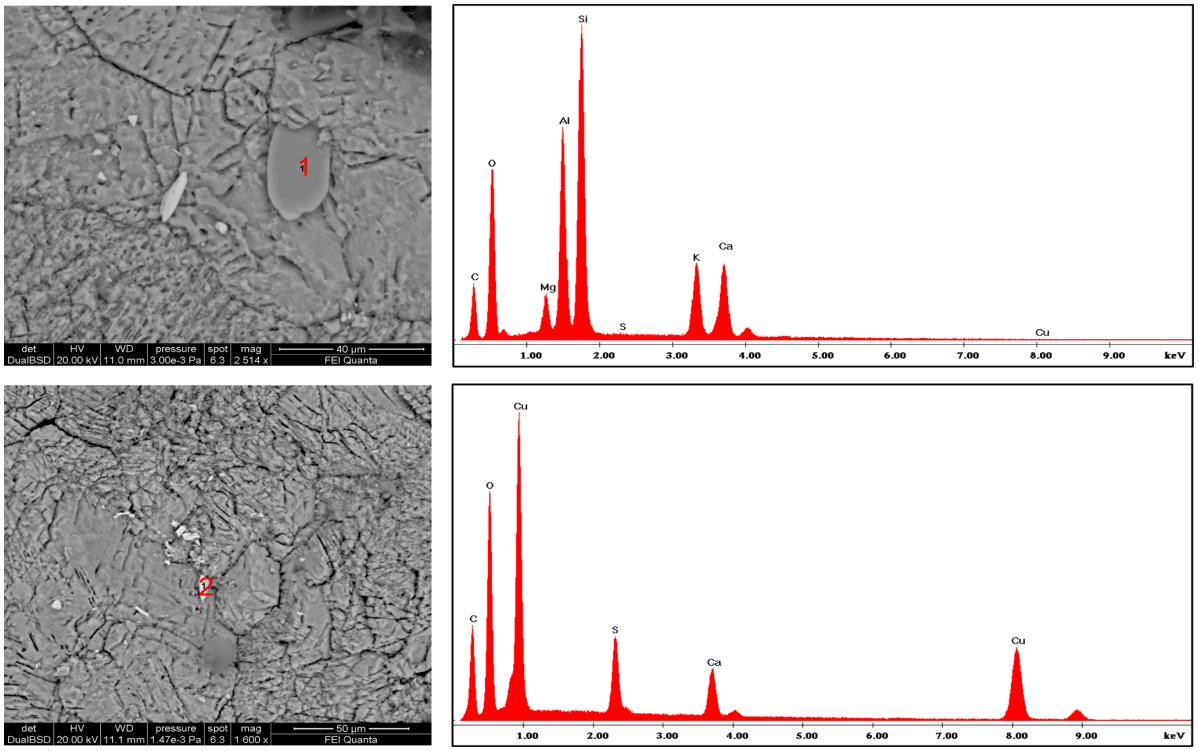

Figure 28. BSE micrograph after cleaning of Carrara Marble with PVA/B-AG with EDTA (PD10) and the corresponding EDS spectra of the selected points in red.

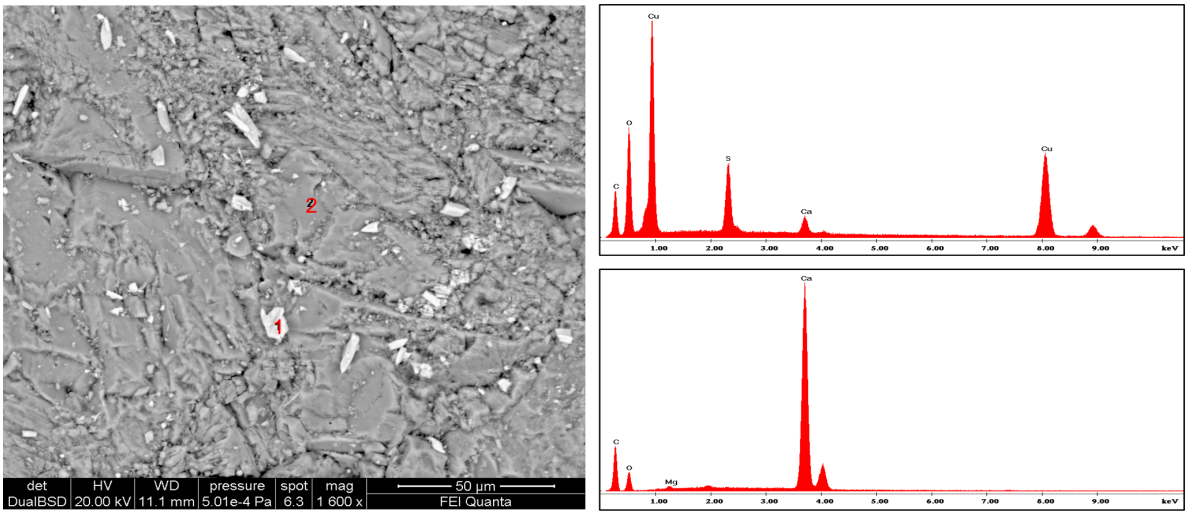

Figure 29. BSE micrograph after cleaning of Carrara Marble with PVA/B-AG with PST (PD11) and the corresponding EDS spectra of the selected points in red.

3.2.2.2 COLORIMETRIC CHANGE

Carrara Marble blocks were cleaned for four hours with two different HVPDs. The first area was cleaned with PVA/B-AG with EDTA (PD10) while the second area was cleaned with PVA/B-AG with PST (PD11). All delta values reported are determined against the control. The goal is to reduce the delta values of the colorimetric parameters and obtain a high removal efficiency.

After the first application of PD10 (see Table VII), there is already a perceptible change in the color of the stone. The cleaned surface remains darker than the original, but the Δa* parameter is 7 times lower and the Δb* parameter 9 times lower. The magnitude of ΔE_{ab}* also

decrease from 59.86 to 10.56 with a removal efficiency of 82.6%. This demonstrates that the cleaning method leaves the surface closer to its original state color-wise. After the second application, the Δa* parameter is 50 times lower and the Δb* parameter 100 times lower. However, the magnitude of ΔE_{ab}* increase to 17.18 and the calculated removal efficiency reduce to 71.3%. This can be traced to the significantly higher ΔL* parameter, which poses an issue because the surface lightening might be due to the partial erosion or solubilization of the substrate.

After the first application of PD11 (see Table VII), there is also an appreciable change in the color of the stone. The ΔL* parameter come close to zero, the Δa* parameter become 5 times lower, and the Δb* parameter 3 times lower. The magnitude of ΔE_{ab}* decrease from 51.28 to 11.83, with a removal efficiency of 76.93%, demonstrating the effectiveness of the cleaning method. After the second application, the Δa* parameter is 20 times lower and the Δb* parameter 8 times lower. However, the magnitude of ΔE_{ab}* increase to 25.25, reducing the calculated removal efficiency to 50.76%. The problem lies again with the higher ΔL* parameter, which translates to surface lightening brought either by partial erosion or solubilization of calcium carbonate from the surface.

Table VII. Average colorimetric parameters of Area 1 and Area 2 of Carrara Marble surfaces with plain stone as control. Area 1 was cleaned with PVA/B-AG with EDTA (PD10) while Area 2 was cleaned with PVA/B-AG with PST (PD11).

	AREA 1				AREA 2			
	ΔL*	Δa*	Δb*	ΔE_{ab}*	ΔL*	Δa*	Δb*	ΔE_{ab}*
1st Application	-5.36	-8.72	-2.04	10.56	-0.71	-9.38	-3.50	11.83
2nd Application	17.13	-1.12	0.77	17.18	25.10	-2.24	1.32	25.25

Overall, PD10 exhibit a better cleaning power than PD11 for Carrara Marble. Two applications are required to approximate the substrate color prior to contamination, as seen in the cumulative decrease of the a* and b* parameters. However, it is possible that part of the calcium carbonate gets eroded or solubilized. It is therefore important that, in the adoption of this cleaning method, the second application is modulated by the operator.

3.2.2.3 HVPD-CONTAMINANT INTERACTION

The first HVPD applied to Carrara Marble for 4 hours was PVA/B-AG with EDTA (PD10) (see Figure 35). Similar to the blank, the bands can be assigned as follows: 3360 cm^{-1} for O-H stretching, 2944 cm^{-1} for asymmetrical -CH_2 stretching, 2863 and 2907 cm^{-1} for C-H stretching, 1644 cm^{-1} for O-H bending, 1334 and 1403 cm^{-1} for asymmetric B-O-C stretching, 1151 cm^{-1} for C-C stretching and C-O-C stretching, 1110 cm^{-1} for in-plane C-H bending and

C-N stretching, 1069 cm^{-1} for C-O-C stretching and glycosidic linkage, and 929 cm^{-1} for -CH_2 stretching.[45,66] There are two bands of interest in the spectrum. First, there is a band at 834 cm^{-1} for Cu-O stretching, which demonstrates the metal-ligand complex formation of copper ions with EDTA.[101] Second, the band at 1644 cm^{-1} has a shoulder at 1586 cm^{-1}, which might be due to the partial shifting of the band for O-H bending. Due to the conformational change brought by the coordination, the highly negative oxygen atoms of the chelant protrude outwards in a square-pyramidal molecular geometry.[96,102] This enhances the hydrogen bonding interactions with the hydroxyl group of the polymer chains and significantly increases the degree of association as a reversible cross-linker.[103]

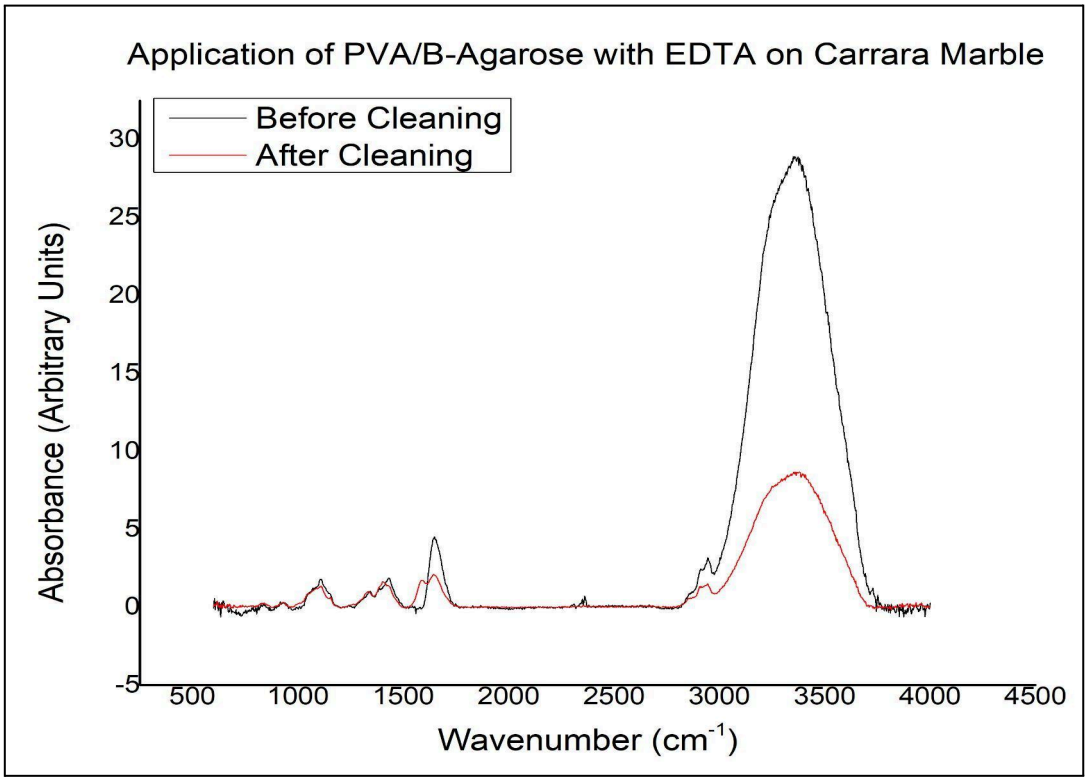

Figure 30. Superimposed ATR-FTIR spectra of PVA/B-AG with EDTA (PD10) before and after second cleaning Carrara Marble.

The second HVPD applied to Carrara Marble for 4 hours was PVA/B-AG with PST (PD11) (see Figure 36). Similar to the blank, the bands can be assigned as follows: 3397 cm^{-1} for O-H stretching, 2931 cm^{-1} for the asymmetrical -CH_2 stretching, 2863 and 2907 cm^{-1} for C-H stretching, 1338 and 1403 cm^{-1} for asymmetric B-O-C stretching, 1069 cm^{-1} for C-O-C stretching and glycosidic linkage, 1049 cm^{-1} for C-O stretching, and 929 cm^{-1} for -CH_2 stretching.[66,80] Similar to PD10, there is a band at 827 cm^{-1} for Cu-O stretching, showing the binding of copper ions with PST. The band at 1644 cm^{-1} also has a shoulder at 1593 cm^{-1} due to the partial shifting of the band for O-H bending. The complexation of copper and PST forms a square planar ring, which promotes hydrogen bonding with the hydroxyl groups of the polymer. In fact, the shifted band has a higher intensity than the original. There is also a

shift to 890 cm^{-1} of the C-O stretching band which reinforces the notion that coordination promotes association as a reversible cross-linker.[97]

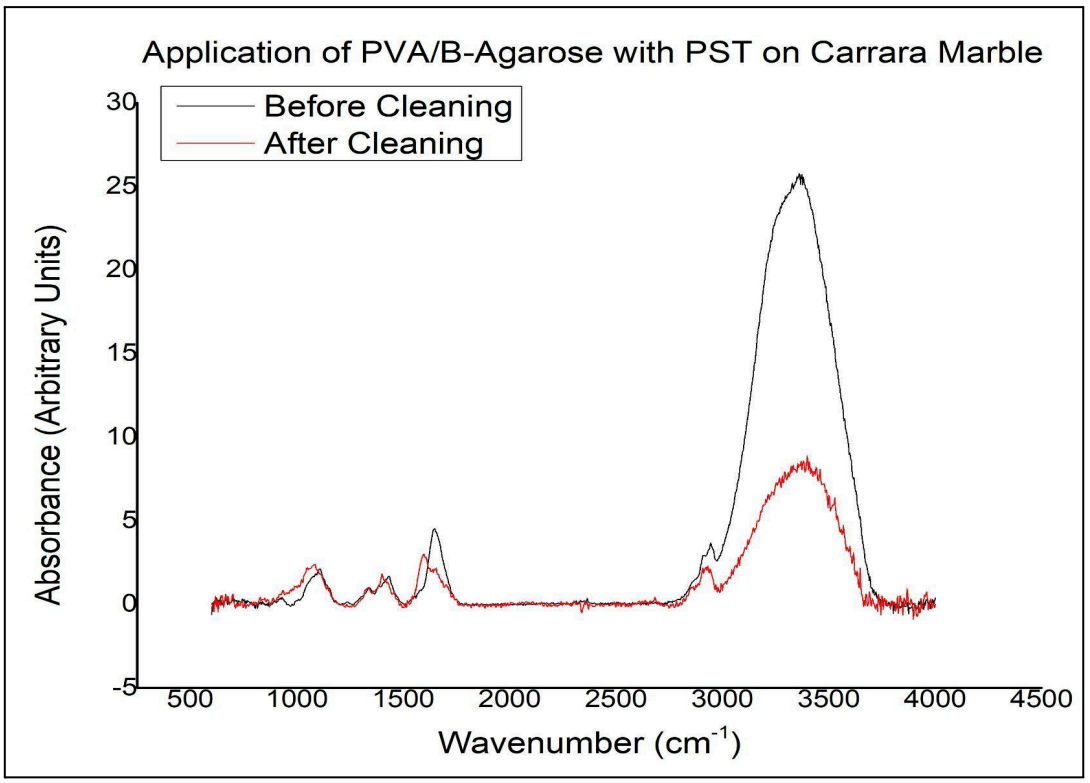

Figure 31. Superimposed ATR-FTIR spectra of PVA/B-AG with PST (PD11) before and after second cleaning Carrara Marble.

3.2.3 CLEANING OF LECCE STONE

3.2.3.1 MORPHOLOGICAL STRUCTURE

The contamination of Lecce Stone led to a very different surface morphology (see Figure 37). The surface was covered entirely with different small crystals, creating a spatially heterogeneous texture. After cleaning with PD10, the surface roughness is not returned to the original state but a lot of crystals are gone. After cleaning with PD11, spheroidal crystals embedded in crevices and pitting get exposed and this is indicative that an antecedent layer has already been removed. There are no fibrils seen in the areas examined too, which suggests little to no HVPD residues were left.

For the area cleaned with PD10, the BSE image shows a high contrast between the stone grains and the corrosion products (see Figure 38). The heavier atoms are more dispersed throughout the matrix of lighter atoms. The first point of interest is a white crystal. The EDS spectrum has copper $L_{\alpha 1}$ and $K_{\alpha 1}$ peaks at 0.90 keV and 8.00 keV, respectively, oxygen $K_{\alpha 1}$ peak at 0.50 keV, carbon $K_{\alpha 1}$ peak at 1.20 keV, sulfur $K_{\alpha 1}$ peak at 2.30 keV, and a calcium $K_{\alpha 1}$ peak at 3.60 keV. This confirms that copper sulfates and hydroxides are still scattered throughout the surface. The second point of interest is one of the gray grains, which only had

the calcium $K_{\alpha 1}$ peak, carbon $K_{\alpha 1}$ peak, and oxygen $K_{\alpha 1}$ peak, suggesting the disinterring of the original substrate surface.

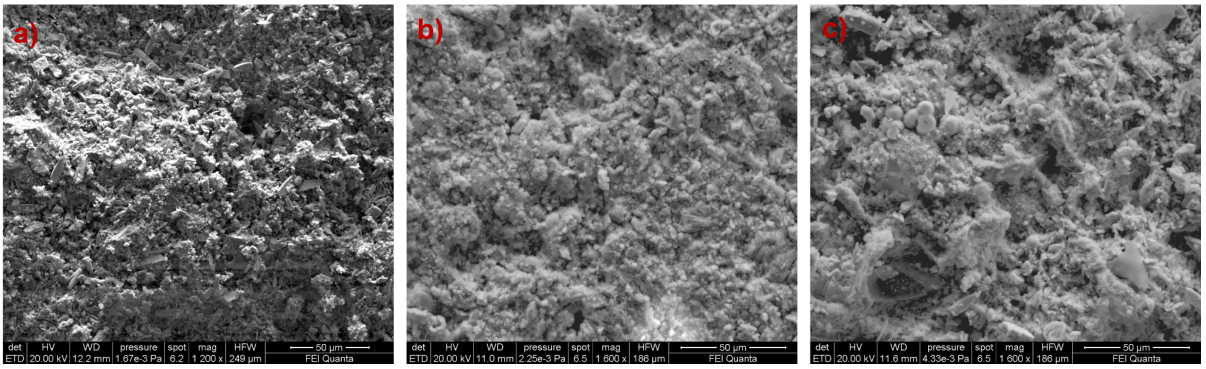

Figure 32. SE micrographs of Lecce Stone after (a) contamination with bronze corrosion products, (b) cleaning with PVA/B-AG with EDTA (PD10), and (c) cleaning with PVA/B-AG with PST (PD11).

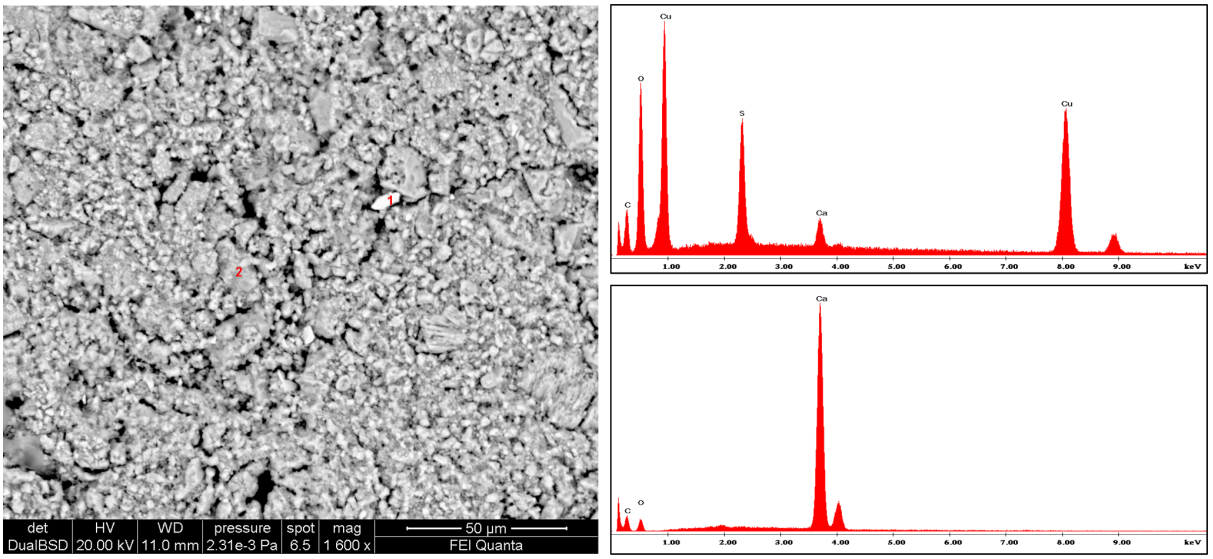

Figure 33. BSE micrograph after cleaning of Lecce Stone with PVA/B-AG with EDTA (PD10) and the corresponding EDS spectra of the selected points in red.

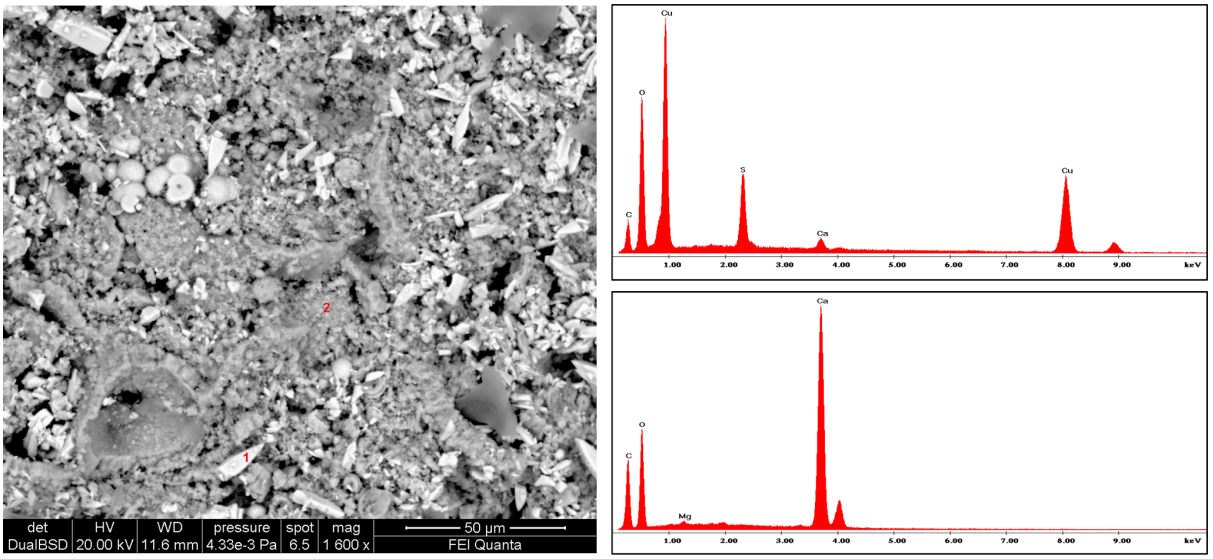

Figure 34. BSE micrograph after cleaning of Lecce Stone with PVA/B-AG with PST (PD11) and the corresponding EDS spectra of the selected points in red.

For the area cleaned with PD11, the BSE image also shows a high contrast. It is noticeable, however, that the extent of cleaning is less effective. The heavier atoms are still concentrated in the crystals across the matrix composed of lighter atoms (see Figure 39). The first point of interest is a white crystal containing either copper sulfates or hydroxides. There is a copper $L_{\alpha 1}$ peak at 0.90 keV, a copper $K_{\alpha 1}$ peak at 8.00 keV, a sulfur $K_{\alpha 1}$ peak at 2.30 keV, and an oxygen peak at $K_{\alpha 1}$ peak. The second point of interest is one of the gray grains. There is a calcium $K_{\alpha 1}$ peak at 3.60 keV, carbon $K_{\alpha 1}$ peak at 1.20 keV, oxygen $K_{\alpha 1}$ peak at 0.50 keV, and magnesium $K_{\alpha 1}$ peak at 1.20 keV. This suggests that there is already an exposure of the original substrate surface but there remains a lot of corrosion products yet to be removed.

3.2.3.2 COLORIMETRIC CHANGE

Lecce Stone blocks were cleaned for four hours with two different HVPDs. The first area was cleaned with PVA/B-AG with EDTA (PD10) while the second area was cleaned with PVA/B-AG with PST (PD11). All delta values reported are determined against the control. The aim is to lessen the degree of the difference and to obtain a high removal efficiency.

After the first application of PD10 (see Table VIII), there is already a noticeable change in the color of the stone. The cleaned surface is darker than the original surface, but the Δa* parameter is about 5 times lower and the Δb* parameter is about 3 times lower. The magnitude of ΔE_{ab}* decrease from 29.14 to 24.53, with a removal efficiency of 15.83%. Despite the drastic decrease in the green and blue component, the darkening is significant. After the second application, the surface was much lighter than the original. The Δa* value and the Δb* values are both 5 times lower. The magnitude of ΔE_{ab}* decrease to 13.07 with a removal efficiency of 55.14%. However, the significant increase in the ΔL* parameter suggests a partial erosion or solubilization of the surface.

After the first application of PD11 (see Table VIII), there was already a significant change in the color of the stone. The surface remains darker than the original and the Δa* parameter is lower and the Δb* parameter cross over from negative to positive. The magnitude of ΔE_{ab}* decrease from 29.14 to 20.40 with a removal efficiency is 29.64%. After the second application, the surface is now lighter than the original, the Δa* value is 20 times lower and the Δb* value is 3 times higher. The magnitude of ΔE_{ab}* decrease 15.66 with a removal efficiency of 46.01%. There is also a significant increase in the ΔL* parameter is symptomatic of a partial erosion or solubilization of the surface.

Table VIII. Average colorimetric parameters of Area 1 and Area 2 of Lecce Stone surfaces with plain stone as control. Area 1 was cleaned with PVA/B-AG with EDTA (PD10) while Area 2 was cleaned with PVA/B-AG with PST (PD11).

	AREA 1				AREA 2			
	ΔL*	Δa*	Δb*	ΔE_{ab}*	ΔL*	Δa*	Δb*	ΔE_{ab}*
1st Application	-23.09	-4.42	-5.43	24.53	-13.68	-8.80	0.84	20.40
2nd Application	11.94	-0.96	4.71	13.07	15.13	-1.97	3.45	15.66

Overall, it seems that cleaning with PD10 result in a more extensive change compared to cleaning with PD11. The results show that cleaning is more challenging for Lecce Stone despite having smaller crystals on the surface. There seems to be an external layer mainly composed of the green-colored corrosion products and an internal layer composed of blue-colored corrosion products. Multiple applications are therefore required but the succeeding ones have to be modulated to avoid the partial erosion or solubilization of the original surface.

3.2.3.3 HVPD-CONTAMINANT INTERACTION

The first HVPD applied to Lecce Stone for 4 hours was PVA/B-AG with EDTA (PD10) (see Figure 41). Similar to the blank, the bands can be assigned as follows: 3370 cm^{-1} for O-H stretching, 2856 cm^{-1} for C-H stretching, 1658 cm^{-1} for O-H bending, 1334 and 1416 cm^{-1} for asymmetric B-O-C stretching, 1106 cm^{-1} for in-plane C-H bending and C-N stretching, 1083 cm^{-1} for C-O-C stretching, and 929 cm^{-1} for -CH_2 stretching.[45,66] One of the main differences is the shoulder peak at 1549 cm^{-1} which could be the shifted band from 1658 cm^{-1}. This highlights the increased interaction of the coordination compounds with the hydroxyl groups of the polymer chain as a reversible cross-linker. [103] This is supported by the shifting to 890 cm^{-1} of the band for C-O stretching, which could be due to the change in bond length resulting from the new interaction. There is also a weak band at 827 cm^{-1} for Cu-O stretching, indicating the formation of a copper-EDTA complex.[101]

The second HVPD applied to Lecce Stone for 4 hours was PVA/B-AG with PST (PD11) (see Figure 42). Similar to the blank, the bands can be assigned as follows: 3367 cm^{-1} for O-H stretching, 2927 cm^{-1} for the symmetrical -CH_2 stretching, 2863 cm^{-1} for C-H stretching, 1648 cm^{-1} for O-H bending, 1338 and 1416 cm^{-1} for asymmetric B-O-C stretching, 1106 cm^{-1} for in-plane C-H bending, and 933 cm^{-1} for -CH_2 stretching.[66,80] The band at 827 cm^{-1} corresponds to Cu-O stretching of the copper-PST complex.[104] However, unlike other results, there is no shifting in the band at 1648 cm^{-1} for O-H bending. It is possible that the sample analyzed did not contain much of the copper-PST complex to elicit a significant change in association with the hydroxyl group of the chains. [104]

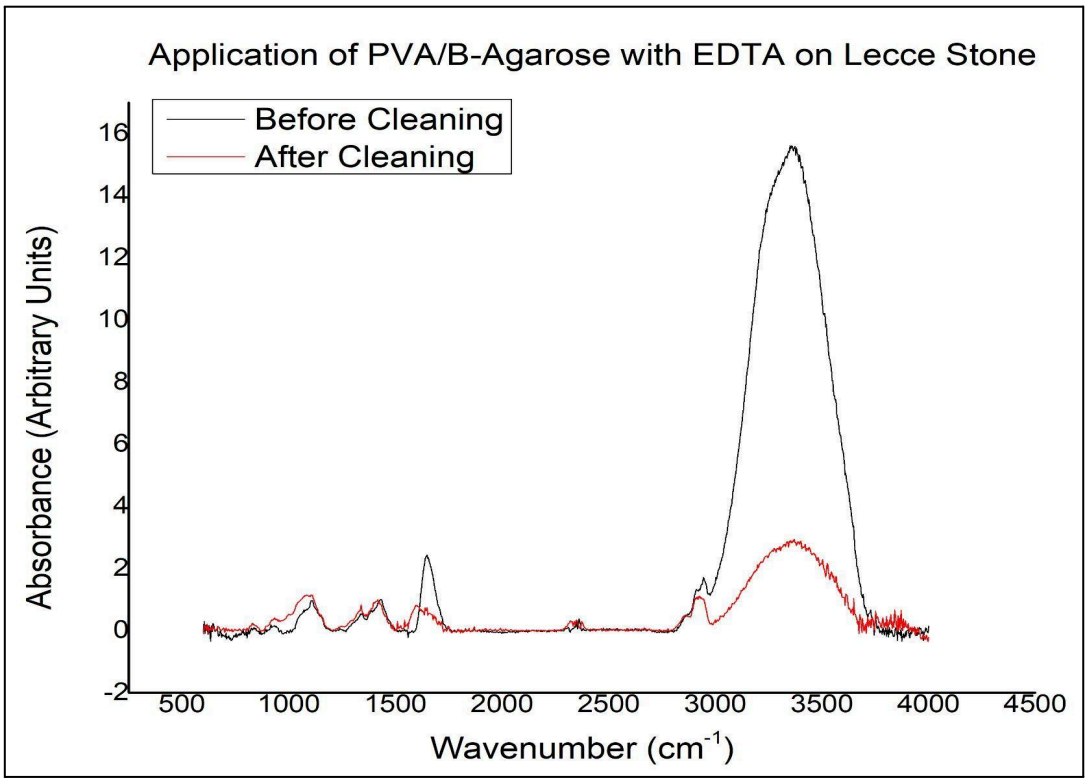

Figure 35. Superimposed ATR-FTIR spectra of PVA/B-AG with EDTA (PD10) before and after second cleaning Lecce Stone.

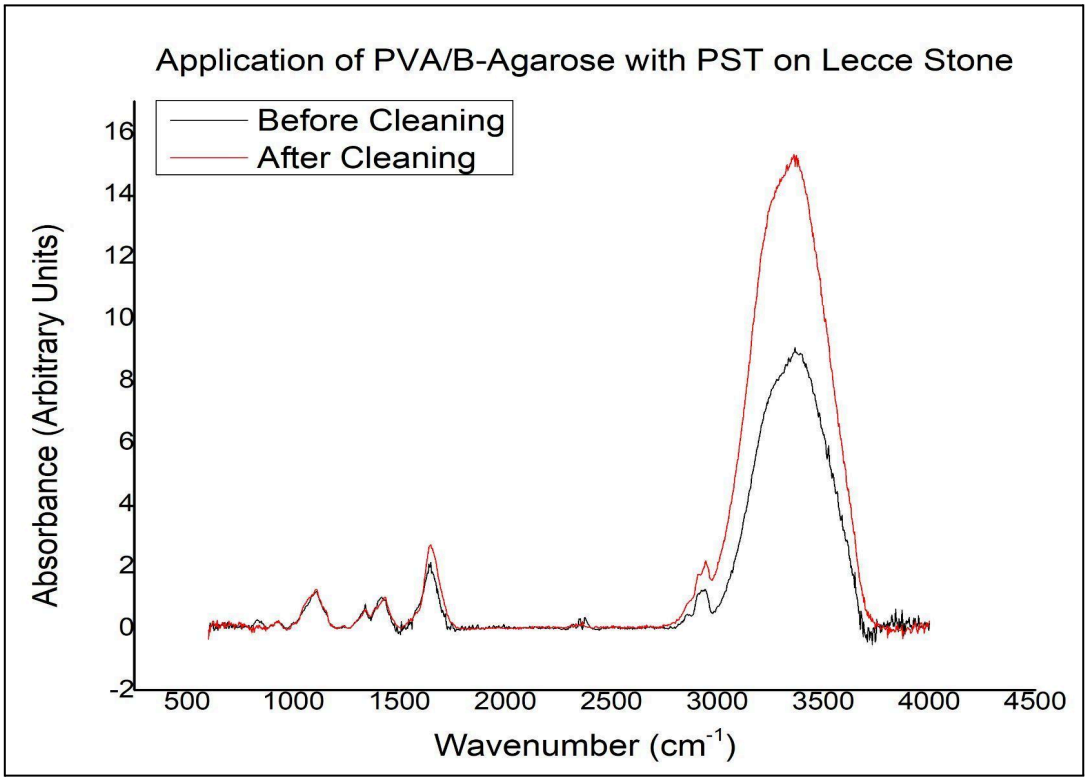

Figure 36. Superimposed ATR-FTIR spectra of PVA/B-AG with PST (PD11) before and after second cleaning Lecce Stone.

3.2.4 CLEANING OF TRAVERTINE

3.2.4.1 MORPHOLOGICAL STRUCTURE

The contamination of Travertine significantly changed its surface morphology into an asperous one filled with crystals of various shapes and sizes (see Figure 43). Based on the micrographs, cleaning with PD10 and PD11 remove a great portion of the corrosion products but not completely. The texture of the surface do not return to its original state and remain irregular. Some spheroidal crystals and pitting are exposed, suggesting there are also several layers of corrosion products formed. On a positive note, there were no HVPD residues left behind after cleaning in the areas examined.

For the area cleaned with PD10, the BSE image shows a high contrast between the stone grains and the corrosion products (see Figure 45). The first point of interest is a white crystal. Similar to other results, the EDS spectrum has copper $L_{\alpha 1}$ and $K_{\alpha 1}$ peaks at 0.90 keV and 8.00 keV, oxygen $K_{\alpha 1}$ peak at 0.50 keV, carbon $K_{\alpha 1}$ peak at 1.20 keV, sulfur $K_{\alpha 1}$ peak at 2.30 keV, and calcium $K_{\alpha 1}$ peak at 3.60 keV. The crystal therefore constituted copper-based compounds and some calcium carbonate originally present in the stone. The second point of interest was one of the gray grains, which only has the calcium $K_{\alpha 1}$ peak, carbon $K_{\alpha 1}$ peak, and oxygen $K_{\alpha 1}$ peak. It is mainly composed of calcium carbonate.

For the area cleaned with PD11, the BSE image also shows a high contrast but it is evident that the cleaning was not as effective (see Figure 45). There are crystals of varying shapes and sizes still dispersed throughout the surface. The first point of interest is a white crystal crystal. There is a copper $L_{\alpha 1}$ peak at 0.90 keV, a copper $K_{\alpha 1}$ peak at 8.00 keV, a sulfur $K_{\alpha 1}$ peak at 2.30 keV, and an oxygen peak at $K_{\alpha 1}$ peak, which implies the presence of copper sulfates and hydroxides. The second point of interest was one of the gray grains. There was a calcium $K_{\alpha 1}$ peak at 3.60 keV, carbon $K_{\alpha 1}$ peak at 1.20 keV, and oxygen $K_{\alpha 1}$ peak at 0.50 keV, corresponding to calcium carbonate.

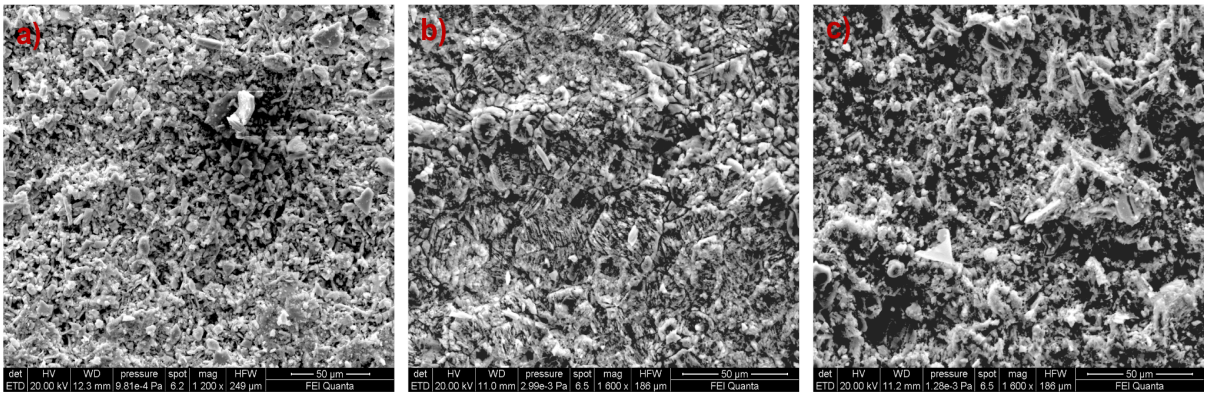

Figure 37. SE micrographs of Travertine after (a) contamination with bronze corrosion products, (b) cleaning with PVA/B-AG with EDTA (PD10), and (c) cleaning with PVA/B-AG with PST (PD11).

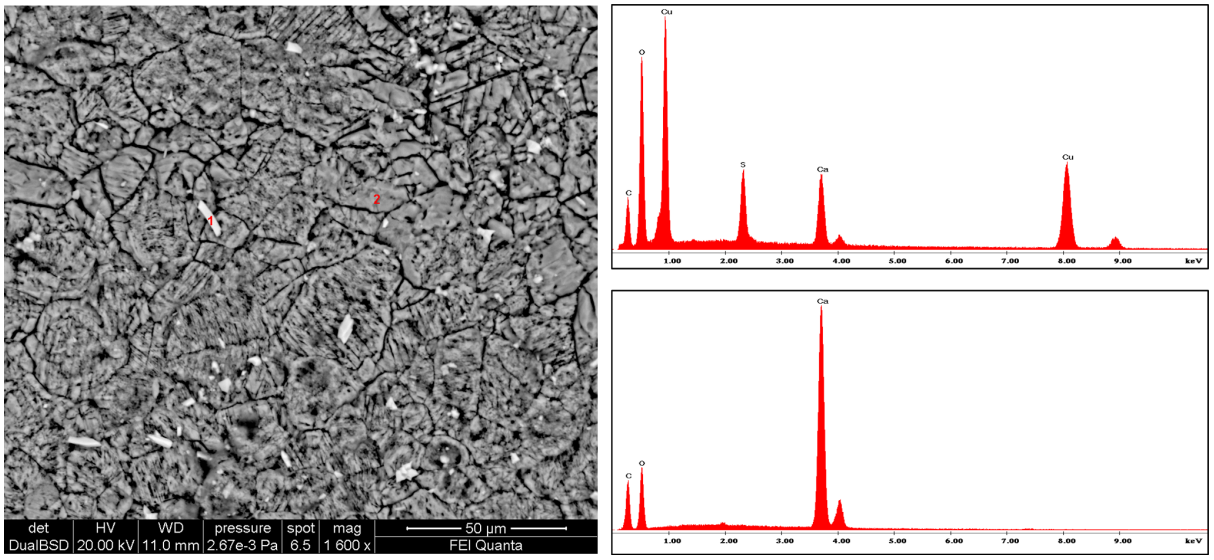

Figure 38. BSE micrograph after cleaning of Travertine with PVA/B-AG with EDTA (PD10) and the corresponding EDS spectra of the selected points in red.

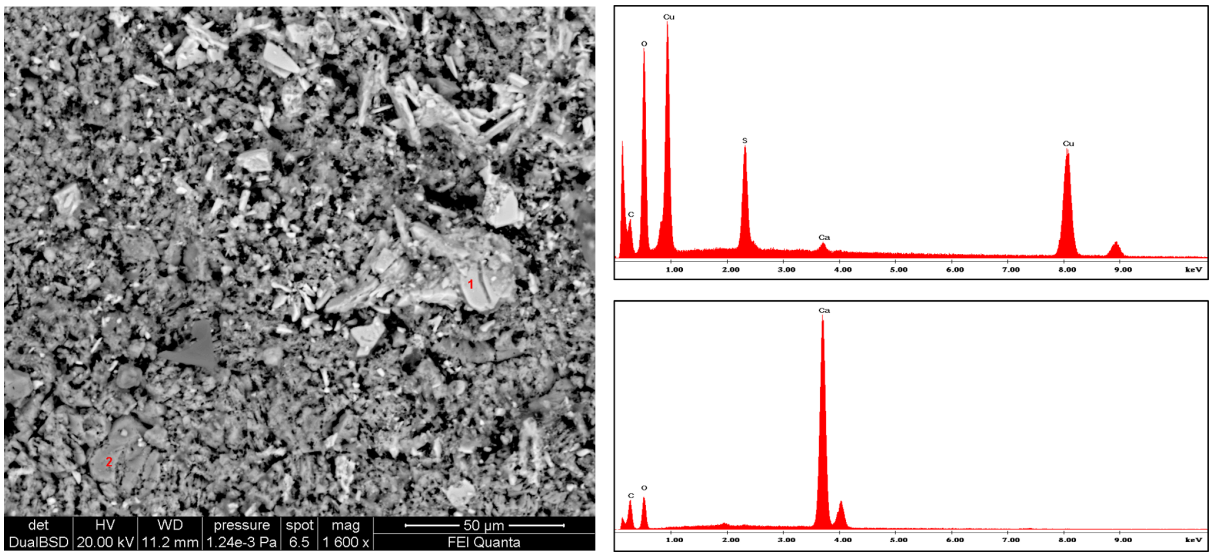

Figure 39. BSE micrograph after cleaning of Travertine with PVA/B-AG with PST (PD11) and the corresponding EDS spectra of the selected points in red.

3.2.4.2 COLORIMETRIC CHANGE

Travertine blocks were also cleaned for four hours with two different HVPDs. The first area was cleaned with PVA/B-AG with EDTA (PD10) while the second area was cleaned with PVA/B-AG with PST (PD11). All delta values reported are determined against the control. The goal is to reduce the delta values of the colorimetric parameters and obtain a high removal efficiency.

After the first application of PD10 (see Table IX), there is already an extensive change in the color of the stone. The surface become darker than the original, but the Δa* parameter is 4 times lower while the Δb* parameter is 2 times lower. The magnitude of ΔE_{ab}* decrease from 36.08 to 25.66 with removal efficiency of 28.86%. After the second application, the surface become lighter than the original surface. The Δa* parameter is 12 times lower and the Δb*

parameter 16 times lower, approaching closer to zero in value. The magnitude of ΔE_{ab}* decrease to 19.44 with a removal efficiency of 46.11%. Similar to the other stones, there is a significant increase in the ΔL* parameter which suggests the partial erosion or solubilization of calcium carbonate.

Table IX. Average colorimetric parameters of Area 1 and Area 2 of Travertine surfaces with plain stone as control. Area 1 was cleaned with PVA/B-AG with EDTA (PD10) while Area 2 was cleaned with PVA/B-AG with PST (PD11).

	AREA 1				AREA 2			
	ΔL*	Δa*	Δb*	ΔE_{ab}*	ΔL*	Δa*	Δb*	ΔE_{ab}*
1st Application	-20.77	-6.65	-8.55	25.66	-25.97	-7.30	-6.14	27.76
2nd Application	19.22	-2.18	1.01	19.44	13.81	-0.75	3.32	14.35

After the first application of PD11, there was already an apparent change in the color of the stone (see Table IX). The surface get darker than the original surface, but the Δa* parameter is 3 times lower while the Δb* parameter 2 times lower. The magnitude of ΔE_{ab}* decrease from 31.34 to 27.76, with a removal efficiency is 11.44%. After the second application of PD11, there is visibly more change. The surface become lighter than the original surface. The Δa* parameter is 30 times lower and the Δb* parameter 3 times lower. The magnitude of ΔE_{ab}* decrease to 14.35 with a removal efficiency of 54.2%. The case of excessive lightening is observed again, which could be due to the partial erosion or solubilization of the stone.

Overall, it seems that cleaning with PD11 result in a more extensive change compared to cleaning with PD10 for Travertine. The results show that cleaning is also challenging for Travertine which also has several layers of products. The external layer seems mainly composed of the green-colored corrosion products while the internal layer seems composed of blue-colored corrosion products. Multiple applications are therefore required for the complete removal of the products and the succeeding ones have to be modulated to avoid the partial erosion or solubilization of the stone surface.

3.2.4.3 HVPD-CONTAMINANT INTERACTION

The first HVPD applied to Travertine for 4 hours was PVA/B-AG with EDTA (PD10) (see Figure 47). Similar to the blank, the bands can be assigned as follows: 3353 cm^{-1} for O-H stretching, 2934 cm^{-1} for symmetrical -CH_2 stretching, 2907 cm^{-1} for C-H stretching, 1644 cm^{-1} for O-H bending, 1338 and 1403 cm^{-1} for asymmetric B-O-C stretching, 1110 cm^{-1} for in-plane C-H bending and C-N stretching, 1069 cm^{-1} for C-O-C stretching and glycosidic linkage, and 933 cm^{-1} for -CH_2 stretching. [45,66] Consistent with the other results, there is a band at 827 cm^{-1} for Cu-O stretching, highlighting the metal-ligand complex formation of

EDTA and the copper ion.[101] There is also a shoulder formed due to the shifting of the band at 1644 cm^{-1} to 1589 cm^{-1}, which is due to the association of the coordination compound with the hydroxyl groups of the polymer.[101]

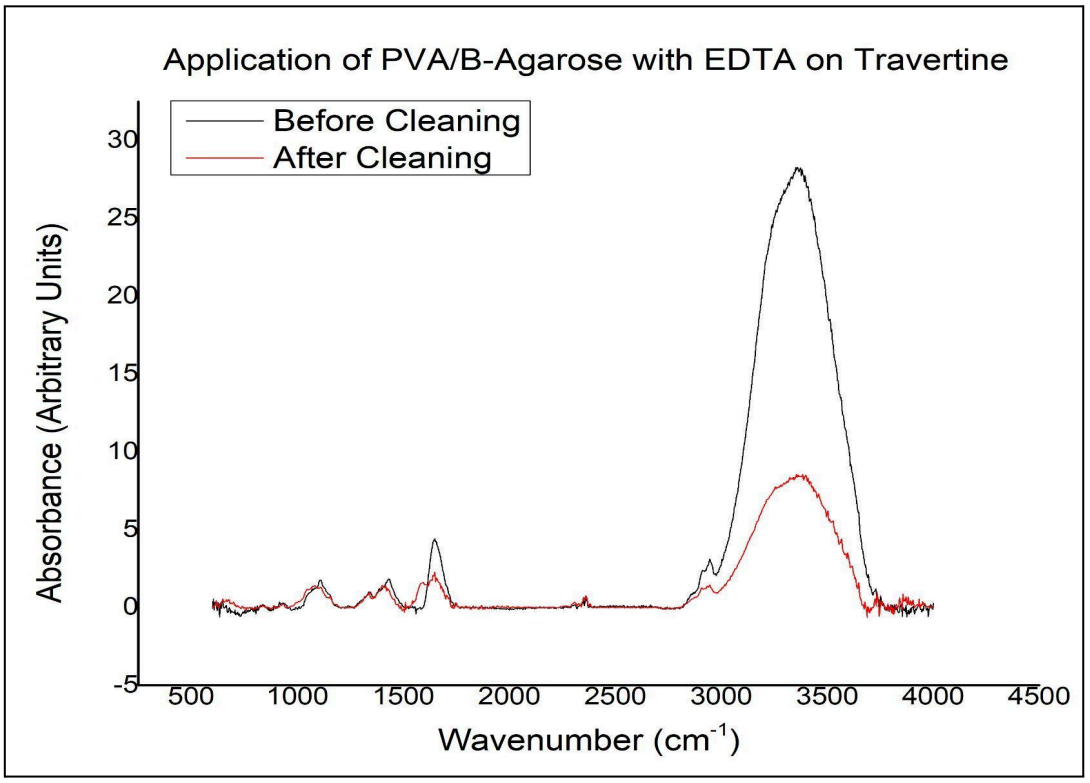

Figure 40. Superimposed ATR-FTIR spectra of PVA/B-AG with EDTA (PD10) before and after cleaning Travertine.

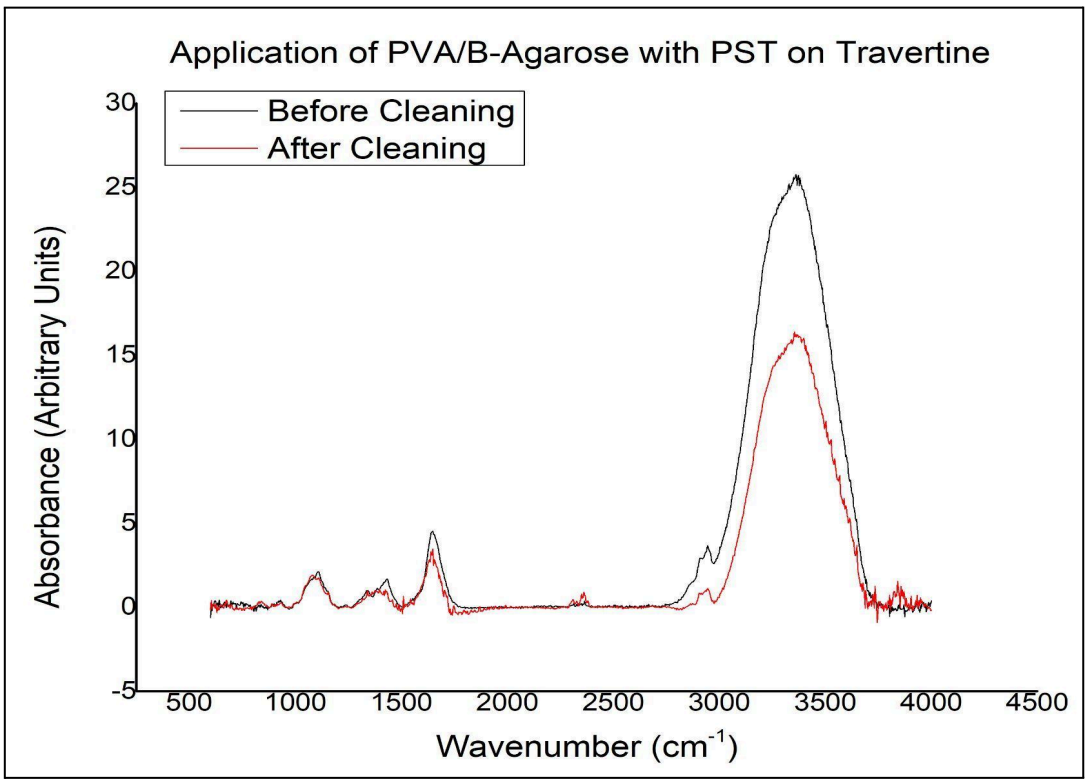

Figure 41. Superimposed ATR-FTIR spectra of PVA/B-AG with PST (PD11) before and after cleaning Travertine.

The second HVPD applied to Travertine for 4 hours was PVA/B-AG with PST (PD11) (see Figure 48). Similar to the blank, the bands can be assigned as follows: 3353 cm^{-1} for O-H stretching, 2934 cm^{-1} and 2944 cm^{-1} for the asymmetrical and symmetrical -CH_2 stretching, 2907 cm^{-1} for C-H stretching, 1644 cm^{-1} for O-H bending, 1338 and 1423 cm^{-1} for asymmetric B-O-C stretching, 1106 cm^{-1} for the in-plane C-H bending, at 1069 cm^{-1} for C-O-C stretching, and at 933 cm^{-1} for -CH_2 stretching.[66,80] There is a band at 827 cm^{-1} for Cu-O stretching, showing the complex formation of the chelant and the contaminant. There is no shifting in the band at 1648 cm^{-1} for O-H bending. Such as the case in Lecce Stone, it is possible that the sample analyzed did not contain much of the copper-PST complex to elicit a significant change in association with the hydroxyl group of the chains.[104]

3.2.5 SUMMARY OF RESULTS

The three lithotypes were contaminated with products leaching from artificial corrosion patinas in a bronze alloy. Based on morphological studies, crystals of different typologies are found on the substrate surfaces containing copper, sulfur, and oxygen. Since Carrara Marble has lower porosity, there are less nucleation sites but crystal growth is observed. Most of the products seem to be concentrated on the surface, resulting in higher delta values in colorimetry. Lecce Stone has higher porosity, with small pores and a pore capillary network. The high surface area provide multiple nucleation sites but not much crystal growth. The pore interconnectivity also allow for a more extensive product diffusion which translated to lower delta values in colorimetry. Lastly, Travertine has the highest porosity with larger pore sizes of irregular shape. This also provide multiple nucleation sites and promoted crystal growth. There is product diffusion as well but not that extensive, yielding to a delta value in between that of Lecce Stone and Carrara Marble.[49,53,54]

Two kinds of HVPDs were applied to clean the stone surfaces: PVA/B-AG with EDTA (PD10) and PVA/B-AG with PST (PD11) (see Table X). For Carrara Marble, both cleaning methods result in the reduction of crystals found on the surface. The stone grains become visible again but the corrosion-induced striations remain. From colorimetric data, PD10 has a higher removal efficiency. For Lecce Stone, both cleaning methods are able to remove an external layer of corrosion products but leave exposed an internal layer with raw and spheroidal crystals. In terms of crystal size, however, PD10 leave smaller crystals dispersed throughout the surface while PD11 left larger crystals in localized regions. The existence of layers is reflected in the colorimetry results where the green component drastically decreases first before the blue component. Colorimetric data also show that PD10 has a higher removal efficiency. For Travertine, both cleaning methods significantly removed crystals from the

surface but there remains another layer of corrosion products. PD10 leave smaller crystals while PD11 leave

Table X. Digital images of stone surfaces before and after cleaning with PD10 (left) and PD11 (right).

	Contaminated Stone	Cleaned Stone
CM		
LS		
T	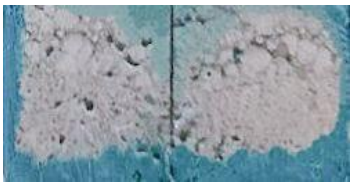	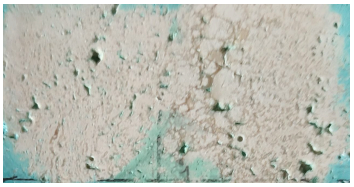

larger crystals and aggregates. From colorimetric data, however, PD11 has a close but slightly higher removal efficiency. It must be noted here that this does not necessarily contradict the other results because there is still the inherent heterogeneity of the surfaces that must be accounted for.

Comparing the three lithotypes, the cleaning methods are most effective for Carrara Marble because all of the corrosion products are concentrated on the surface. For Lecce Stone and Travertine, the cleaning methods also remove a lot of the corrosion products, albeit less extensively. Due to their porosities, several layers of corrosion products form which make removal more challenging. Two applications have to be done regardless of lithotype to approximate the color of the original surface. It is important though to modulate the succeeding applications to avoid excessive lightening of the surface, brought by the partial erosion or solubilization of calcium carbonate from the surface. It is also better to limit each application to four hours to avoid leaving HVPD residues on the surface.

In terms of effectiveness, EDTA appears to be generally more powerful chelant compared to PST. Both are labile and can move around the network but they have a significant difference in their formation constants (K_f) with copper (II). At room temperature, EDTA has a K_f of 5.01×10^{18} L/mol while PST has a K_f of 1.00×10^{14} L/mol.[105,106] From the FT-IR spectra, the metal-ligand complex formed by EDTA also has a higher degree of association with the hydroxyl groups of the network as seen in the shifting of the band for O-H bending. There is also a certain degree of association with the complex formed by PST, but not significant enough to see a visible shift in the spectra.

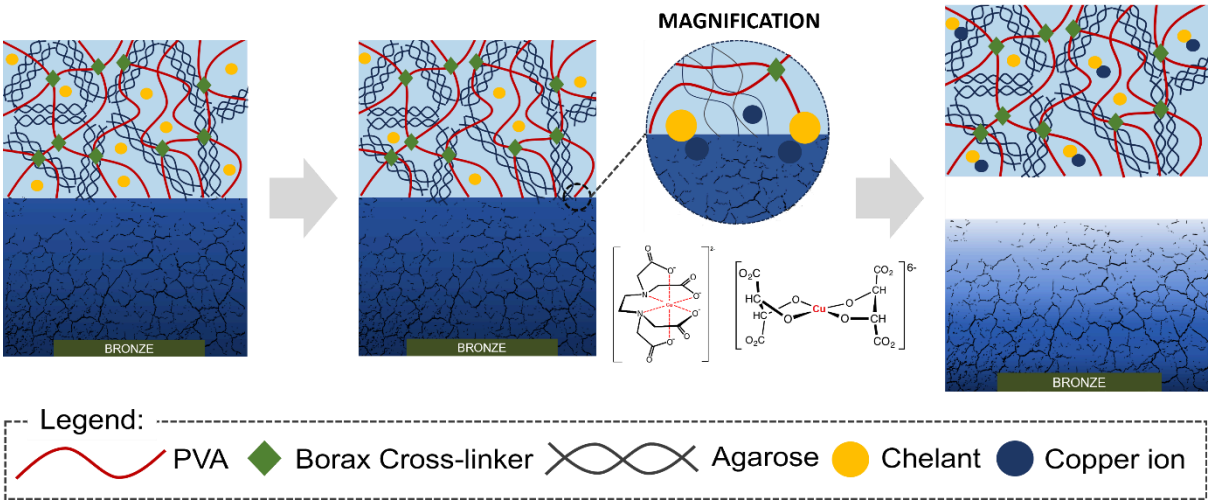

Figure 42. Proposed general mechanism of the cleaning of bronze corrosion products from the stone surface using PVA/B-AG HVPDs loaded with chelants.

3.3 CLEANING OF PARALOID® B72

3.3.1 ARTIFICIAL ACCELERATED AGING

3.3.1.1 COLORIMETRIC CHANGE

The three lithotypes were coated with approximately 2 mm of 3.0% w/v Paraloid® B72. After aging, the area was then divided into four for the application of two HVPDs at different treatment periods. In the summarized tables, the different colorimetric parameters reveal which direction the change happened relative to the control (see Table XI and XII).

For the L* parameter, the delta values are all negative. The darkening of the surface is clearly visible and the most drastic change is with Lecce Stone. For the a* parameter, the delta values are all positive which means that the surface shifts towards red. The highest magnitude of change is with Travertine. For the b* parameter, the delta values vary slightly. For Carrara Marble, the delta values are negative which indicates that the surface color shift towards blue. Meanwhile, for Lecce Stone and Travertine, the delta values are positive which indicates that their surfaces appear more yellow. The magnitude of ΔE_{ab}* is consistently greater than 20 across all samples, signifying an apparent chromatic change due to aging.

It is difficult to point out the exact reason for the differences in the response of the polymer for each stone. However, the extent of interaction between the polymer and the substrate might be contributing. For Carrara Marble, the polymer-substrate contact is limited to the surface of the stone. The photo-oxidative reactions taking place therefore might be more homogeneous. For Lecce Stone and Travertine, due to their high porosities, the polymer-substrate contact likely extends to a certain depth underneath the surface. For Lecce Stone, which has smaller pores and a capillary network, some of the polymers are not directly exposed to light and oxygen. For Travertine, which has larger pores, there might be an

oxygen gradient but most areas are still reachable by light. Hence, the polymer degradation processes might vary depending on the part being examined. Darkening is most extensive for Lecce Stone because probably chain cross-linking reactions dominate, promoting polymer aggregation in localized areas. Yellowing and reddening is most extensive for Travertine because probably photolysis and radical reactions govern, leading to the formation of chromophores with carbonyl groups, double bonds, and conjugated structures.[57,61,62(bk)]

Tabke XI. Average colorimetric parameters of Area 1 and Area 2 in which the two selected HVPDs would be applied for 2 hours. Area 1 would be cleaned with PVA/B (PD1) and Area 2 would be cleaned with PVA/B-AG (PD9).

	AREA 1				AREA 2			
	ΔL*	Δa*	Δb*	ΔE_{ab}*	ΔL*	Δa*	Δb*	ΔE_{ab}*
Carrara Marble	-24.43	0.09	-3.18	24.67	-23.65	0.23	-2.80	23.92
Lecce Stone	-24.55	1.99	4.22	25.01	-25.53	2.60	5.51	26.29
Travertine	-16.78	4.09	14.23	22.72	-17.07	3.96	12.56	22.56

Table XII. Average colorimetric parameters of Area 1 and Area 2 in which the two selected HVPDs would be applied for 24 hours. Area 3 would be cleaned with PVA/B (PD1) while Area 4 would be cleaned with PVA/B-AG (PD9).

	AREA 3				AREA 4			
	ΔL*	Δa*	Δb*	ΔE_{ab}*	ΔL*	Δa*	Δb*	ΔE_{ab}*
Carrara Marble	-20.08	0.069	-2.46	20.34	-19.06	0.13	-2.53	19.32
Lecce Stone	-25.24	2.69	6.60	26.34	-26.40	2.74	5.98	27.26
Travertine	-21.40	3.56	11.79	26.86	-17.40	4.17	14.44	23.36

3.3.2 CLEANING OF CARRARA MARBLE

3.3.2.1 COLORIMETRIC CHANGE

Two HVPDs were selected for the removal of Paraloid® B72, specifically, PVA/B (PD1) and PVA/B-AG (PD9). In the first and second areas, the HVPDs were applied on the surface of Carrara Marble for two hours (see Table XIII). In the third and fourth areas, the two HVPDs were applied on the surface for a day. They were covered with Parafilm to avoid drying (see Table XIV).

After the first application of PD1 for 2 hours, the ΔE_{ab}* value decrease from 24.67 to 20.95 with the ΔL* parameter having the greatest contribution. The extent of darkening is reduced by the cleaning but the area remain darker than the original surface. There is also a reversal in the signs of the Δa* and Δb* parameters but close to zero in value. Since the coating was thick, some degradation products initially trapped within the polymer chains might be drawn

out to the surface.[81,86] After the second and third application, all the parameters start decreasing in value. Subsequently, the magnitude of ΔE_{ab}* decrease to 16.46 with a removal efficiency of 33.22%. However, the issue of darkening remains to be addressed in order for the surface to return to the original color.

Meanwhile, after the first application of PD9 for 2 hours, the ΔE_{ab}* value decrease from 23.92 to 17.83. In line with the other results, the ΔL* parameter has the highest contribution and there is also a reversal in the signs of the Δa* and Δb* parameters. After the second and third application, the Δa* and Δb* parameters decrease but the ΔL* increased. This raise the magnitude of the ΔE_{ab}* value to 22.11 with a final removal efficiency is 7.56%. It is possible that the darkening is due to the rearrangement of the polymer chains in the aged resin and their aggregation during the cleaning process. This is seen in the delamination and flaking off of the aged resin. [81,86]

Table XIII. Average colorimetric parameters of Carrara Marble surfaces with plain stone as control. Area 1 was cleaned with PVA/B (PD1) while Area 2 was cleaned with PVA/B-AG (PD9) for 2 hours.

	AREA 1				AREA 2			
	ΔL*	Δa*	Δb*	ΔE_{ab}*	ΔL*	Δa*	Δb*	ΔE_{ab}*
1st Application	-20.82	-1.62	0.27	20.95	-17.67	-1.18	1.34	17.83
2nd Application	-16.40	-0.75	1.10	16.49	-22.04	-0.85	1.00	22.11
3rd Application	-16.37	-1.26	0.63	16.46	-21.99	-1.17	1.08	22.11

After the first application of PD1 for 24 hours, the ΔE_{ab}* value decrease from 20.34 to 14.55. The ΔL* parameter decrease while the Δa* and Δb* parameters change in sign. After the second application, the ΔE_{ab}* value increase to 17.43 with a removal efficiency of 14.29%. The issue remains to be the darkening of the surface, which might be due to the rearrangement of polymer chains induced by the adhesive forces of HVPD.

Table XIV. Average colorimetric parameters of Carrara Marble surfaces with plain stone as control. Area 3 was cleaned with PVA/B (PD1) while Area 4 was cleaned with PVA/B-AG (PD9) for 24 hours.

	AREA 3				AREA 4			
	ΔL*	Δa*	Δb*	ΔE_{ab}*	ΔL*	Δa*	Δb*	ΔE_{ab}*
1st Application	-14.32	-1.67	0.33	14.55	-14.63	-1.52	0.44	14.84
2nd Application	-17.32	-1.40	0.35	17.43	-13.79	-1.51	0.06	13.95

Meanwhile, after the first application of PD9, the ΔE_{ab}* value decrease from 19.32 to 14.84. The ΔL* parameter decrease while the Δa* and Δb* parameters change in sign close to zero. After the second application, the ΔE_{ab}* value decrease to 13.95 with a final removal efficiency of 27.80%.

Overall, based on colorimetry results, the best method of cleaning Carrara Marble is the multiple applications of PD9 for 24 hours. This method yield the lowest ΔE_{ab}* value and no darkening is observed during the process.

3.3.2.2 WATER VAPOR PERMEABILITY

The water vapor permeability of Carrara Marble was monitored for seven days at different points of the study (see Figure 55). During the initial days, there is a steady increase in the water vapor permeating through the stone. However, during the last days, there is minimal variation in the water vapor permeating through the stone. This is expected because the interconnected pores eventually get saturated and the stone reaches equilibrium with the environment. For the plain stone, the water vapor permeability plateaus at 72.31 g/m^2. After coating the stone blocks with Paraloid® B72, the value lowers to 61.28 g/m^2 which is equivalent to a 15.25% change relative to the control. This is expected because the exposed surfaces have been covered, thereby making the penetration of water vapor difficult. After aging the resin, there is not much difference. The value is 61.54 g/m^2 which is equivalent to a 14.89% change relative to the control. After the cleaning, the value slightly increased to 63.59 g/m^2, which reduces the difference to 12.06% relative to the control. While the results show that the aged resin has not been completely removed yet, the latest value approaches the original value which confirms that the aged resin is being removed by the HVPDs.[81,82]

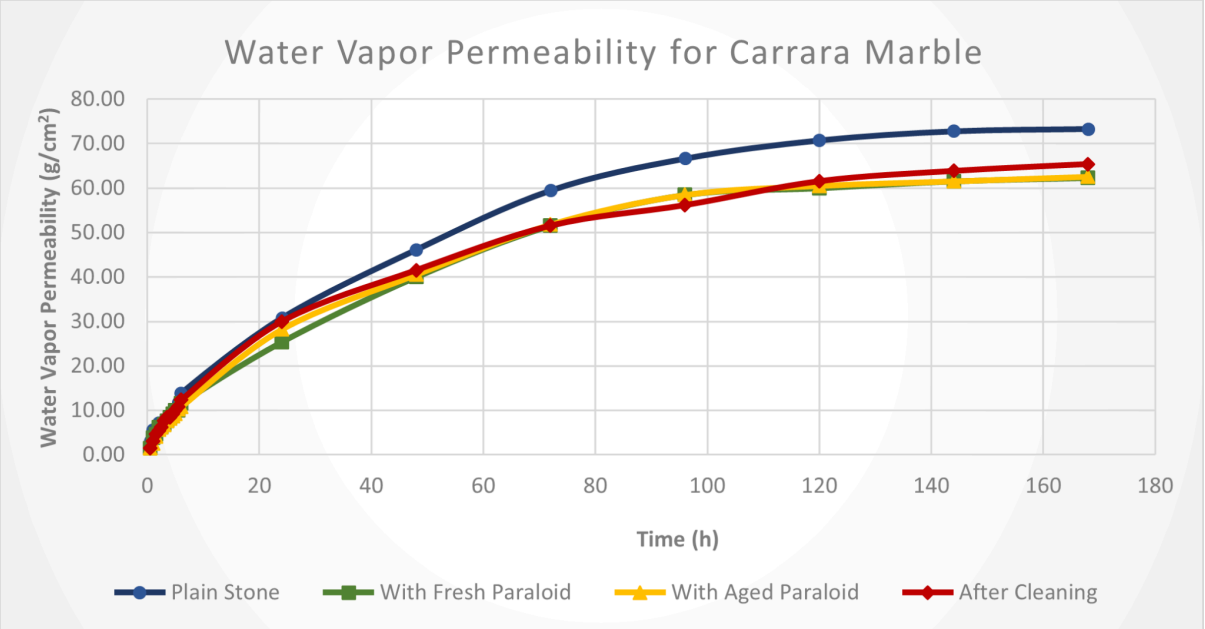

Figure 43. Water vapor permeability curve of Carrara Marble before coating (blue), after coating with Paraloid® B72 (green), after artificial accelerated aging (yellow), and after cleaning (red).

3.3.2.3 HVPD-CONTAMINANT INTERACTION

The first HVPD applied to Carrara Marble was PVA/B (PD1) for a period of 2 hours and 24 hours. Between the two FTIR spectra, the bands present are very similar except the band intensity after 24 hours of cleaning is slightly higher than after 2 hours.

The vibrational modes originating from the PVA polymer chain cross-linked with Borax are still visible in the spectra. The bands can be assigned as follows: 3360 cm^{-1} for O-H bending, 2940 cm^{-1} for C-H stretching, 2930 cm^{-1} for symmetrical -CH_2 stretching, 1648 cm^{-1} for O-H bending, 1340 and 1420 cm^{-1} for asymmetric B-O-C stretching, 1090 cm^{-1} for in-plane C-H bending, 1070 cm^{-1} for C-O-C stretching, 930 cm^{-1} for -CH_2 stretching, 890 cm^{-1} for -CH_2 rocking, and 830 cm^{-1} for C-C stretching and out-of-plane C-H bending.[66,80]

Since the aged resin is an acrylate polymer, most of the spectral changes after cleaning are found between 800 to 2000 cm^{-1}.[x] While the intensity seems the same, the band width around 1650 cm^{-1} broaden probably due to the overlap with the band for ester C=O stretching. The bands around 1420 and 1340 cm^{-1} also seem less resolved due to the overlapping of the bands for the antisymmetric and symmetric bending of the methyl group in the α position. Some other bands that are weak but are of interest include: 1240 cm^{-1} for ester C-O stretching, 1070 cm^{-1} for O-C-C stretching of the ethyl ester., and for 810 cm^{-1} corresponds to the -CH_2 rocking of the alkyl group attached to the ester.[14,15,17,42,66] These signals are not intense which make

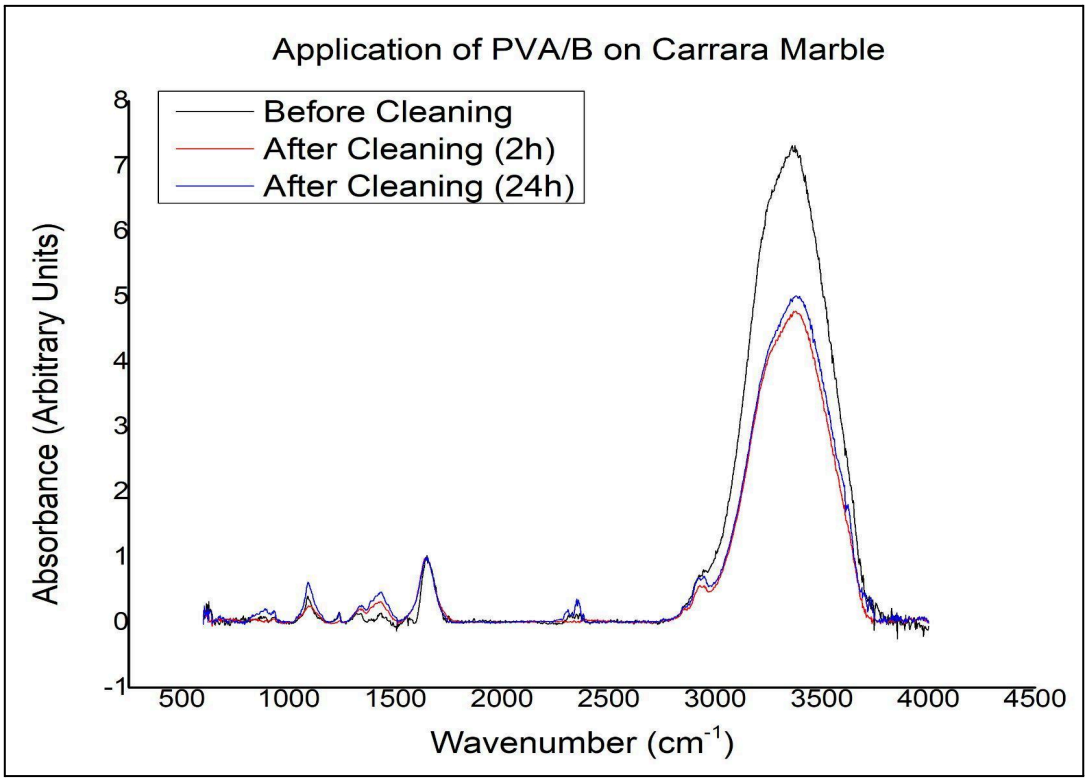

Figure 44. Superimposed ATR-FTIR spectra of PVA/B (PD1) before and after cleaning Carrara Marble for 2 and 24 hours.

assignment with confidence difficult. From the spectra alone, there does not seem to be a lot of molecular interaction between PVA/B and the aged acrylate resin.

The second HVPD applied to Carrara Marble was PVA/B-AG (PD9) for a period of 2 hours and 24 hours. The bands present in the two spectra are similar and can be assigned as follows: 3380 cm^{-1} for O-H bending, 2925 cm^{-1} for symmetrical -CH_2 stretching, 2940 cm^{-1} for C-H stretching, 1648 cm^{-1} for O-H bending, 1330 and 1410 cm^{-1} for asymmetric B-O-C stretching, 1110 cm^{-1} for in-plane C-H bending, 1070 cm^{-1} for C-O-C stretching and glycosidic linkage, 940 cm^{-1} for -CH_2 stretching, and 820 cm^{-1} for C-C stretching and out-of-plane C-H bending. [66,80] The bands corresponding to the aged resin are also visible in the spectra. The bands are found around 1650 cm^{-1} for ester C=O stretching, 1420 and 1340 cm^{-1} for the antisymmetric and symmetric bending of the methyl group in the α position, 1150 cm^{-1} for the C-C(=O)-O antisymmetric stretching, 1080 cm^{-1} for O-C-C stretching of the ethyl ester, and 810 cm^{-1} for the -CH_2 rocking of the alkyl group attached to the ester. [81,82]

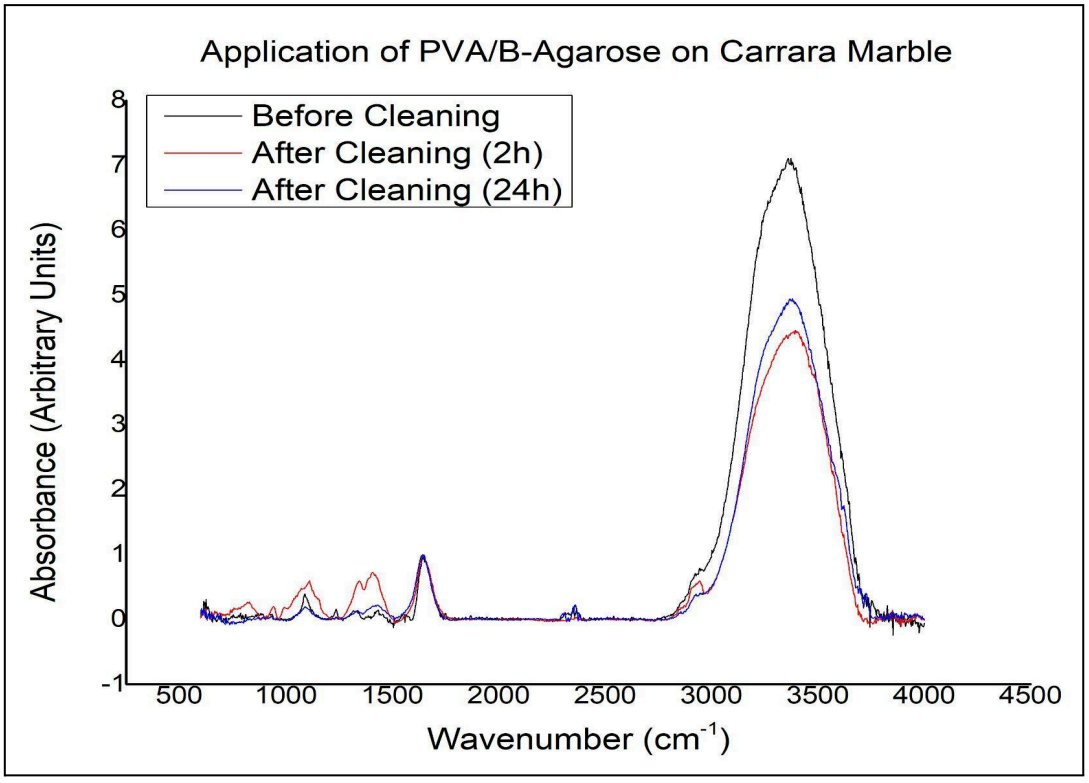

Figure 45. Superimposed ATR-FTIR spectra of PVA/B-AG (PD9) before and after cleaning Carrara Marble for 2 and 24 hours.

One point of interest here is that the band intensity after 2 hours of cleaning is much higher than after 24 hours of cleaning. This is in opposition to the results seen in PVA/B and therefore requires further investigation on the nature of the interaction between the HVPDs and aged resin. What can only be hypothesized for now is that the cleaning mechanism of PD9 is different from PD1. It is possible that, with the inclusion of agarose, there is a change in the HVPD compatibility with the resin. Agarose can alter the microenvironment of the

polymer network to make it favorable for the partial adhesion of the resin. The adhesive forces between the HVPD and the resin do not outweigh cohesive forces among the acrylate chains though, hence mostly flaking off or delamination is observed long-term.[107]

3.3.3 CLEANING OF LECCE STONE

3.3.3.1 COLORIMETRIC CHANGE

Two HVPDs were selected for the removal of Paraloid® B72: PVA/B (PD1) and PVA/B-AG (PD9). In the first and second areas, the HVPDs were applied on the surface of Lecce Stone for two hours (see Table XV). In the third and fourth areas, the two HVPDs were applied on the surface for a day. They were covered with Parafilm to avoid drying (see Table XVI).

After the first application of PD1 for 2 hours, the magnitude of ΔE_{ab}* halve from 25.01 to 12.57. The ΔL* parameter contribute significantly since it decreases to less than half its value. The Δa* parameter and the Δb* parameter decrease to a third of its value. After the second application, there is a slight decrease in all parameters. However, after the third application, the ΔL* parameter increase again which raise the ΔE_{ab}* value as a consequence, with a final removal efficiency of 42.00%.

Meanwhile, after the first application of PD9 for 2 hours, the magnitude of ΔE_{ab}* also halve from 26.29 to 13.02. The ΔL* parameter halve and the low values Δa* and Δb* parameters further decrease. After the second application, there is a slight decrease in all three parameters which brought down ΔE_{ab}* to 13.02. However, after the third application, the ΔL* parameter increase which then affected the ΔE_{ab}* value and the removal efficiency of 44.29%. Based on these results, a third application is not advised. More investigations regarding the mechanism of cleaning is essential to determine the cause of darkening.

Table XV. Average colorimetric parameters of Lecce Stone surfaces with plain stone as control. Area 1 was cleaned with PVA/B (PD1) while Area 2 was cleaned with PVA/B-AG (PD9) for 2 hours.

	AREA 1				AREA 2			
	ΔL*	Δa*	Δb*	ΔE_{ab}*	ΔL*	Δa*	Δb*	ΔE_{ab}*
1st Application	-11.91	-2.25	2.83	12.57	-13.12	-1.28	3.34	13.66
2nd Application	-8.05	-1.81	2.24	8.79	-12.70	-1.48	2.44	13.02
3rd Application	-14.14	-1.32	2.42	14.50	-14.39	-0.83	2.29	14.64

After the first application of PD1 for 24 hours, the magnitude of ΔE_{ab}* decrease from 26.34 to 14.78. The ΔL* parameter is still negative but halved in value. The Δa* and Δb* parameters also decrease. After the second application, all three parameters decreased so the ΔE_{ab}* lowered to 13.50 with a removal efficiency is 48.74%.

Meanwhile, after the first application of PD9 for 24 hours, the magnitude of ΔE_{ab}* decrease from 27.26 to 15.24. The ΔL* parameter almost halve while the Δa* and Δb* decrease. For the second application, all three parameters slightly decrease so the ΔE_{ab}* lowered to 14.78 with a removal efficiency of 45.80%.

Table XVI. Average colorimetric parameters of Carrara Marble surfaces with plain stone as control. Area 3 was cleaned with PVA/B (PD1) while Area 4 was cleaned with PVA/B-AG (PD9) for 24 hours.

	AREA 3				AREA 4			
	ΔL*	Δa*	Δb*	ΔE_{ab}*	ΔL*	Δa*	Δb*	ΔE_{ab}*
1st Application	-14.35	-1.28	3.23	14.78	-14.87	-1.06	3.02	15.24
2nd Application	-13.24	-1.12	2.19	13.50	-14.48	-0.96	2.49	14.78

Overall, based on the colorimetry results, it is difficult to determine the best method to clean Lecce Stone. Regardless of the HVPD, multiple applications are required for the removal of Paraloid® B72 and the ΔE_{ab}* values for all tests do not significantly vary and the issue of darkening is not addressed. However, the use of PD9 for 24 hours results in the lowest Δa* and Δb* parameters by the end of the cleaning process.

3.3.3.2 WATER VAPOR PERMEABILITY

The water vapor permeability of Lecce Stone was monitored for seven days at different points of the study (see Figure 60). There is initially a linear increase in the water vapor permeating through the stone. At a certain point, the water vapor permeating through the stone hardly fluctuates due to the saturation of the interconnected pores and the equilibrium of the stone with the environment. For the plain stone, the water vapor permeability reaches 208.72 g/m^2. After coating the stone blocks with Paraloid® B72, the value significantly lowers to 151.54 g/m^2 which is equivalent to a 27.40% change relative to the control. This is expected because Lecce Stone has a relatively high porosity and the coating essentially blocks a great portion of the pores on the surface. After aging the resin, there is not much difference. The value is 154.53 g/m^2 which is equivalent to a 25.96% change relative to the control. After the cleaning, the value slightly increased to 177.44 g/m^2, which reduces the difference to 14.99% relative to the control. While it is difficult to attribute the result into one particular HVPD, it can be stated that these two HVPDs are fundamentally capable of removing the aged resin. [81,82]

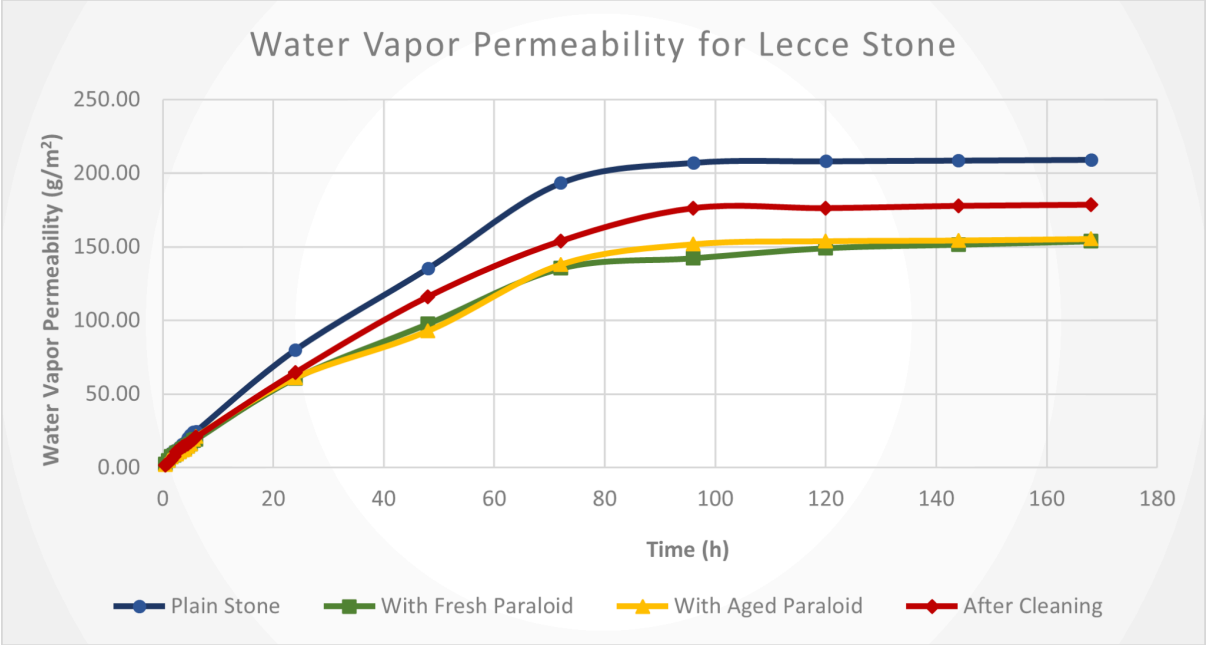

Figure 46. Water vapor permeability curve of Lecce Stone before coating (blue), after coating with Paraloid® B72 (green), after artificial accelerated aging (yellow), and after cleaning (red).

3.3.3.3 HVPD-CONTAMINANT INTERACTION

The first HVPD applied to Lecce Stone was PVA/B (PD1) for a period of 2 hours and 24 hours. Comparing the two spectra, the bands present are almost identical. The only difference is that cleaning for 24 hours mostly resulted in a higher band intensity relative to cleaning for 2 hours. A longer contact time resulted in a better removal of the aged resin given the hydrophilic nature of the HVPD.

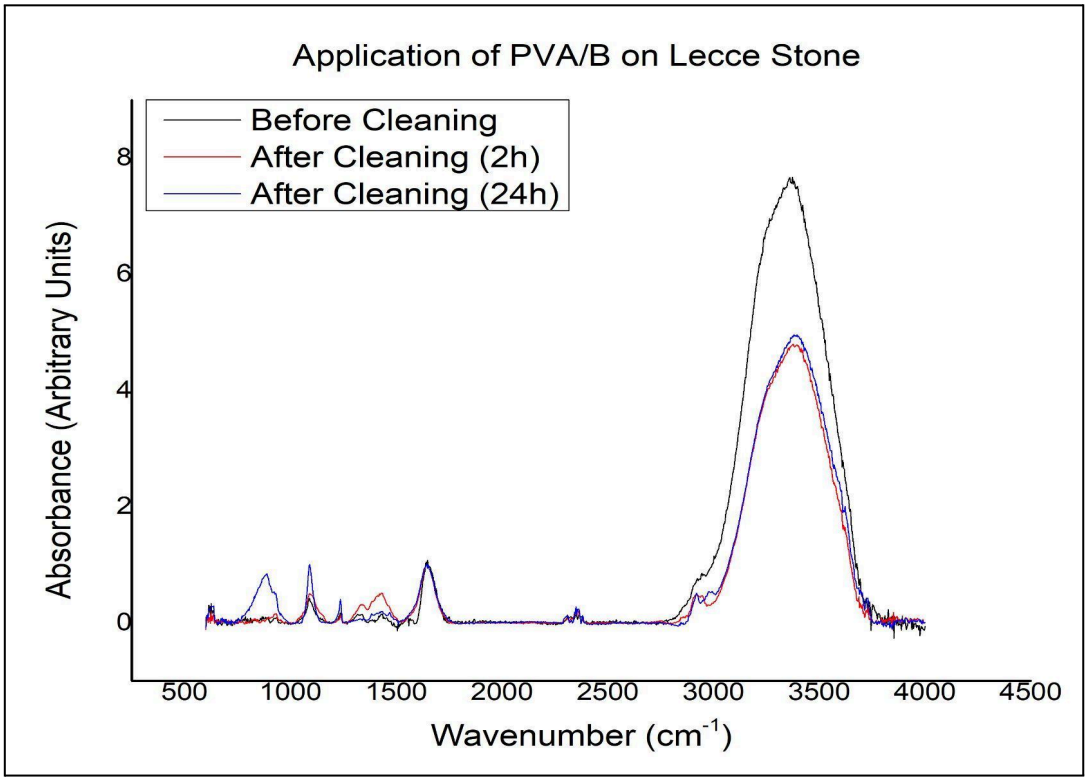

Figure 47. Superimposed ATR-FTIR spectra of PVA/B (PD1) before and after cleaning Lecce Stone for 2 and 24 hours.

The bands for PD1 can be assigned as follows: 3380 cm^{-1} for O-H bending, 2920 cm^{-1} for symmetrical -CH_2 stretching, 2970 cm^{-1} for C-H stretching, 1648 cm^{-1} for O-H bending, 1330 and 1430 cm^{-1} for asymmetric B-O-C stretching, and 925 cm^{-1} for -CH_2 stretching. [66,80] The spectral changes brought about by cleaning the aged resin are found in the lower wavenumber region. Generally, the band intensities are higher and band widths are larger due to the overlapping of new and old bands. These include the bands around 1650 cm^{-1} for ester C=O stretching, 1430 and 1330 cm^{-1} for the antisymmetric and symmetric bending of the methyl group in the α position, 1240 cm^{-1} for ester C-O stretching, 1090 cm^{-1} corresponds to O-C-C stretching of the ethyl ester, and 890 cm^{-1} for -CH_2 rocking of the alkyl group attached to the ester. [14,15,17,42,66]

The second HVPD applied to Lecce Stone was PVA/B-AG (PD9) for a period of 2 hours and 24 hours. The bands present in the two spectra are similar but the band intensity after 2 hours of cleaning is much higher than after 24 hours of cleaning. This follows the trend in cleaning Carrara Marble, which further supports the possibility that PD9 can temporarily adhere the resin before the cohesive forces supersede the adhesive forces which leads to flaking off or delamination. The bands for PD9 can be assigned as follows: 3380 cm^{-1} for O-H bending, 2925 cm^{-1} for symmetrical -CH_2 stretching, 2940 cm^{-1} for C-H stretching, 1648 cm^{-1} for O-H

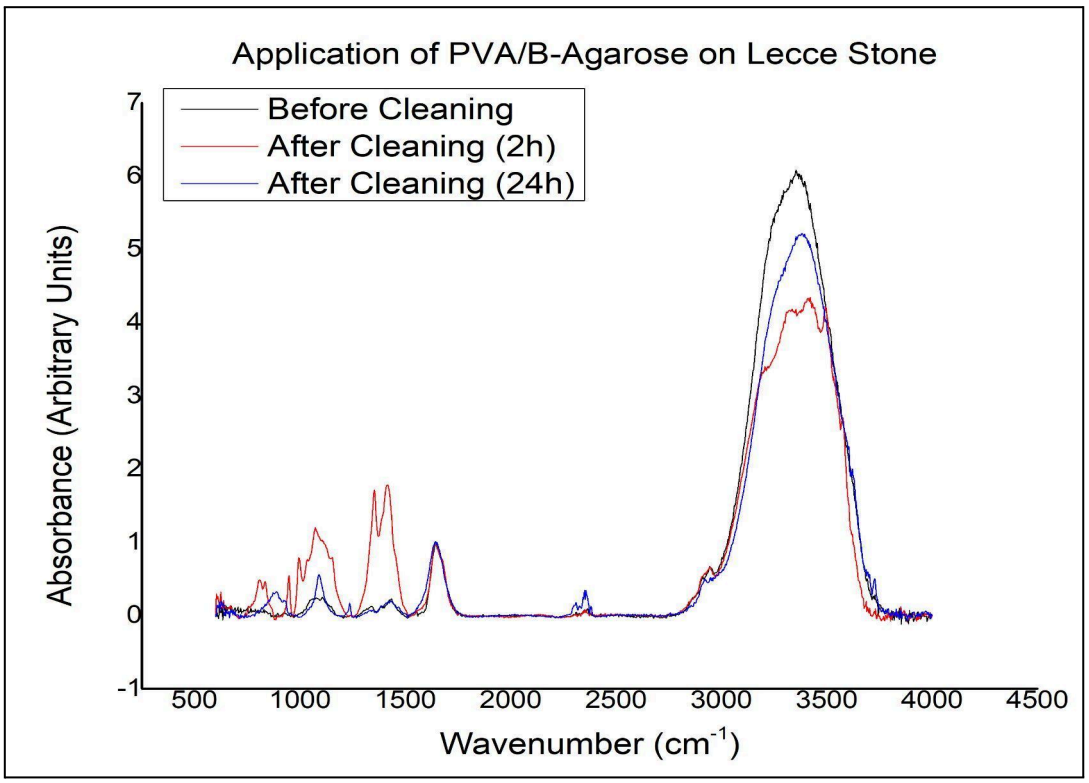

Figure 48. Superimposed ATR-FTIR spectra of PVA/B-AG (PD9) before and after cleaning Lecce Stone for 2 and 24 hours.

bending, 1350 and 1420 cm^{-1} for asymmetric B-O-C stretching, 1080 cm^{-1} for C-O-C stretching and glycosidic linkage, 940 cm^{-1} for -CH_2 stretching, and 830 cm^{-1} for C-C stretching and out-of-plane C-H bending. [66,80]

The bands corresponding to the aged resin are also present but overlap with the bands of the HVPD, as observed in the higher band intensities and larger band widths. The bands are found around 1650 cm^{-1} for ester C=O stretching, 1420 and 1340 cm^{-1} for the antisymmetric and symmetric bending of the methyl group in the α position, 1240 cm^{-1} for the ester C-O stretching, 1150 cm^{-1} for the C-C(=O)-O antisymmetric stretching, 1080 cm^{-1} for O-C-C stretching of the ethyl ester, and 810 cm^{-1} for the -CH_2 rocking of the alkyl group attached to the ester. [14,15,17,42,66]

3.3.4 CLEANING OF TRAVERTINE

3.3.4.1 COLORIMETRIC CHANGE

Two HVPDs were selected for the removal of Paraloid® B72: PVA/B (PD1) and PVA/B-AG (PD9). In the first and second areas, the HVPDs were applied on the surface of Travertine for two hours (see Table XVII). In the third and fourth areas, the two HVPDs were applied on the surface for a day. They were covered with Parafilm to avoid drying (see Table XVIII).

For the first application of PD1 for 2 hours, the ΔE_{ab}* value halved from 22.72 to 12.25. The ΔL* parameter decrease but still has a considerable contribution to the overall delta value. The Δa* and Δb* parameter approach zero. After the second application, there is a significant decrease in the ΔL* parameter, resulting in a lower ΔE_{ab}* value of 9.87. After the third application, the ΔL* parameter slightly increase again but the ΔE_{ab}* value decrease to 9.81, with a removal efficiency of 56.82%.

Meanwhile, for the first application of PD9 for 2 hours, the magnitude of ΔE_{ab}* also halve from 22.56 to 10.10. The ΔL* parameter reduce to a third of its value while the Δa* and Δb* parameters come close to neutral. After the second application, there is further decrease in all

Table XVII. Average colorimetric parameters of Travertine surfaces with plain stone as control. Area 1 was cleaned with PVA/B (PD1) while Area 2 was cleaned with PVA/B-AG (PD9) for 2 hours.

	AREA 1				AREA 2			
	ΔL*	Δa*	Δb*	ΔE_{ab}*	ΔL*	Δa*	Δb*	ΔE_{ab}*
1st Application	-11.62	-2.85	-1.85	12.25	-5.92	-2.62	0.31	10.10
2nd Application	-2.20	-2.18	1.09	9.87	-0.07	-1.92	0.72	4.60
3rd Application	-9.43	-2.32	-0.30	9.81	-11.55	-2.01	1.64	12.98

three parameters which bring down ΔE_{ab}* to 4.60. However, after the third application, all three parameters increase which then raise ΔE_{ab}* to 12.98, with a removal efficiency is 42.48%. Similar to the results in Lecce Stone, a third application is not advised.

For the first application of PD1 for 24 hours, the magnitude of ΔE_{ab}* decrease from 20.34 to 11.85. The ΔL* parameter is still negative but almost half in value. The Δa* and Δb* parameter decrease in value. For the second application, all three parameters slightly increase and so does the ΔE_{ab}* consequently to 12.65 with a removal efficiency is 52.89%.

Meanwhile, for the first application of PD9 for 24 hours, the magnitude of ΔE_{ab}* decrease from 19.32 to 11.85 since all three parameters decrease. For the second application, the ΔL* parameter slightly increase, raising ΔE_{ab}* to 12.65 with a removal efficiency is 56.79%.

Table XVIII. Average colorimetric parameters of Carrara Marble surfaces with plain stone as control. Area 3 was cleaned with PVA/B (PD1) while Area 4 was cleaned with PVA/B-AG (PD9) for 24 hours.

	AREA 3				AREA 4			
	ΔL*	Δa*	Δb*	ΔE_{ab}*	ΔL*	Δa*	Δb*	ΔE_{ab}*
1st Application	-9.30	-2.98	-2.57	11.85	-13.08	-2.92	-2.02	13.91
2nd Application	-10.76	-2.49	-1.89	12.65	-9.82	-2.14	-0.05	10.09

Overall, on the basis of colorimetry results, the best method of cleaning Travertine is the two applications of PD9 for 24 hours. For a coating thickness of 2 mm, at least two applications are necessary for the removal of Paraloid® B72. The use of PD1 results in close ΔE_{ab}* values but there is a persisting issue of darkening after two applications.

3.3.4.2 WATER VAPOR PERMEABILITY

The water vapor permeability of Travertine was monitored for seven days at different points of the study (see Figure 65). The curve begins with a steady increase in the water vapor permeating through the stone until it eventually becomes more or less constant. The interconnected pores get saturated, and the stone reaches equilibrium with the environment. For the plain stone, the water vapor permeability remains constant at 477.54 g/m^2. After coating the stone blocks with Paraloid® B72, the value significantly lowers to 324.62 g/m^2 which is equivalent to a 32.01% change relative to the control. For a highly porous stone such as Travertine, this is expected because the pores in the surfaces have been filled and covered. After artificially aging the resin, there is a slight difference. The value is 338.97 g/m^2 which is equivalent to a 29.00% change relative to the control. After the cleaning, the value increased to 369.74 g/m^2, which reduces the difference to 22.56% relative to the control.

These results show that the HVPDs can remove a significant portion of the aged resin, albeit incomplete. [81,82]

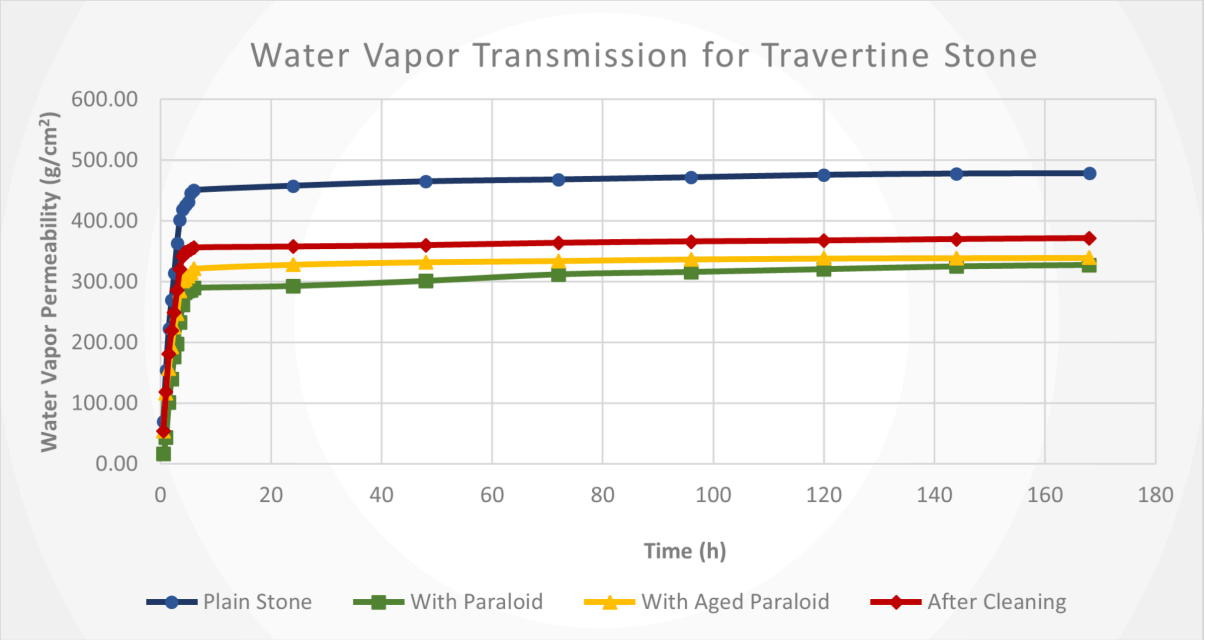

Figure 49. Water vapor permeability curve of Travertine before coating (blue), after coating with Paraloid® B72 (green), after artificial accelerated aging (yellow), and after cleaning (red).

3.3.4.3 HVPD-CONTAMINANT INTERACTION

The first HVPD applied to Travertine was PVA/B (PD1) for a period of 2 hours and 24 hours. The bands present in the two spectra are similar and can be assigned as follows: 3380 cm^{-1} for O-H bending, 2950 cm^{-1} for symmetrical -CH_2 stretching, 2925 cm^{-1} for C-H stretching, 1648 cm^{-1} for O-H bending, 1330 and 1420 cm^{-1} for asymmetric B-O-C stretching, and 930 cm^{-1} for -CH_2 stretching. [66,80] The spectral changes due to the removal of aged resin are found in the

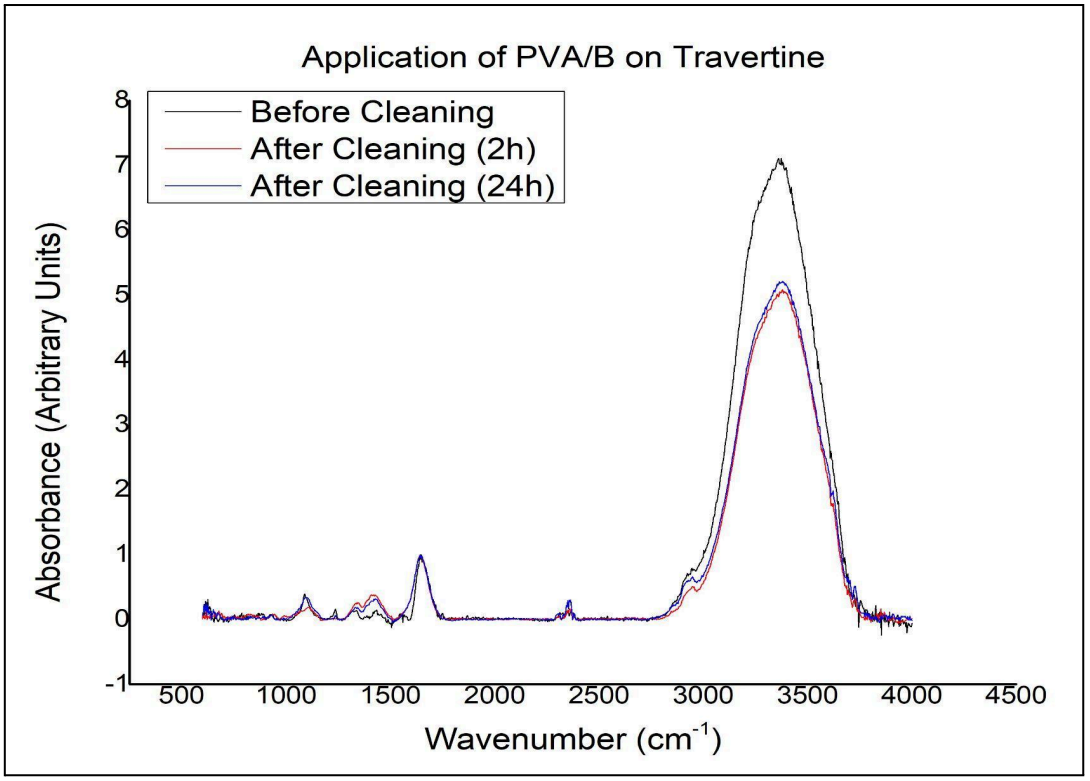

Figure 50. Superimposed ATR-FTIR spectra of PVA/B (PD1) before and after cleaning Travertine for 2 and 24 hours.

lower wavenumber region. The observable changes are the broadening of band widths due to the overlapping of new and old bands. These include the bands around 1650 cm^{-1} for ester C=O

stretching, 1420 and 1330 cm^{-1} for the antisymmetric and symmetric bending of the methyl group in the α position, 1240 cm^{-1} corresponding to the ester C-O stretching, 1100 cm^{-1} for C-C(=O)-O antisymmetric stretching, and 1090 cm^{-1} for O-C-C stretching of the ethyl ester.[14,15,17,42,66]

The second HVPD applied to Travertine was PVA/B-AG (PD9) for a period of 2 hours and 24 hours. Similar to the cases of Carrara Marble and Lecce Stone, the band intensity after 2 hours of cleaning is much higher than after 24 hours of cleaning, possibly due to the differences in the cleaning mechanism of PD9 and PD1. The bands can be assigned as follows: 3380 cm^{-1} for O-H bending, 2925 cm^{-1} for symmetrical -CH_2 stretching, 2950 cm^{-1} for C-H stretching, 1648 cm^{-1} for O-H bending, 1340 and 1410 cm^{-1} for asymmetric B-O-C stretching, 1070 cm^{-1} for C-O-C stretching and glycosidic linkage, 940 cm^{-1} for -CH_2 stretching, and 890 cm^{-1} for C-C stretching and out-of-plane C-H bending.[66,80] The bands corresponding to the aged resin are also found in the spectra. However, most of them overlap with the bands of the HVPD which results in higher band intensity and larger band width. The bands are found around 1650 cm^{-1} for ester C=O stretching, 1410 and 1340 cm^{-1} for the antisymmetric and symmetric bending of the methyl group in the α position, 1240 cm^{-1} for the ester C-O stretching, 1120 cm^{-1} for the C-C(=O)-O antisymmetric stretching, 1070 cm^{-1}

for O-C-C stretching of the ethyl ester, and 810 cm^{-1} for the -CH_2 rocking of the alkyl group attached to the ester. [14,15,17,42,66]

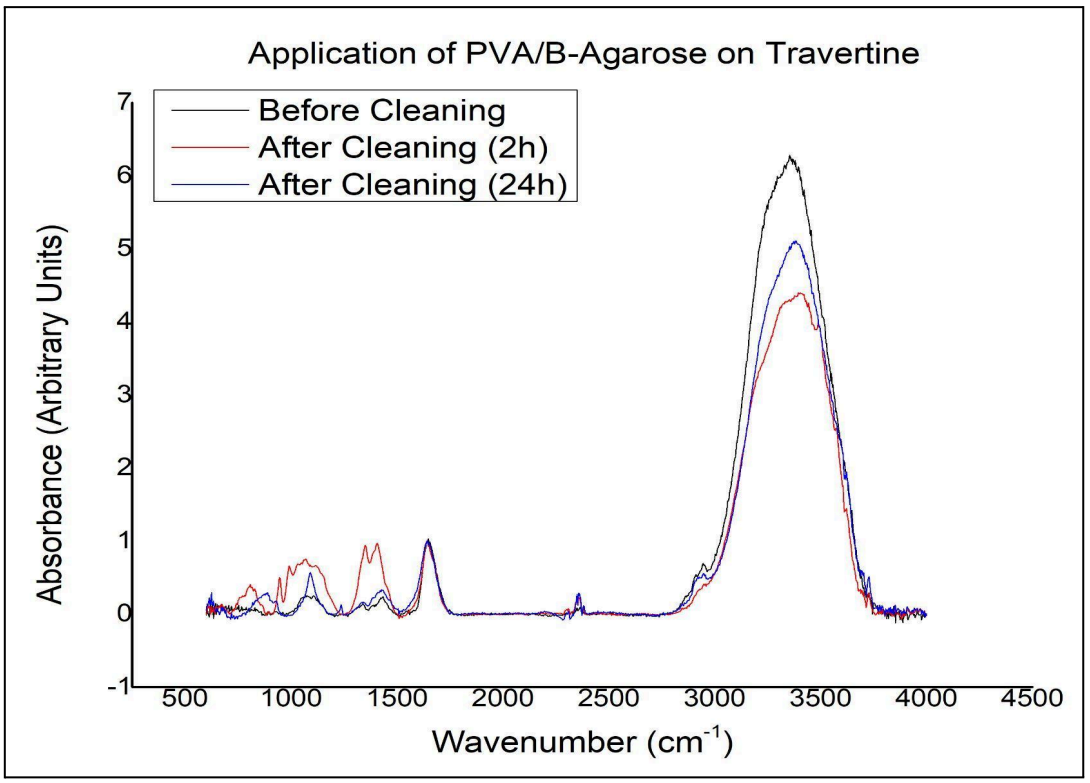

Figure 51. Superimposed ATR-FTIR spectra of PVA/B (PD1) before and after cleaning Travertine for 2 and 24 hours.

3.3.5 SUMMARY OF RESULTS

The aging of Paraloid® B72 resulted in chromatic variations on the surface of the stones (Table XIX). The color coordinates change differently depending on the lithotype, which suggests that the surface morphology and porosity of the stones affect the degradation mechanism of the resin. For Carrara Marble, which has a relatively even surface, the polymer likely undergoes photolysis reaction more homogeneously. For Lecce Stone, which has a capillary network, photolysis happens on the surface but the lack of oxygen in the small interconnected pores promotes cross-linking reactions as well. This is probably why darkening is most extensive in this particular stone. For Travertine, which has larger pores, photolysis happens on the surface but there are also significant radical reactions. These form chromophores bearing carbonyl groups, double bonds, and conjugation which absorb in the blue and violet regions of the spectrum. This is likely the reason for the yellowing and reddening of the coating.[14,15,61]

Based on the cleaning tests, multiple applications are necessary for the removal of the aged resin. While all four could not fully address the issue of darkening, the use of PD9 twice for 24 hours showed the most promise. PD1 was also effective but the ΔL* parameter fluctuates after

Table XIX. Digital images of stone surfaces before and after cleaning with PD1 (left) and PD9 (right) for 2 hours (top) and 24 hours (bottom).

	Plain Stone	With Fresh Paraloid B72	With Aged Paraloid B72	Cleaned Stone
CM				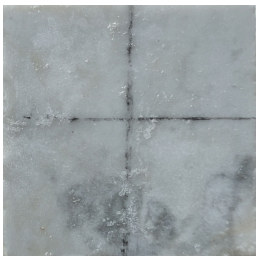
LS				
T		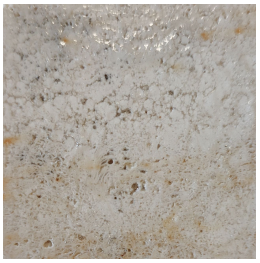		

each application. The third application often results in further darkening, which might be happening for several reasons. It might have to do with the mechanism of cleaning of PVA/B, which induces the migration and increased concentration per area of the polymer chains prior to flaking off or delamination. The molecular orientation of acrylates are known to affect their crystallinity or amorphousness, and consequently, their optical properties.[81,86]

Both HVPDs interact with the acrylate chains and their by-products which eventually leads to delamination but it is possible that, with the presence of agarose, there is a change in compatibility with the resin.[107] Agarose can alter the microenvironment of the polymer network to make it favorable for the partial adhesion of the resin. The adhesive forces between the HVPD and the resin do not outweigh cohesive forces among the acrylate chains though, hence delamination is observed long-term. This point can be further deepened through additional studies on the interaction between the polymers in the HVPD and the acrylate resin, along with monitoring changes in the stone's surface morphology.[108,109]

The effectiveness of the HVPDs as cleaning tools are supported by the other test results. The flaking off and delamination of the resin was physically observed. For the used samples of

PVA/B-AG, bands corresponding to Paraloid® B72 are clearly present in the FT-IR ATR spectra. The removal of Paraloid® B72 also resulted in the improvement of the breathability of the stone. It did not return to its original permeability, however, which suggests that part of the resin is still left on the stone. Additional cleaning with the HVPDs or other methods might be necessary since cracks, crevices, and pores are not easy to reach.

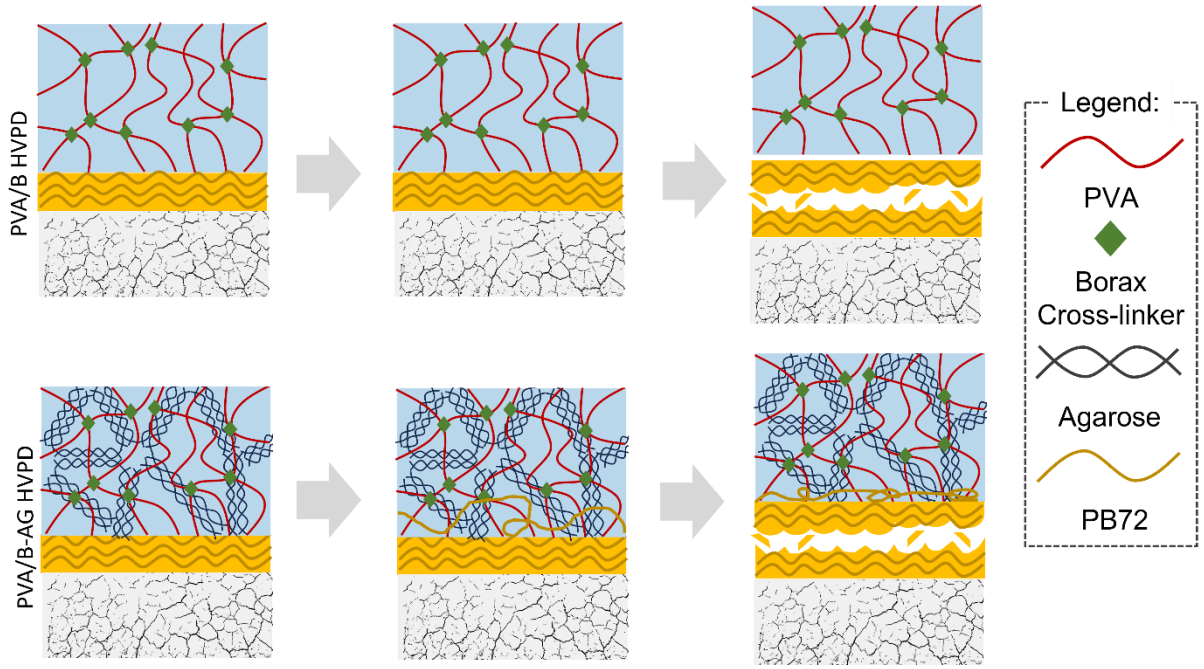

Figure 52. Proposed general mechanism of the removal of Paraloid® B72 from the stone surface using PVA/B and PVA/B-AG HVPDs.

CONCLUSION

The aim of the research was to evaluate the performance of PVA/B-based HVPDs in removing bronze corrosion products and aged Paraloid® B72 from Carrara Marble, Lecce Stone, and Travertine surfaces through a multi-technical approach. On a macroscale, the HVPDs should be able to address the chromatic variation and return the surface as close to its original state as possible. On a microscale, the contaminants should be removed without altering the surface morphology or the other properties of the stone.

Prior to any application, the HVPDs were first characterized to determine suitability on the basis of their rheological properties, water holding capacity, loss of volatile fraction, and residue formation. Rheological measurements revealed that while the interpenetration of agarose and the loading of chelants into the polymer network create stiffer materials, all six HVPDs have a G'_0 value above 400 Pa, which means that they can be peeled off. The water holding capacity test showed that there is minimal desorption of the aqueous phase from the HVPDs, but the test on their loss of volatile fraction showed considerable drying after 4 hours of exposure. Preliminary trials also demonstrated that treatment beyond 4 hours resulted in residue formation on the substrate. Hence, when using these HVPDs, it is advisable to do multiple applications at shorter intervals.

For the cleaning of bronze corrosion products, FORS analysis revealed that two applications of PVA/B-AG with EDTA or PST are able to approximate the original color of the stone. The Δa^* and Δb^* parameters approach zero, which translates to a less green and less blue appearance. However, the ΔL^* parameter can increase so the second application must be modulated in order to avoid lightening. Both metal-ligand complexes are highly stable in water and can interact well with the hydroxyl groups of the polymer chains, as seen in the FT-IR spectra. Between the two chelants, however, EDTA proved to have higher removal efficiency than PST for Carrara Marble and Lecce Stone, owing to its higher formation constant.

At a closer look using SEM-EDS, cleaning with the two HVPDs drastically reduced the copper-based crystals on the surface of the stone. However, this is where the differences between lithotypes come into play. Cleaning had a more extensive effect on Carrara Marble relative to Lecce Stone and Travertine. This can be attributed to the differences in porosity of the stones: it is easier to clean when the corrosion products are concentrated on the surface and not penetrating cracks and pores into the subsurface.

For the cleaning of aged Paraloid® B72, FORS analysis showed that multiple applications of PVA/B and PVA/B-AG are necessary to remove the insoluble resin. The Δa* and Δb* parameters decreased significantly, seen as a reduction in the reddening and yellowing. However, the ΔL* parameter remained high, so darkening still needs to be addressed. It is possible that multiple degradation mechanisms took place. The chromophores formed *via* radical reactions, which are responsible for the red and yellow appearance, can be sequestered easily by the HVPDs. However, it is more difficult to get the cross-linked polymer chains.

Between the two HVPDs, the use of PVA/B-AG twice at 24-hour durations proved to be most efficient. It is possible that agarose changes the polarity of the dispersion which makes it more favorable than PVA/B alone. This is supported by the FT-IR spectra of the used HVPDs, where bands corresponding to Paraloid® B72 were clearly visible in the used PVA/B-AG. The cleaning mechanisms of the two HVPDs might also be different. The adhesive forces between the acrylate resin and PVA/B-AG might be stronger which leads to partial adhesion of the contaminant to the HVPD aside from flaking off or delaminating from the stone. With regards to water vapor permeability, the breathability of the stones improved after the cleaning procedures. These results are promising because a hydrophobic organic material was removed using the hydrophilic HVPD without the addition of organic solvents or other cleaning systems.

Overall, PVA/B-based HVPDs proved to be an eco-friendly and versatile cleaning tool. Further research elucidating the interaction between the HVPD components and the contaminants, as well as the complex mechanisms of cleaning, will open possibilities for its wider adoption in the conservation of cultural heritage.

REFERENCES

1. Weber H. Conservation and Restoration of Natural Stone in Europe. *Bulletin of the Association for Preservation Technology*. 1985;17(2):15-23. doi:10.2307/1494130
2. Siegesmund S, Weiss T, Vollbrecht A. Natural stone, weathering phenomena, conservation strategies and case studies: introduction. *Geological Society, London, Special Publications*. 2002;205(1):1-7. doi:10.1144/GSL.SP.2002.205.01.01
3. Fiorino S. China and Italy (1, 2017 - 4, 2021). Istituto di Scienze del Patrimonio Culturale. Published August 15, 2019. Accessed August 23, 2023. https://www.ispc.cnr.it/en/2019/08/15/china-and-italy-1-2017-4-2021/
4. Hannibal JT, Park LE. A Guide to Selected Sources of Information on Stone Used for Buildings, Monuments, and Works of Art. *Journal of Geological Education*. 1992;40(1):12-24. doi:10.5408/0022-1368-40.1.12
5. Viles HA. Durability and conservation of stone: Coping with complexity. *Quarterly Journal of Engineering Geology and Hydrogeology*. 2013;46:367-375. doi:10.1144/qjegh2012-053
6. Russa MFL, Ruffolo SA, Belfiore CM, et al. Study of the effects of salt crystallisation on degradation of limestone rocks. *Periodico di Mineralogia*. 2013;82(1). doi:10.2451/2013PM0007
7. Alves C, Figueiredo CAM, Sanjurjo-Sánchez J, Hernández AC. Effects of Water on Natural Stone in the Built Environment—A Review. *Geosciences*. 2021;11(11):459. doi:10.3390/geosciences11110459
8. Warscheid Th, Braams J. Biodeterioration of stone: a review. *International Biodeterioration & Biodegradation*. 2000;46(4):343-368. doi:10.1016/S0964-8305(00)00109-8
9. Weiss T, Siegesmund S, Kirchner D, Sippel J. Insolation weathering and hygric dilatation: two competitive factors in stone degradation. *Env Geol*. 2004;46(3):402-413. doi:10.1007/s00254-004-1041-0
10. Vasconcelos G, Lourenço PB. Experimental characterization of stone masonry in shear and compression. *Construction and Building Materials*. 2009;23(11):3337-3345. doi:10.1016/j.conbuildmat.2009.06.045
11. Scott DA. *Copper and Bronze in Art: Corrosion, Colorants, Conservation*. Getty Conservation Institute; 2002.
12. Gaylarde CC, Gaylarde PM, Beech IB. Deterioration of limestone structures associated with copper staining. *International Biodeterioration & Biodegradation*. 2008;62(2):179-185. doi:10.1016/j.ibiod.2008.01.007
13. Spile S, Suzuki T, Bendix J, Simonsen KP. Effective cleaning of copper stained calcareous stone. *Herit Sci*. 2016;4(1):29. doi:10.1186/s40494-016-0102-5
14. Favaro M, Mendichi R, Ossola F, et al. Evaluation of polymers for conservation treatments of outdoor exposed stone monuments. Part I: Photo-oxidative weathering. *Polymer Degradation and Stability*. 2006;91(12):3083-3096. doi:10.1016/j.polymdegradstab.2006.08.012
15. Favaro M, Mendichi R, Ossola F, Simon S, Tomasin P, Vigato PA. Evaluation of polymers for conservation treatments of outdoor exposed stone monuments. Part II: Photo-oxidative and salt-induced weathering of acrylic–silicone mixtures. *Polymer Degradation and Stability*. 2007;92(3):335-351. doi:10.1016/j.polymdegradstab.2006.12.008
16. Macchia A, Laurenzi Tabasso M, Salvi AM, et al. Analytical characterization of corrosion products of copper and its alloys on stained stone surfaces. *Surface and Interface Analysis*. 2013;45(7):1073-1080. doi:10.1002/sia.5220
17. Melo MJ, Bracci S, Camaiti M, Chiantore O, Piacenti F. Photodegradation of acrylic resins used in the conservation of stone. *Polymer Degradation and Stability*. 1999;66(1):23-30. doi:10.1016/S0141-3910(99)00048-8
18. Bonelli N, Chelazzi D, Baglioni M, Giorgi R, Baglioni P. Confined Aqueous Media for the Cleaning of Cultural Heritage: Innovative Gels and Amphiphile-Based Nanofluids. In: Dillmann P,

Bellot-Gurlet L, Nenner I, eds. *Nanoscience and Cultural Heritage*. Atlantis Press; 2016:283-311. doi:10.2991/978-94-6239-198-7_10
19. Baglioni M, Giorgi R, Berti D, Baglioni P. Smart cleaning of cultural heritage: a new challenge for soft nanoscience. *Nanoscale*. 2012;4(1):42-53. doi:10.1039/C1NR10911A
20. Angelova LV, Matarrese C, Fratini E, Weiss RG, Dei L, Carretti E. Chelating agents in aqueous, partially-hydrolyzed, poly(vinyl acetate) dispersions crosslinked with borax. Physicochemical characterization and an application. *Colloids and Surfaces A: Physicochemical and Engineering Aspects*. 2018;556:61-71. doi:10.1016/j.colsurfa.2018.07.044
21. Berlangieri C, Andrina E, Matarrese C, et al. Chelators confined into 80pvac-borax highly viscous dispersions for the removal of gypsum degradation layers. *Pure and Applied Chemistry*. 2017;89(1):97-109. doi:10.1515/pac-2016-0815
22. Matarrese C. Co-solvents and chelating agents confined in complex fluids for the cleaning of surfaces of works of art. Accessed August 23, 2023. https://flore.unifi.it/handle/2158/984618
23. Mazzuca C, Severini L, Domenici F, et al. Polyvinyl alcohol based hydrogels as new tunable materials for application in the cultural heritage field. *Colloids and Surfaces B: Biointerfaces*. 2020;188:110777. doi:10.1016/j.colsurfb.2020.110777
24. Guaragnone T, Casini A, Chelazzi D, Giorgi R. PVA-based peelable films loaded with tetraethylenepentamine for the removal of corrosion products from bronze. *Applied Materials Today*. 2020;19:100549. doi:10.1016/j.apmt.2019.100549
25. Natali I, Carretti E, Angelova L, Baglioni P, Weiss RG, Dei L. Structural and Mechanical Properties of "Peelable" Organoaqueous Dispersions with Partially Hydrolyzed Poly(vinyl acetate)-Borate Networks: Applications to Cleaning Painted Surfaces. *Langmuir*. 2011;27(21):13226-13235. doi:10.1021/la2015786
26. Al-Emam E, Soenen H, Caen J, Janssens K. Characterization of polyvinyl alcohol-borax/agarose (PVA-B/AG) double network hydrogel utilized for the cleaning of works of art. *Herit Sci*. 2020;8(1):106. doi:10.1186/s40494-020-00447-3
27. Han X, Li M, Fan Z, Zhang Y, Zhang H, Li Q. PVA/Agar Interpenetrating Network Hydrogel with Fast Healing, High Strength, Antifreeze, and Water Retention. *Macromolecular Chemistry and Physics*. 2020;221(22):2000237. doi:10.1002/macp.202000237
28. Carbonate Rocks. Geology is the Way. Accessed September 11, 2023. https://geologyistheway.com/sedimentary/carbonate-rocks/
29. Bell FG. ENGINEERING GEOLOGY | Problematic Rocks. In: Selley RC, Cocks LRM, Plimer IR, eds. *Encyclopedia of Geology*. Elsevier; 2005:543-554. doi:10.1016/B0-12-369396-9/00220-3
30. Murray JW. The Deposition of Calcite and Aragonite in Caves. *The Journal of Geology*. 1954;62(5):481-492. doi:10.1086/626192
31. Daoxian Y. Variations of Karst Geomorphology over Geoclimatic Gradients. *Treatise on Geomorphology*. 2013;6:319-326. doi:10.1016/B978-0-12-374739-6.00107-X
32. Herz N, Dean NE. Stable isotopes and archaeological geology: the Carrara marble, northern Italy. *Applied Geochemistry*. 1986;1(1):139-151. doi:10.1016/0883-2927(86)90045-4
33. The study of stone for conservation purposes: Lecce stone (southern Italy) | Geological Society, London, Special Publications. Accessed August 23, 2023. https://www.lyellcollection.org/doi/abs/10.1144/sp391.8
34. Calia A, Laurenzi Tabasso M, Maria Mecchi A, Quarta G. The study of stone for conservation purposes: Lecce stone (southern Italy). *Geological Society, London, Special Publications*. 2014;391(1):139-156. doi:10.1144/SP391.8
35. García-del-Cura MÁ, Benavente D, Martínez-Martínez J, Cueto N. Sedimentary structures and physical properties of travertine and carbonate tufa building stone. *Construction and Building Materials*. 2012;28(1):456-467. doi:10.1016/j.conbuildmat.2011.08.042
36. Gomez-Heras M, McCabe S. Weathering of stone-built heritage: A lens through which to read the Anthropocene. *Anthropocene*. 2015;11:1-13. doi:10.1016/j.ancene.2015.12.003

37. Camuffo D. Physical weathering of stones. *Science of The Total Environment*. 1995;167(1):1-14. doi:10.1016/0048-9697(95)04565-I
38. Winkler EM. Weathering and weathering rates of natural stone. *Environ Geol Water Sci*. 1987;9(2):85-92. doi:10.1007/BF02449939
39. Winkler EM. Natural Rust on Stone. In: Winkler EM, ed. *Stone: Properties, Durability in Man's Environment*. Applied Mineralogy. Springer; 1975:164-168. doi:10.1007/978-3-7091-3819-9_9
40. Livingston RA. Acid rain attack on outdoor sculpture in perspective. *Atmospheric Environment*. 2016;146:332-345. doi:10.1016/j.atmosenv.2016.08.029
41. Stagno V, Genova C, Zoratto N, Favero G, Capuani S. Single-Sided Portable NMR Investigation to Assess and Monitor Cleaning Action of PVA-Borax Hydrogel in Travertine and Lecce Stone. *Molecules*. 2021;26(12):3697. doi:10.3390/molecules26123697
42. Chiantore O, Lazzari M. Photo-oxidative stability of paraloid acrylic protective polymers. *Polymer*. 2001;42(1):17-27. doi:10.1016/S0032-3861(00)00327-X
43. Carvalho L da C. Metallic Corrosion Processes and Information from Corrosion Products. In: Pollard AM, Armitage RA, Makarewicz CA, eds. *Handbook of Archaeological Sciences*. 1st ed. Wiley; 2023:1089-1102. doi:10.1002/9781119592112.ch54
44. Watkinson D. Preservation of Metallic Cultural Heritage. In: *Shreir's Corrosion*. Elsevier; 2010:3307-3340. doi:10.1016/B978-044452787-5.00172-4
45. Canevali C, Fasoli M, Bertasa M, et al. A multi-analytical approach for the study of copper stain removal by agar gels. *Microchemical Journal*. 2016;129:249-258. doi:10.1016/j.microc.2016.07.007
46. Stagno V, Ciccola A, Curini R, Postorino P, Favero G, Capuani S. Non-Invasive Assessment of PVA-Borax Hydrogel Effectiveness in Removing Metal Corrosion Products on Stones by Portable NMR. *Gels*. 2021;7(4):265. doi:10.3390/gels7040265
47. Piccardo P, Bongiorno V, Campodonico S. 10 - Artistic patinas on ancient bronze statues. In: Dillmann P, Watkinson D, Angelini E, Adriaens A, eds. *Corrosion and Conservation of Cultural Heritage Metallic Artefacts*. European Federation of Corrosion (EFC) Series. Woodhead Publishing; 2013:193-212. doi:10.1533/9781782421573.3.193
48. Di Carlo G, Giuliani C, Riccucci C, et al. Artificial patina formation onto copper-based alloys: Chloride and sulphate induced corrosion processes. *Applied Surface Science*. 2017;421:120-127. doi:10.1016/j.apsusc.2017.01.080
49. Constantinides I, Adriaens A, Adams F. Surface characterization of artificial corrosion layers on copper alloy reference materials. *Applied Surface Science*. 2002;189(1):90-101. doi:10.1016/S0169-4332(02)00005-3
50. FitzGerald KP, Nairn J, Skennerton G, Atrens A. Atmospheric corrosion of copper and the colour, structure and composition of natural patinas on copper. *Corrosion Science*. 2006;48(9):2480-2509. doi:10.1016/j.corsci.2005.09.011
51. Macchia A, Sammartino MP, Tabasso ML. A new method to remove copper corrosion stains from stone surfaces. *Journal of Archaeological Science*. 2011;38(6):1300-1307. doi:10.1016/j.jas.2011.01.005
52. Zhang X, He W, Odnevall Wallinder I, Pan J, Leygraf C. Determination of instantaneous corrosion rates and runoff rates of copper from naturally patinated copper during continuous rain events. *Corrosion Science*. 2002;44(9):2131-2151. doi:10.1016/S0010-938X(02)00015-X
53. Payer JH, Ball G, Rickett BI, Kim HS. Role of transport properties in corrosion product growth. *Materials Science and Engineering: A*. 1995;198(1-2):91-102. doi:10.1016/0921-5093(95)80063-Z
54. Benavente D, del Cura MAG, García-Guinea J, Sánchez-Moral S, Ordóñez S. Role of pore structure in salt crystallisation in unsaturated porous stone. *Journal of Crystal Growth*. 2004;260(3):532-544. doi:10.1016/j.jcrysgro.2003.09.004

55. Troiano F, Vicini S, Gioventù E, Lorenzi PF, Improta CM, Cappitelli F. A methodology to select bacteria able to remove synthetic polymers. *Polymer Degradation and Stability*. 2014;107:321-327. doi:10.1016/j.polymdegradstab.2013.12.029
56. Artesani A, Di Turo F, Zucchelli M, Traviglia A. Recent Advances in Protective Coatings for Cultural Heritage–An Overview. *Coatings*. 2020;10(3):217. doi:10.3390/coatings10030217
57. Princi E. *Handbook of Polymers in Stone Conservation*. Smithers Rapra; 2014.
58. Čubrić IS, Čubrić G, Katić Križmančić I, Kovačević M. Evaluation of Changes in Polymer Material Properties Due to Aging in Different Environments. *Polymers*. 2022;14(9):1682. doi:10.3390/polym14091682
59. Fistos T, Fierascu I, Doni M, Chican IE, Fierascu RC. A Short Overview of Recent Developments in the Application of Polymeric Materials for the Conservation of Stone Cultural Heritage Elements. *Materials*. 2022;15(18):6294. doi:10.3390/ma15186294
60. Feller RL. *Accelerated Aging: Photochemical and Thermal Aspects*. Getty Publications; 1995.
61. Hutchinson JM. Physical aging of polymers. *Progress in Polymer Science*. 1995;20(4):703-760. doi:10.1016/0079-6700(94)00001-I
62. Lazzari M, Chiantore O. Thermal-ageing of paraloid acrylic protective polymers. *Polymer*. 2000;41(17):6447-6455. doi:10.1016/S0032-3861(99)00877-0
63. Bracci S, Sacchi B. In situ Assessment of Conservation Treatments and Monitoring of Their Effectiveness. In: Gherardi F, Maravelaki PN, eds. *Conserving Stone Heritage: Traditional and Innovative Materials and Techniques*. Cultural Heritage Science. Springer International Publishing; 2022:231-274. doi:10.1007/978-3-030-82942-1_8
64. Casini A, Chelazzi D, Baglioni P. Advanced methodologies for the cleaning of works of art. *Sci China Technol Sci*. 2023;66(8):2162-2182. doi:10.1007/s11431-022-2348-7
65. Baglioni P, Chelazzi D, Giorgi R, Poggi G. Colloid and Materials Science for the Conservation of Cultural Heritage: Cleaning, Consolidation, and Deacidification. *Langmuir*. 2013;29(17):5110-5122. doi:10.1021/la304456n
66. Alemam E. Cleaning of Wall Paintings by Polyvinyl alcohol–Borax/Agarose (PVA–B/AG) Double Network Hydrogels: Characterization, Assessment, and Applications.
67. Sansonetti A, Bertasa M, Canevali C, Rabbolini A, Anzani M, Scalarone D. A review in using agar gels for cleaning art surfaces. *Journal of Cultural Heritage*. 2020;44:285-296. doi:10.1016/j.culher.2020.01.008
68. Arnott S, Fulmer A, Scott WE, Dea ICM, Moorhouse R, Rees DA. The agarose double helix and its function in agarose gel structure. *Journal of Molecular Biology*. 1974;90(2):269-284. doi:10.1016/0022-2836(74)90372-6
69. Wang C, Shen Z, Hu P, et al. Facile fabrication and characterization of high-performance Borax-PVA hydrogel. *J Sol-Gel Sci Technol*. 2022;101(1):103-113. doi:10.1007/s10971-021-05584-0
70. Bertasa M, Canevali C, Sansonetti A, et al. An in-depth study on the agar gel effectiveness for built heritage cleaning. *Journal of Cultural Heritage*. 2021;47:12-20. doi:10.1016/j.culher.2020.10.007
71. Cagno S, Macchia A, Prestileo F. *YOCOCU 2014: Professionals' Experiences in Cultural Heritage Conservation in America, Europe, and Asia*. Cambridge Scholars Publishing; 2016.
72. Baglioni M, Rengstl D, Berti D, Bonini M, Giorgi R, Baglioni P. Removal of acrylic coatings from works of art by means of nanofluids: understanding the mechanism at the nanoscale. *Nanoscale*. 2010;2(9):1723-1732. doi:10.1039/C0NR00255K
73. Brajer I. The removal of aged acrylic coatings from wall paintings using microemulsions. Published online 2014.
74. Boral S, Saxena A, Bohidar HB. Syneresis in agar hydrogels. *International Journal of Biological Macromolecules*. 2010;46(2):232-236. doi:10.1016/j.ijbiomac.2009.12.008
75. Mao R, Tang J, Swanson BG. Water holding capacity and microstructure of gellan gels. *Carbohydrate Polymers*. 2001;46(4):365-371. doi:10.1016/S0144-8617(00)00337-4

76. Guo L. Preparation and Properties of Hyaluronic Acid Hydrogel Modified by L-cysteine Hydrochloride - IOPscience. Accessed September 11, 2023. https://iopscience.iop.org/article/10.1088/1755-1315/651/4/042022/meta
77. Ramli H, Zainal NFA, Hess M, Chan CH. Basic principle and good practices of rheology for polymers for teachers and beginners. *Chemistry Teacher International*. 2022;4(4):307-326. doi:10.1515/cti-2022-0010
78. Ross-Murphy SB. Rheological characterization of polymer gels and networks. *Polymer Gels and Networks*. 1994;2(3):229-237. doi:10.1016/0966-7822(94)90007-8
79. Almeida RM, Marques AC. Characterization of Sol–Gel Materials by Infrared Spectroscopy. In: Klein L, Aparicio M, Jitianu A, eds. *Handbook of Sol-Gel Science and Technology*. Springer International Publishing; 2016:1-31. doi:10.1007/978-3-319-19454-7_33-1
80. Socrates G. *Infrared and Raman Characteristic Group Frequencies: Tables and Charts*. John Wiley & Sons; 2004.
81. Tsakalof A, Manoudis P, Karapanagiotis I, Chryssoulakis I, Panayiotou C. Assessment of synthetic polymeric coatings for the protection and preservation of stone monuments. *Journal of Cultural Heritage*. 2007;8(1):69-72. doi:10.1016/j.culher.2006.06.007
82. Esposito Corcione C, De Simone N, Santarelli ML, Frigione M. Protective properties and durability characteristics of experimental and commercial organic coatings for the preservation of porous stone. *Progress in Organic Coatings*. 2017;103:193-203. doi:10.1016/j.porgcoat.2016.10.037
83. Grieken RV, Delalieux F, Gysels K. Cultural heritage and the environment. *Pure and Applied Chemistry*. 1998;70(12):2327-2331. doi:10.1351/pac199870122327
84. Occhipinti R, Stroscio A, Maria Belfiore C, Barone G, Mazzoleni P. Chemical and colorimetric analysis for the characterization of degradation forms and surface colour modification of building stone materials. *Construction and Building Materials*. 2021;302:124356. doi:10.1016/j.conbuildmat.2021.124356
85. Tortora M, Chiarini M, Spreti N, Casieri C. 1H-NMR-relaxation and colorimetry for evaluating nanopolymeric dispersions as stone protective coatings. *Journal of Cultural Heritage*. 2020;44:204-210. doi:10.1016/j.culher.2019.12.014
86. Tanaka F. *Polymer Physics: Applications to Molecular Association and Thermoreversible Gelation*. Cambridge University Press; 2011.
87. Rubinstein M, Semenov AN. Dynamics of entangled solutions of associating polymers. *Macromolecules*. Published online 2001:1058-1068. doi:10.1021/ma0013049
88. Van Oene H. Chapter 7 - Rheology of Polymer Blends and Dispersions. In: Paul DR, Newman S, eds. *Polymer Blends*. Academic Press; 1978:295-352. doi:10.1016/B978-0-12-546801-5.50013-X
89. Feng Y, Taraban M, Yu YB. The Effect of Ionic Strength on the Mechanical, Structural and Transport Properties of Peptide Hydrogels. *Soft Matter*. 2012;8(46):11723-11731. doi:10.1039/C2SM26572A
90. Karlsson RMP, Larsson PT, Pettersson T, Wågberg L. Swelling of Cellulose-Based Fibrillar and Polymeric Networks Driven by Ion-Induced Osmotic Pressure. *Langmuir*. 2020;36(41):12261-12271. doi:10.1021/acs.langmuir.0c02051
91. Urbonaite V, van der Kaaij S, de Jongh HHJ, et al. Relation between gel stiffness and water holding for coarse and fine-stranded protein gels. *Food Hydrocolloids*. 2016;56:334-343. doi:10.1016/j.foodhyd.2015.12.011
92. Dreval' VYe, Tager AA, Utyumova NS. Effect of inorganic salts on the viscosity of polyvinyl alcohol solutions in water and dimethylsulphoxide. *Polymer Science USSR*. 1977;19(7):1812-1818. doi:10.1016/0032-3950(77)90196-4
93. Tretinnikov O, Zagorskaya S. Effect of inorganic salts on the crystallinity of polyvinyl alcohol. *Journal of Applied Spectroscopy*. 2012;78. doi:10.1007/s10812-012-9551-0

94. Singh T, Meena R, Kumar A. Effect of Sodium Sulfate on the Gelling Behavior of Agarose and Water Structure Inside the Gel Networks. *J Phys Chem B*. 2009;113(8):2519-2525. doi:10.1021/jp809294p
95. Sevost'yanova NI, Martynenko LI, Spitsyn VI. IR spectroscopic study of ethylenediaminediacetic acid and its salts. *Russ Chem Bull*. 1972;21(4):751-754. doi:10.1007/BF00854466
96. KASAPOĞLU N, BAYKAL A, TOPRAK M, KÖSEOĞLU Y, BAYRAKDAR H. Synthesis and Characterization of NiFe_2O_4 Nano-Octahedrons by EDTA-Assisted Hydrothermal Method. *Turkish Journal of Chemistry*. 2007;31(6):659-666. doi:-
97. MATHIVANAN V, HARIS M. Characterization of pure and copper-doped iron tartrate crystals grown in silica gel. *Pramana - J Phys*. 2013;81(1):177-187. doi:10.1007/s12043-013-0564-x
98. Lemaire E, Ayela C, Atli A. Eco-friendly materials for large area piezoelectronics: self-oriented Rochelle salt in wood. *Smart Mater Struct*. 2018;27(2):025005. doi:10.1088/1361-665X/aaa209
99. Premature fracture of high-strength suspension springs caused by corrosion fatigue cracking - ScienceDirect. Accessed September 11, 2023. https://www.sciencedirect.com/science/article/pii/S2590123022004194
100. Mays TJ. A new classification of pore sizes. In: Llewellyn PL, Rodriquez-Reinoso F, Rouqerol J, Seaton N, eds. *Studies in Surface Science and Catalysis*. Vol 160. Characterization of Porous Solids VII. Elsevier; 2007:57-62. doi:10.1016/S0167-2991(07)80009-7
101. Aghazadeh M, Karimzadeh I, Ganjali M, Gharailou D, Hamad S. EDTA-grafted Cu2+-doped superparamagnetic nanoparticles: facile novel synthesis and their structural and magnetic characterizations. *Applied Physics A*. 2019;125. doi:10.1007/s00339-019-2803-6
102. Lanigan K, Pidsosny K. Reflectance FTIR spectroscopic analysis of metal complexation to EDTA and EDDS. *Vibrational Spectroscopy - VIB SPECTROSC*. 2007;45:2-9. doi:10.1016/j.vibspec.2007.03.003
103. Huang YS, Zhou Y, Zeng X, Zhang D, Wu S. Reversible Crosslinking of Commodity Polymers via Photocontrolled Metal–Ligand Coordination for High-Performance and Recyclable Thermoset Plastics. *Advanced Materials*. n/a(n/a):2305517. doi:10.1002/adma.202305517
104. Ariponnammal S, Velvizhi R. Structural, Spectroscopic, and Magnetic Studies on Copper Tartrate Crystals. *Zeitschrift für Naturforschung A*. 2019;74(9):813-819. doi:10.1515/zna-2018-0498
105. Chempendix - Formation Constants for metal-EDTA Complexes. Accessed September 10, 2023. https://sites.google.com/site/chempendix/formation-constants/formation-constants-for-metal-edta-complexes
106. Ramasubramanian M, Popov BN, White RE, Chen KS. *Equilibrium Characteristics of Tartrate and EDTA-Based Electroless Copper Deposition Baths*. Sandia National Lab. (SNL-NM), Albuquerque, NM (United States); 1997. Accessed September 10, 2023. https://www.osti.gov/biblio/510442
107. Markovic G, Visakh PM. 1 - Polymer blends: State of art. In: Visakh PM, Markovic G, Pasquini D, eds. *Recent Developments in Polymer Macro, Micro and Nano Blends*. Woodhead Publishing; 2017:1-15. doi:10.1016/B978-0-08-100408-1.00001-7
108. Vicente JD. *Rheology*. BoD – Books on Demand; 2012.
109. Lenhart JL, Cole PJ. Adhesion Properties of Lightly Crosslinked Solvent-Swollen Polymer Gels. *The Journal of Adhesion*. 2006;82(10):945-971. doi:10.1080/00218460600875953